Influenza Matrix Protein M1 – An *in vitro* Membrane Binding Study

D I S S E R T A T I O N

Zur Erlangung des akademischen Titels
d o c t o r r e r u m n a t u r a l i u m
(Dr. rer. nat.)
im Fach Biophysik

eingereicht an der
Mathematisch-Naturwissenschaftlichen Fakultät I
der Humboldt-Universität zu Berlin

von
Diplom-Biologin
Nadine Jungnick

Präsident der Humboldt-Universität zu Berlin
Prof. Dr. Jan-Hendrik Olbertz

Dekan der Mathematisch-Naturwissenschaftlichen Fakultät I
Professor Dr. Andreas Herrmann

Gutachter: 1. Prof. Dr. Andreas Herrmann
2. PD Dr. Michael Veit
3. Professor Dr. Thomas Günther Pomorski

eingereicht: 20.9.2011

Datum der Promotion: 19.12.2011

Zusammenfassung

Die Aufklärung der Prozesse, die zur Zusammensetzung des Influenza A Virus führen, ist Bestandteil für die Bekämpfung dieser Infektionskrankheit. Der Viruspartikel setzt sich aus einer Hülle, der darunter liegenden Matrix und dem Genom zusammen. Das Genom ist als Bündel aus acht Ribunucleoproteinkomplexen organisiert. Die Hülle besteht aus einer Membran, die mit Sphingomyelin und Cholesterol angereichert ist und den darin eingebetteten Membranproteinen Hämagglutinin, Neuraminidase und dem Protonenkanal M2. Die unter der Hülle liegende Matrix wird von einem einzigen Influenzaprotein formiert: Dem Matrixprotein M1. Es spielt eine Schlüsselrolle im Replikationszyklus des Virus in der Zelle. Es interagiert mit dem genetischen Material, mit den Membranproteinen und der Lipidmembran der Hülle.

Die vorliegende Arbeit gibt Auskunft, welche Lipide eine Rolle in der M1-Membran-Wechselwirkung spielen. Die Liste der identifizierten Lipide umfasst neben dem bereits bekannten Phosphatidylserin auch Phosphatidylglycerol und Phosphatidsäure. Verschiedene Phosphatidylinositole konnten ebenfalls identifiziert werden. Als stärkster M1 Bindungspartner trat dabei Phosphatidylinositol-4-Phosphat zutage.

Weitere auf Mutanten basierende Untersuchungen zeigten, dass der membranbindende Bereich nicht auf eine einzelne Domäne in M1 festgelegt werden kann. Die N-terminale M1-Domäne mit ihrem Oberflächen-exponierten, positiv geladenen Areal und die C-terminale Domäne interagierten mit Modellmembranen.

Das Resultat dieser Interaktionen konnte mittels mikroskopischer Untersuchungen an gigantischen unilamellaren Vesikeln dokumentiert werden. Für M1 und für eine Mutante, die nur aus der N-terminalen M1-Domäne besteht, konnte eine von anderen viralen Proteinen unabhängige homooligomere Organisation auf der Membran gezeigt werden. Diese M1-Cluster könnten während der Zusammensetzung des Viruspartikels als Fundament für die Eingliederung aller weiteren viralen Komponenten dienen.

Schlagworte: Fluoreszenzmikroskopie, Influenza A Matrixprotein M1, Protein-Membran-Interaktionen, unilamellare Vesikel.

Abstract

Knowledge about the assembly process of the influenza A virus particle is essential for the development of effective approaches for prevention and treatment of this virus infection. The virus particle consists of an envelope, an underlying matrix, and the encapsulated genome. The genetic material is organized as bundle of eight ribonucleoprotein complexes that encode for eleven proteins. The envelope consists of a lipid bilayer that is enriched in sphingomyelin and cholesterol. The viral spike proteins, hemagglutinin and neuraminidase, as well as the proton channel M2 are embedded into this membrane. The matrix can be found below the envelope. It is formed by one single protein, the matrix protein M1. M1 plays a crucial role during the replication of the virus in the cell. It interacts with the genetic material, with the envelope proteins and with the lipid bilayer of the envelope.

The results of this study reveal in detail which lipids are targeted by M1. The set of identified lipids contains phosphatylglycerol and phosphatidic acids as new binding partners, beside the known phophatidylserine. Additionally, several phosphatidylinositols were identified. Phosphatidylinositol-4-phosphate was the strongest binding partner from this group.

Mutant-based analysis revealed that M1 owns more than one membrane binding site. The positively charged area in the N-terminal and the C-terminal domain mediated membrane association of the respective mutant protein.

The final constitution of M1 on the membrane was characterized by confocal fluorescence microscopy on giant unilamellar vesicles. Full length M1 and a mutant that consisted only of the N-terminal part of M1 showed lateral clustering of homooligomers on the vesicle surface. The clusters formed independently of any other viral component. A function as fundament for the incorporation of the other viral components can be assumed for these clusters.

Keywords: Unilamellar vesicles, influenza matrix protein M1, protein-membrane interaction, fluorescence microscopy

Abbreviations

APS	Ammonium persulfate
A_λ	Absorption at wavelength λ in nm
C_6-NBD-PC	1-Palmitoyl-2-[6-[(7-nitro-2-1,3-benzoxadiazol-4-yl)amino]hexanoyl]-*sn*-glycero-3-phosphatidylcholine
Chol	Cholesterol
DLS	dynamic light scattering
DOPC	Dioleoyl-phosphatidylcholine
DOPS	Dioleoyl-phosphatidylserine
EDTA	Ethylenediaminetetraacetic acid
FM	Fluorescein-5-maleimide
FRAP	Fluorescence recovery after photobleaching
FRET	Förster resonance energy transfer
GUV	giant unilamellar vesicle
HA	Hemagglutinin
LUV	large unilamellar vesicle
M1	Matrix protein 1
MOPS	3-(N-morpholino)propanesulfonic acid
NaP	10 mM sodium phosphate buffer, pH 7
NaPKCl	10 mM sodium phosphate buffer with 120 mM potassium chloride, pH 7
Cy-, Cys-	Cysteine
N-NBD-DPPE	N-(7-nitrobenzy-2-oxa-l,3-di azol-4-yl)-1,2-dipalmitoyl-*sn*-glycero-3-phosphatidylethanolamine
OD_λ	optical density at wavelength λ in nm
ORF	open reading frame
PAGE	polyacrylamide gel electrophoresis
PBS	polybasic sequence
PCR	Polymerase chain reaction
PI3P	Phosphatidylinositol-3-phosphate
PI4P	Phosphatidylinositol-4-phosphate
SDS	Sodium dodecyl sulfate
SM	Sphingomyelin
SUV	small unilamellar vesicle
T_m	melting temperature
TMR	5/6-Carboxy-tetramethylrhodamine-ethyl-maleimide

Table of contents

1 Introduction

Infection by the influenza virus results in the death of a quarter- to a half-million people annually. In Germany alone 21,959 people died in 2008 [1] from flu-like diseases. In April 2009, a highly infectious influenza variant emerged in Mexico and caught world-wide attention. This influenza A H1N1 strain, so called "New flu", spread rapidly and was classified as pandemic by the WHO in June 2009 [2]. The fundamental mechanisms governing influenza infection need to be understood in detail to prevent and treat future outbreaks. This effort will require both basic and applied medical research, and studies on the molecular level. Biochemical and biophysical methods promise substantial progress in the discovery of the mechanisms of influenza virus replication and assembly in the cell.

1.1 Influenza

The history of the influenza disease can be traced back to the ancient Greeks. Hippocrates described bronchial infections with symptoms similar to influenza [3]. More accurate records of influenza pandemics are available since the 16th century. During the following centuries several major outbreaks occurred [4] of which the most recent were the Spanish flu with over 50 million deaths in 1918 [5,6] and the Hong Kong flu 1968 with reported one million deaths [7,8].

Wild aquatic birds are the widely accepted reservoir hosts for influenza viruses [9,10]. Research on avian influenza-based human viruses revealed a two-step transmission mechanism, where an avian strain infected an intermediate swine host and was then transmitted to humans [11]. Direct transmission between humans and birds has been described for H5N1 virus strains between 2003 – 2005 in Asia [11]. In most cases the transmission rates between animals and humans were low [12]. Pandemic viruses like the H1N1 virus from 2009 were exceptionally contagious and spread rapidly among humans around the world [13,14]. This particular H1N1 virus was first detected in Mexico and characterized on the molecular level. It contained components of human, avian, and swine specific viruses [13,15].

The mechanism upon which different viral genes are combined is called re-assortment and occurs when different influenza hosts live in close proximity and cross infections occur. During an infection with different viruses, new virus particles are assembled which contain genetic material from both influenza strains [16].

The Influenza A and B genus, together with the genera of Influenza C, Thogotoviruses, and the Isavirus belong to the family *Orthomyxoviridae*. Recently additional viruses have been discovered and pooled in a fifth yet unnamed genus [17] which also harbor the major characteristic of the *Orthomyxoviridae* – the segmented and single-stranded RNA genome of negative polarity. The individual influenza genera can be distinguished by host range, genome and viron structure. Influenza A and B have a similar viron structure and a segmented genome consisting of eight pieces which encode 11 proteins in total (see chapter 1.1.1). Influenza C has in contrast to A and B only seven genomic segments. The distinction between A and B lies in the specificity of the nucleoprotein (NP) which is necessary for the organization of the genome and also determines the host range [18]. Whereas influenza B causes mostly mild symptoms upon infection in humans, pandemics with severe phenotypes are mainly caused by the influenza A virus.

1.1.1 The influenza virus particle

Influenza virus particles are pleomorphic. Beside spheres with an approximate size of 100 – 150 nm [19], filamentous particles can also be observed [20]. The envelope of the particles consists of a lipid bilayer in which three different membrane proteins are embedded (Figure 1). The trimeric hemagglutinin (HA) mediates binding to the host membrane and fusion of the viral and the target membrane. For influenza A 16 different avian HA subtypes (H1 – H16) have been classified by their serological behavior [21,22]. Three HA serotypes (H1, H2, and H3) have been found to be adapted to the human population [23]. The second membrane protein, neuraminidase (NA), is tetrameric and removes the receptor molecules recognized by HA from the outer membrane surface. Nine NA serotypes (N1 – N9) have been described [22]. The tetrameric protein M2, the third membrane protein, acts as a proton channel. Influenza B particles contain both HA and NA but M2 is replaced by a proton channel named NB [24]. In Influenza C the multifunctional hemagglutinin-esterase-fusion protein (HEF) carries the activities of HA and NA [18]. The proton channel is formed by the CM2 protein [25].

Directly beneath the envelope lies a shell of M1 protein. M1 oligomerization and interactions with the membrane as well as with HA, NA and M2 have been postulated as being necessary for the formation of this layer [26,27,28]. M1 encloses the virus core that contains the seven (influenza C) or eight (influenza A and B) viral ribonucleoprotein (vRNP) complexes [29] which carry the genetic material of the virus. Each vRNP complex consists of a single-

stranded, negatively oriented RNA that is coiled into a panhandle-like structure by oligomerized NP. The polymerase complex with the proteins PB1, PB2, and PA is located at the terminal end of the panhandle [30]. The polymerase complex mediates the transcription of viral RNA.

Two additional proteins complete the particle structure. The multifunctional NS1 protein has a modulating effect on the transcription of viral RNA and an enhancing effect on translation of viral mRNA [31]. The nuclear export protein (NEP – previously NS2) is responsible for the export of newly formed vRNP complexes from the nucleus [32].

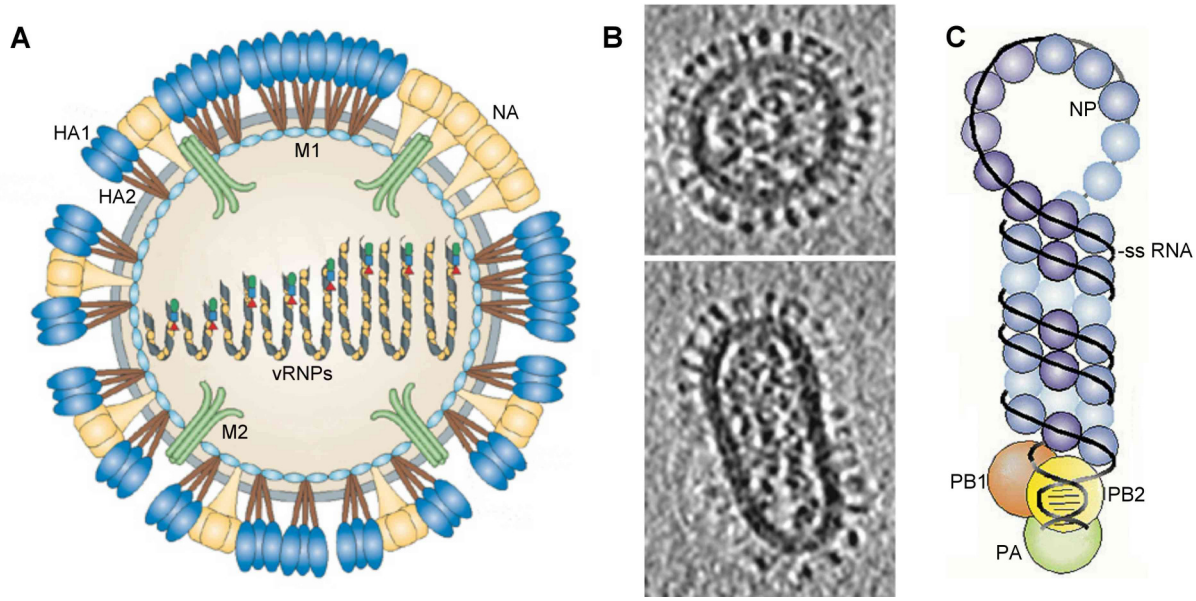

Figure 1 The influenza particle. (A) Model of the Influenza A particle depicting the envelope with the spike proteins hemagglutinin (HA), neuraminidase (NA) and the proton channel M2 embedded into the lipid bilayer. Oligomerized M1 interacts with the envelope components and encloses the viral ribonucleoprotein (vRNP) complexes. Adapted from [33]. (B) Electron micrograph of a spherical and an elongated virus particle with visible spike proteins and genomic material in the center [34]. (C) A model of a vRNP [30].

1.1.2 Influenza replication cycle

The replication of influenza can basically be divided into three stages: (i) internalization, (ii) production of the viral components, and (iii) assembly and release. Figure 2 summarizes the replications cycle. Initially, HA binds to cell surface receptors on the host membrane. These receptors are glycoproteins and glycolipids containing oligosaccharides with terminal sialic acids. Sialic acids comprise a molecule group based on neuraminic acid with the most common member being N-acetylneuraminic acid [35]. The precise linkage of the monosaccharides determines the host preference. In case of avian influenza sialic acids are recognized that

are bound to galactose through α2-3 linkages [23]. Viruses infecting humans attach to α2-6-linked sialic acids [23]. The binding mechanism between HA and the sialic acids carrying glycoproteins and glycolipids is modulated by HAs own oligosaccharides. It was shown for HA with truncated glycosylations that the receptor binding was increased [36,37].

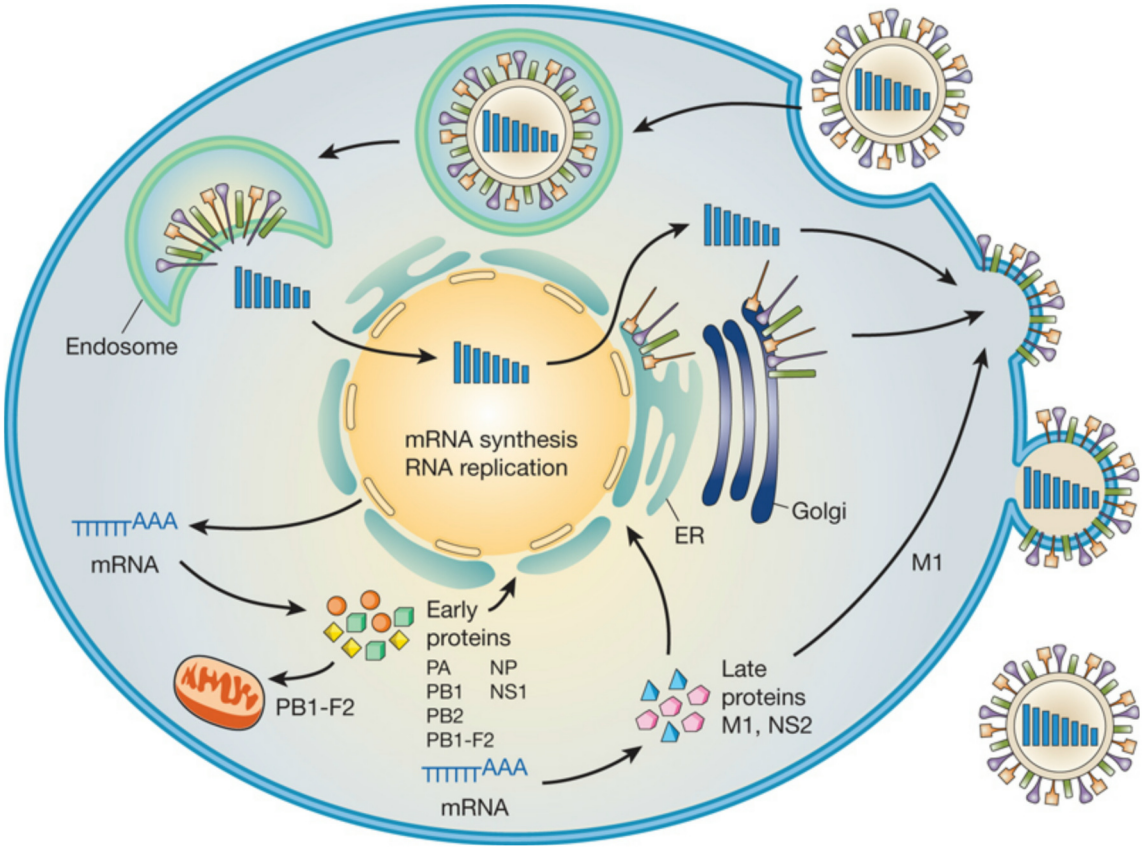

Figure 2 Replication cycle of Influenza A. HA binds in a first step to sialic acids on the surface of the host cell. The bound virus particle is internalized via receptor-mediated endocytosis. The acidification of the late endosome triggers conformational changes in HA, which lead to fusion of endosomal and viral membrane. The vRNPs are released through the fusion pore and transported to the nucleus. Viral mRNA synthesis occurs in the nucleus. The viral mRNAs induce production of the viral membrane proteins HA, NA, and M2 at the endoplasmic reticulum (ER). These membrane proteins are transported towards the assembly site through the Golgi apparatus. The other proteins are translated on cytoplasmic ribosomes. Early proteins, which are necessary for transcription and vRNP replication and assembly, are imported into the nucleus. Late proteins, like M1 and NS2 (NEP) enable the export of the vRNPs. When all components are assembled at the plasma membrane the new progeny virions bud. Adapted from [38].

When the virus is attached to the host membrane the cell internalizes the particle via receptor-mediated endocytosis. It could be shown that the resulting endosome is produced by clathrin-dependent and -independent pathways [39,40]. The endosome is transported by the cytoskeleton to the interior of the cell in close proximity to the nucleus [41]. Upon formation of the late endosome acidification occurs [42]. The lowering of the pH to values of 5.5 - 5 induces a conformational change in HA. This leads to the exposition and insertion of HA's hydrophobic

fusion peptide into the host membrane. In a second rearrangement step of HA the host and viral membrane are drawn together, resulting in fusion and pore formation (Figure 3) [43,44].

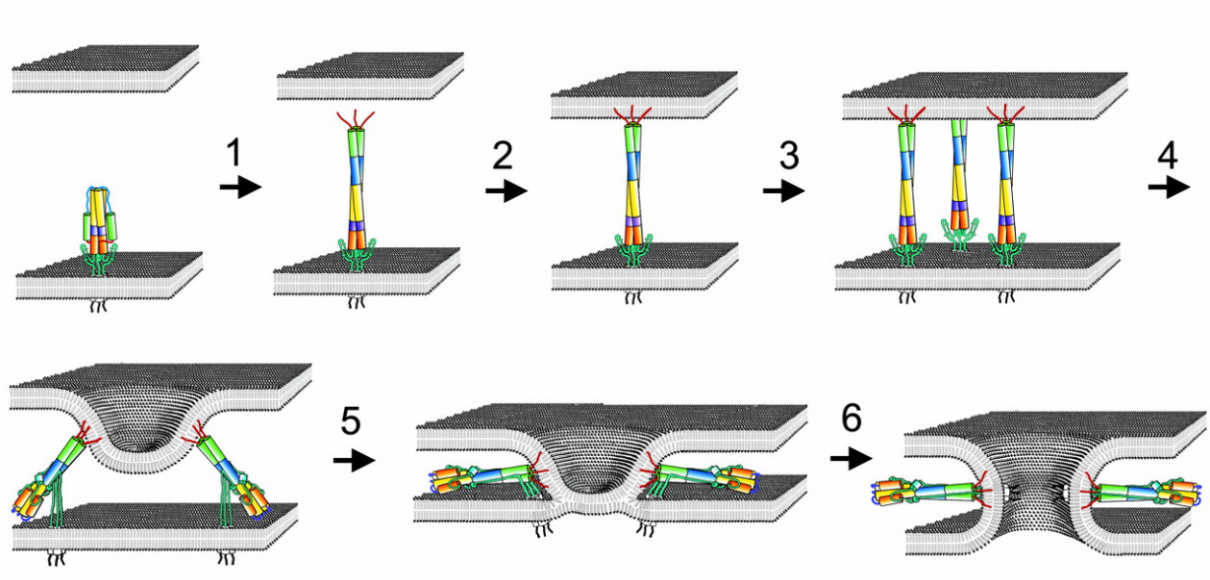

Figure 3 Conformational changes in hemagglutinin upon endosome acidification. Upon acidification conformational changes occur in HA (1) that expose the structurally concealed hydrophobic fusion peptide. The fusion peptides of the HA trimer insert into the host membrane (2, 3) and in a second rearrangement step the host membrane is drawn into close proximity to the viral membrane (4). Further action of HA leads to membrane fusion and the formation of a hemifusion diaphragm (5). Finally, a pore is formed (6). Adapted from [43].

Parallel to this, M2 shuttles protons from the endosomal lumen into the viral core. At this point M1 plays a crucial role. It functions as a link connecting the cytoplasmic tails of the three membrane proteins [26] and the virus membranes [27] to the vRNP complexes [45]. The acidification destabilizes the M1 envelope anchor and releases the genome segments into the cytoplasm for transport towards the nucleus [46]. The three nuclear localization signals (NLS) of NP have been shown to be essential for the import of the vRNP complexes into the nucleus. Import has been shown to be mediated by importin α and β and the nuclear pore complex [41,47,48]. Within the nucleus the trimeric polymerase complex transcribes the negative-sense viral RNA segments into mRNA and replicates them via complementary RNA intermediates into abundant copies of vRNA [49,50]. Simultaneously, the mRNAs are exported to the cytoplasm or endoplasmatic reticulum (ER) where translation of the eleven influenza proteins occurs. HA, NA and M2 are synthesized on the ER from where they are transported via the Golgi apparatus to the apical plasma membrane [51]. A co-localization of HA and NA with cholesterol- and sphingomyelin-enriched microdomains, so called membrane rafts, was shown [52,53,54]; whereas M2 was proposed to be peripherally associated to these liquid ordered membrane domains since only a minor portion of M2 was found to be associated with deter-

gent-resistant membranes [55]. The newly synthesized cytoplasmic proteins M1, NS1, NP, and the polymerase subunits are targeted to the nucleus by their intrinsic NLS. In case of NEP transport may occur by diffusion [32]. In the cytoplasm the remaining M1 was found to be colocalized with cellular membranes including the Golgi vesicles [56,57,58] independent of other viral proteins. The PB1-F2 protein, a splicing variant of the polymerase subunit PB1, interacts with mitochondrial proteins [59]. In the nucleus, PB1, PB2, PA, and NP together with vRNA are assembled into new vRNP complexes. Their export is triggered by a signal cascade initiated by the accumulation of HA at the plasma membrane [60]. The single vRNP complexes are exported from the nucleus after stepwise association of proteins [61]. First, M1 attaches to the vRNPs. This association inactivates the polymerase complex and arrests it at the terminal part of the vRNP complex [62,63]. NEP binds to M1. It contains a nuclear export signal sequence and is the target for the host protein Crm1 [64]. Crm1 facilitates together with RanGTP the export of vRNPs through the nuclear pore [65]. The re-import of the complexes into the nucleus is inhibited by M1 which possibly shields the NLS of NP [46,66]. Once the M1 covered vRNPs are released into the cytoplasm, transport towards the apical plasma membrane is mediated by cytoskeleton filaments [62,67]. Assembly of all components into the viral particle occurs at the apical plasma membrane, since only there vRNPs are present. The current model states that M2 and raft associated HA and NA are linked to each other by polymerized M1 that is bound to the cytoplasmic tails of the membrane proteins and to the membrane. The observation of the M1 oligomerization process should be experimentally possible but has not yet been accomplished. Interaction of M1 with membrane proteins and M1 self-oligomerization [68,69,70] are well studied events, and M1 oligomerization is considered essential for membrane bending and formation of the bud involving the cortical actin filaments [71]. The vRNPs are delivered to the budding site and internalized into the bud by pulling into the cavity by envelope-M1 and M1-vRNP interactions and additionally by pushing through actin filaments [62]. The mechanism how the single vRNPs are organized in the cytoplasm is based on RNA-RNA interaction of specific signal sequences leading to an octameric super-vRNP [72,73,74]. This complex could be visualized [29] in virus cross-sections. The incorporation of the eight vRNPs is not the critical but an essential part of particle formation. Budding of empty virus-like particles could also be induced in the absence of vRNPs [75,76]. The last step is the closure of the bud. Here M2 plays a role in organizing the membrane before pinching-off of the new particle [34,55]. Release of the new particle requires

removal of sialic acids from the cell surface. Otherwise the newly synthesized particles remain bound on the infected cell. This cleavage is accomplished by NA. The catalytic site of NA binds specifically to the sialic acid of the glycoproteins and glycolipids and hydrolyzes the linkages to the respective terminal sialic acid [77,78].

1.1.3 M1 as key organizer at the membrane level

Mutational studies showed an essential function of M1 during virus particle formation. Infectious virus production failed when M1 was lacking or when specific amino acid sequences of M1 were substituted [79]. An additional hint for the importance of M1 arose when the concentration of available M1 was limited. This leads to a delayed and reduced budding of viral particles [80]. Even though its role in virus maturation is of such importance, the function of M1 during the replication cycle is not understood in detail.

The 252 amino acids containing matrix protein is encoded on segment seven, the second smallest of the eight genome pieces. M1 can be isolated from the virus as a 27.8 kDa protein. Its isoelectric point is 9.81. Several attempts have been undertaken to crystallize the protein. Sha and Luo [81] presented in 1997 the structure of the N-terminal domain (AA 2 – 158) isolated from virus at pH 4. This structure of wild type M1 revealed an N-terminal subdomain formed by the first four helices (H1 – H4). A flexible link including the short helix H5 connects the N-terminal subdomain to the middle subdomain that consists of four additional helices. The C-terminal structure could not be solved due to proteolysis [81]. Subsequently two structures of the same N-terminal part of M1 were published and showed only minor folding differences to the structure published by Sha and Luo. Harris *et al.* as well as Arzt *et al.* determined the structure at neutral pH [68,82]. Furthermore, the structure of a M1 mutant with substituted NLS signal [83] was solved and revealed no structural differences to the wild type. Based on the crystal structures, the surface potential of this part of M1 was calculated and local concentrations of either positive or negative charged amino acids could be visualized. The polybasic sequence (PBS) in H6 that contains the three residues (R101, K104, R105) of the NLS motif (101–RKLKR–105) together with K95 and K98 forms a prominent positively charged surface area. Beside the function of the NLS as a nuclear sorting signal a function as membrane binding site was proposed and electrostatic interactions to negatively charged membrane surfaces were suggested as the binding mechanism [27]. Experimental data to prove this mechanism are so far only available to a limited extent. When purified M1 was

exposed to liposomes and liposomes with bound M1 were separated from unbound M1, protein association was only detected for negatively charged vesicles. The negatively charged vesicles in this artificial system were produced from a mixture of specific lipids, namely phosphatidylcholine, cholesterol, and negatively charged phophatidylserine [27,84]. However, interactions with other lipids are not reported. Membrane suspensions derived from lysed cells were also tested. Here a M1 association was visualized [27]. Since cellular membranes consist of more than three different lipids, the role of the huge lipid spectrum needs to be further specified. It is possible that phosphatidylserine is not the only M1 target.

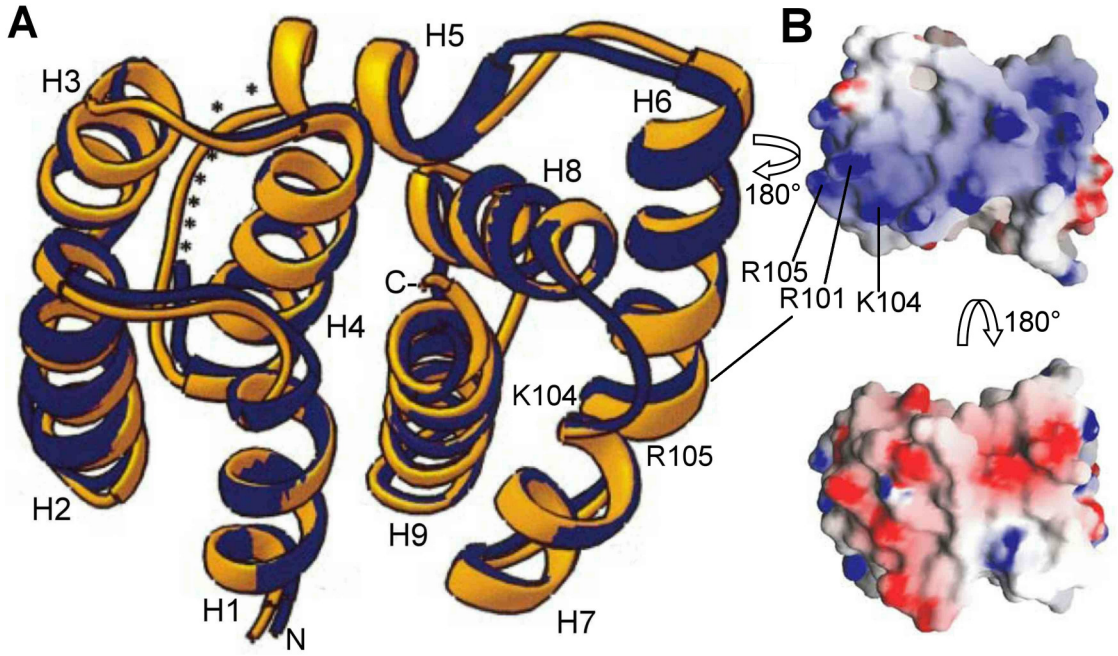

Figure 4 3D structure of the N-terminal part of M1. (A) Superimposed ribbon cartoon of the crystal structures at pH 4 (gold) and pH 7 (blue). The major secondary structure elements are nine α-helices linked by loop regions. β-sheets are not visible. Adapted from [68]. (B) Electrochemical surface potential of the protein from two different views. The protein exhibits enrichment of negative charges (red) and a prominent positively charged (blue) patch including the PBS (95–KAVKLYRKLKR–105) which is located on H6. Modified from [83]

When M1 was expressed in mammalian epithelial cells it was found in the nucleus and attached to membranes [56]. The plasma membrane, the membranes of Golgi apparatus and ER as well as transport and storage vesicles were targeted by M1. Studies performed with fluorescent proteins showed a spotted distribution of M1 [58]. Experiments with fluorescent ER and Golgi markers revealed a co-localization of M1 with the Golgi apparatus [85]. Why M1 was found in association with the Golgi is matter of ongoing research.

1.2 Lipid membranes

Lipid membranes play a crucial role in both the structure and the function of all – prokaryotic and eukaryotic – cells. They define the cellular space in total (plasma membrane) as well as in eukaryotic cells internal organelles (mitochondria and plastids) and compartments (nuclear membrane, smooth and rough endoplasmic reticulum, Golgi apparatus, endosomes, and lysosomes).

They display a uniform overall structure, basically a six nanometer thick double layer of lipid molecules with embedded (integral) and peripheral proteins. Membranes function as barriers which enable regulated transport of molecules from outside inwards and vice versa by protein activity. In addition, many cellular enzymes are attached to membranes where they are concentrated on a lateral plane and facilitate efficient interactions [86]. A continuous exchange of vesicles maintains transport of cargo which is not directly transported via the cytoskeleton or diffusion through the cytoplasm. Beside this, membranes serve as an assembly site for cellular proteins, like clathrin coated pits, or for virus particles.

1.2.1 Cellular lipids

Mammalian cells contain more than thousand different lipid species [87]. Lipids fulfill three general functions: (i) energy storage, (ii) matrix of cellular membranes, (iii) first and second messengers in signal transductions and molecular recognition processes.

Glycerophospholipids are the major lipid component in the membrane. These lipids are composed of three components: (i) the headgroup molecule which is attached via a phosphoester bond to (ii) glycerol. Two fatty acid chains (iii) can be found at the other originally hydroxylated C-atoms of the glycerol, also attached via ester bonds. Major glycerophospholipids found in the cell are phosphatidic acids (PA), phosphatidylcholines (PC), phosphatidylethanolamines (PE), phosphatidylserines (PS), and phosphatidylinsitols (PI) with one to three additional phosphorylations [88].

The second abundant group of molecules is the group of sphingolipids. These molecules show a trimodular composition similar to glycerophospholipids. The skeletal structure component is sphingosine. The amino group of this molecule functions as attachment site for fatty acids, the resulting molecule is classified as ceramide. Substituents can be bound to the primary hydroxyl group of sphingosine through esterification. The most prominent sphingolipid sphingomyelin is depicted in Figure 5. Glycoglycerolipids and glycosphingolipids are glycosylated

forms of membrane lipids [86]. The carbohydrate moiety of the headgroup can range from a single sugar to very complex polymers.

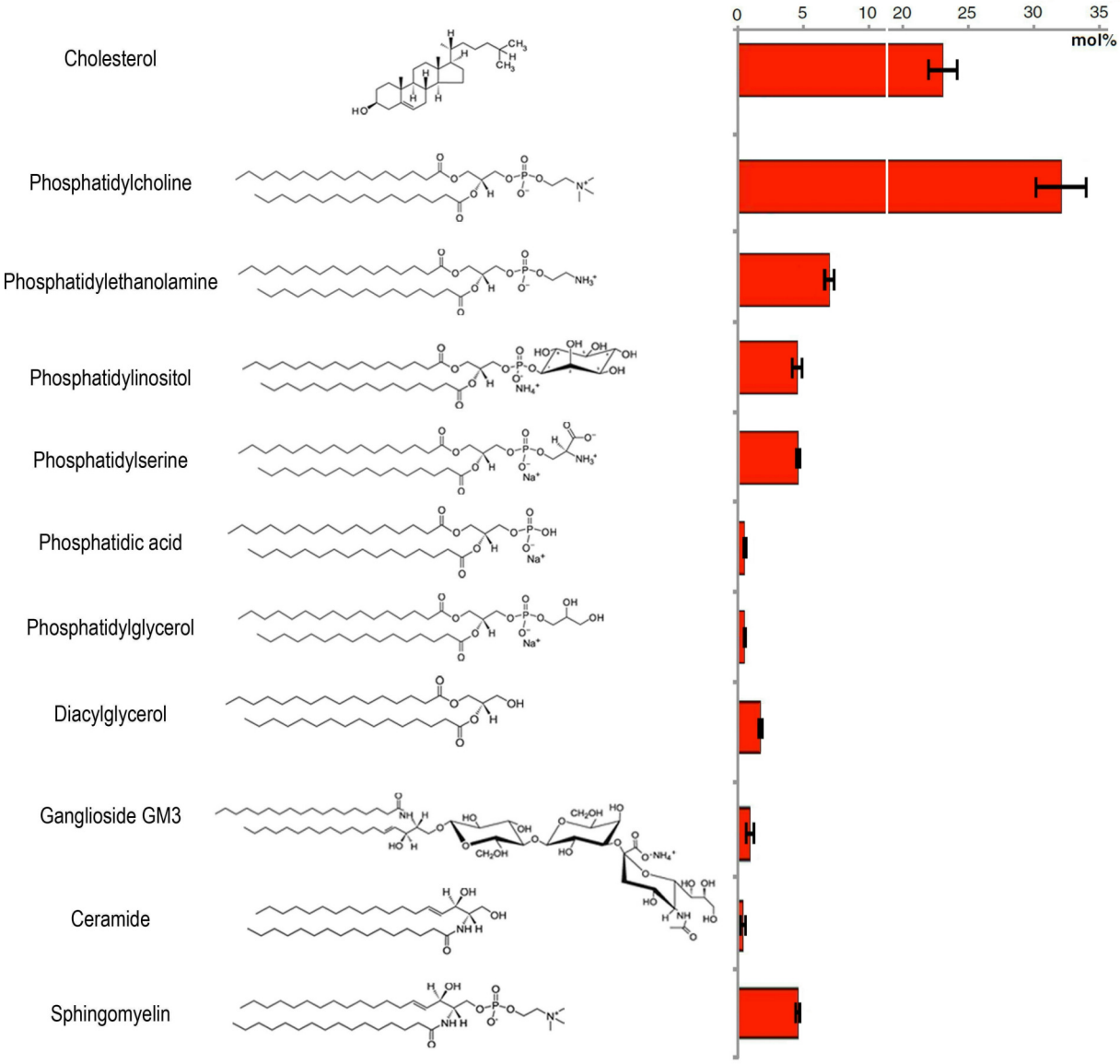

Figure 5 Membrane lipids of epithelial Madin-Darby canine kidney cells. Cholesterol, phosphatidylcholine, and phosphatidylethanolamine represent the major components of epithelial cells. Less abundant are PI, PS, SM, diacylglycerol, PA, PG, ceramides, and gangliosides like GM3. Adapted from [88].

The attached fatty acids differ in chain length and number of double bonds within the chain. The degree of unsaturation in the side chains and the concentration of lipids with unsaturated side chains influence the membrane fluidity. The more unsaturated side chains are present the higher the fluidity of the membrane is.

Another group of membrane molecules are sterols including cholesterol, the most abundant sterol in mammalian cells. These molecules incorporate between phospholipids and sphingo-

lipids. Hydrogen bonds between the sterols hydroxyl group and the lipid headgroups as well as hydrophobic interactions are the driving force for this incorporation.

Minor components of membranes are free fatty acids, lysophospholipds, mono- and diacylglycerides, as well as polyisoprenoid lipids.

The lipid composition is dynamic. For epithelial morphogenesis a major shift of the composition from sphingomyelin to glycosphingolipids, together with an increase in phosphatidylethanolamine and cholesterol content could be observed whereas the opposite changes took place during an epithelial-to-mesenchymal transition [88].

1.2.2 Cellular lipid transport and membrane traffic

Glycerophospholipids are mainly synthesized at the interface of cytosol and membrane. The bacterial phospholipid synthesis is located at the cytosolic site of the plasma membrane, whereas eukaryotic cells produce their lipids mainly at the smooth endoplasmic reticulum. The synthesized lipids are incorporated into the cytoplasmic site of the membrane. The translocation of lipids from one leaflet to the other is accomplished by flip-flop mechanisms. Flip-flop can occur spontaneously or controlled by membrane proteins called flippases. These proteins bind lipids on one membrane leaflet, transport in an energy-dependent step and release the bound lipid at the other leaflet (reviewed in [89]). Action of P-type ATPases like yeast Dnf1p and Dnf2p allows the maintenance of the different compositions of inner and outer leaflet of the plasma membrane. They keep the content of aminophospholipids like PS and PE in the outer leaflet low by specific transport to the inner leaflet where PS is enriched [90].

The ER is the major lipid production site in eukaryotic cells. It overlaps with the nuclear membrane. The other compartments achieve their supply of lipids by two transport mechanisms. Lipid transfer proteins shuttle specific lipids between membranes whereas vesicles allow transport of formed membranes. Transport with lipid carrying proteins involves a continually growing group of proteins. These proteins act at membrane contacts sites between the ER and the Golgi apparatus or the Golgi and the plasma membrane. The ceramide transporter CERT was active between ER and Golgi membranes [91]. Nir2 was identified as a PI/PC transfer protein, shuttling PC from the Golgi to the ER and phosphatidylinositol back, from which phosphatidylinositol-4-phosphate (PI4P) is subsequently synthesized at the Golgi membranes [92]. The activity of these proteins enriches specific lipids at the respective compartments.

The major transport form for lipids is the vesicle. A huge and still growing number of proteins are involved in the establishment and trafficking of vesicles in the cell, regulating vesicle identity, local lipid synthesis, and vesicle targeting. Clathrin-coated vesicles can be formed from the plasma membrane as well as the Golgi apparatus. They mediate endocytic events and endosomal vesicular traffic [93,94,95]. COP (coat protein) vesicles of type I are involved in bidirectional transport in the Golgi apparatus as well as recycling of proteins from the Golgi to the ER [96]. Vesicles organized by COPII emerge from the ER and export secretory proteins towards the Golgi complex [97,98].

All these mechanisms taken together enable the cell to sort lipids and proteins specifically to distinct sites of the cell. These transport pathways are used by viruses, like influenza, to sort their components. For example, influenza hemagglutinin highjacks the secretory pathway on its way from the ER through the Golgi to the viral assembly site at the plasma membrane [99].

1.2.3 The plasma membrane

As mentioned before, membranes function as barriers. This function is especially important at the outermost membrane, the plasma membrane. Nutrients and liquids are taken up through this membrane. Signals are perceived and transmitted inwards. Beside these major functions of the regular cellular life cycle other events can be observed here. Assembly and budding of the new influenza viral particles occur at the plasma membrane [62].

The lipids provide the matrix for incorporated proteins. The plasma membrane exhibits a pronounced difference in the lipid composition of the cytoplasmic and extracellular leaflets. Human erythrocytes were extensively analyzed as a model system for the plasma membrane. Their outer leaflet contains mostly phosphatidylcholine and sphingomyelin while the inner leaflet consists mainly of phosphatidylethanolamine and phosphatidylserine. The phosphatidylinositolphosphates are also not homogeneously distributed across the plasma membrane. Phosphatidic acid, phosphatidylinositol and phosphatidylinositol-4,5-bisphosphate were mainly present at the inner leaflet [100]. This assymetric appearance of lipids leads to a negatively charged cytoplasmic lipid leaflet (see Figure 6A). Beside this leaflet dimorphism a lateral heterogeneity of the lipid distribution was found in the plasma membrane. Lipid domains called rafts are enriched in cholesterol, sphingomyelin, and glycerophospholipids which carry saturated fatty acids, and specific proteins [101,102]. The local enrichment of these specific

lipids creates a liquid ordered phase state. These liquid ordered plasma membrane rafts are surrounded by lipids in a liquid disordered organization [103].

Clustering of proteins was observed in a sterol-dependent manner [104]. The incorporated proteins carry specific raft signals, like cysteine palmitoylation close to the transmembrane domain [105] or glycosylphosphatidylinositol (GPI) anchors with saturated fatty acids [106]. Interestingly, the influenza hemagglutinin was found among those proteins, since it clusters cholesterol dependent in mammalian cells [52,53]. There are hints that rafts are also present at intra cellular membranes like the ER [107] and they may serve as sorting platforms in the cell. Figure 6 summarizes the transversal lipid distribution and presents a model of the lateral organization of the plasma membrane.

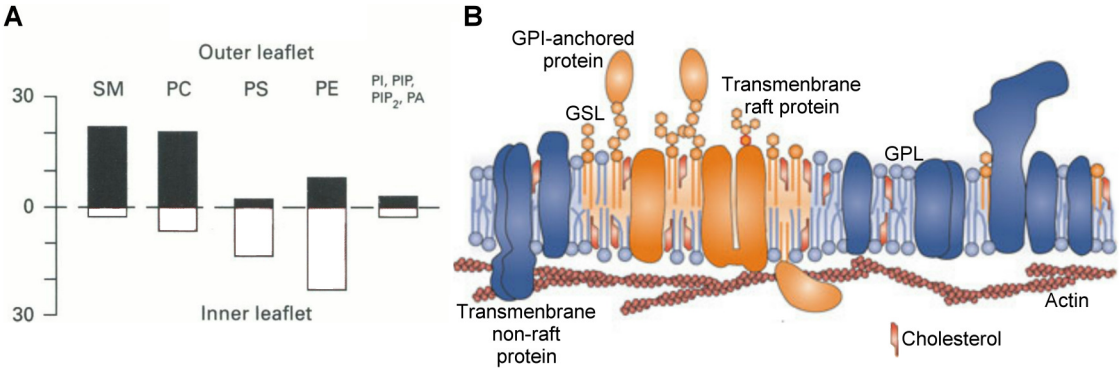

Figure 6 Composition and organization of the plasma membrane. (A) Leaflet composition of the plasma membrane. Adaptad from [100]. SM and PC were shown to reside mostly in the outer leaflet; PS and PE were detected in the inner leaflet. Phosphoinositols and its phosphorylated derivatives were distributed on both leaflets. (B) Model of the lateral heterogeneity within the plasma membrane. GPI-anchored proteins, transmembrane raft proteins cluster together with glycosphingolipids and cholesterol into rafts. Non-raft proteins are excluded. GSL = Glycosphingolipid, GPL = Glycerophospholipid. Modified from [108].

1.2.4 Influenza protein mediated plasma membrane modification

The influenza proteins HA, NA, and M2 belong to the group of integral membrane proteins. All three proteins own one α-helical membrane domain which consists mainly of hydrophobic amino acids [109,110,111]. A lipid raft association was shown for HA and NA [109,112]. The intrinsic equipment that facilitates HA raft association was identified. Mutation of specific amino acids in the transmembrane domain of HA revealed the amino acids 530-WILWISFAI-538 as essential for HA raft association [109]. The transmembrane domain and cytoplasmic tail of HA together own three cysteine residues (C551, C559, C562 in HA of the H7N1 strain) which are acylated [113]. The raft association of HA was reduced when

these cysteines were substituted [53,114]. The raft targeting signals of NA were also assessed via mutagenesis of specific amino acids in the transmembrane domain and cytoplasmic tail. The mutation of the amino acids 27-GINIISIWIS-35 in NAs transmembrane domain led to reduced raft association of NA [110]. Acylation of NA was not reported. From this data it was surmised that HA and NA recruit raft lipids to the assembly site of the virus particle (reviewed in [51,62,115]). The enrichment of HA and NA in rafts at the budding site is the first step during influenza assembly. But the final particle formation can only be accomplished when the membrane is curved, a bud is developed, and fission of the elongated bud occurs. Virus-like particles (VLPs) were formed, when HA or NA were expressed alone in cells [75,116]. Analysis of HA in model membranes revealed, that full length HA or its transmembrane peptide do not bent or tubulate the membrane when they are reconstituted into giant unilamellar vesicles (GUVs) [117]. Similar results were obtained when HA was analyzed in giant plasma membrane vesicles that resemble the plasma membrane. Therefore, cellular factors must be involved in the HA based VLP production. Combined expression of HA, NA, M2 and M1 enhanced VLP formation significantly [75]. This could have been the result from more efficient bud closure and fission of the closed VLPs. An impact of the influenza proton channel M2 in fission of virus particles was shown by production of mutant virus particles with altered M2. The mutation did not hinder the bud formation, but the release of the formed viruses was stopped [111,118]. Bending of membranes independent of other influenza proteins was shown when M2 was reconstituted into GUVs. The 17 amino acids long amphipathic helix in the cytoplasmic tail of M2 mediated this bending [111]. M2 was not found to be a raft protein, even though it carries a palmitoylation in its cytoplasmic tail [115,119]. Co-localization of M2 with HA was shown [120,121]. An interaction between HA and M2 would link M2 to the other viral spike proteins and could induce M2 mediated membrane bending.

A role for M1 in the orchestration of the budding process has been proposed. Several studies showed a direct influence of M1 on the shape of the final virus [80,122]. Single mutations in the NLS region of M1 could induce a shift from spherical viruses towards filamentous ones [123]. The change of the viral shape needs modification of the viral membrane and membrane-bound proteins. M1 was not able to induced VLP formation when it was expressed alone in cells. The VLP production was triggered efficiently when HA, NA, M2, and M1 were expressed together. The formation of a M1 layer inside of the VLPs could be shown [75]. This indicated a connection between these four proteins at the membrane level. An interaction of

M1 with the cytoplasmic tails of all three membrane proteins was shown [28,57,58]. Interestingly, M1-M2 interactions influence the shape of the budding influenza particle [28,120,124]. A current model by Rossman *et al.* [115] summarizes all the described protein-membrane and protein-protein interactions (Figure 7). The model considers clustering of HA and NA in lipid raft domains as an initial step that slightly bends the membrane at the assembly site. This bud initiation is further accomplished by M1 binding to the cytoplasmic tails of HA and NA and M1-mediated vRNP-attachment to the spike proteins (Figure 7A). The next step in the virus formation is elongation of the bud by polymerization of M1. This leads to a perpendicular encapsulation of the vRNPs in relation to the plasma membrane. M2 is recruited to the periphery of the budding site through interactions with M1 (Figure 7B). The amphipathic helix of M2 alters membrane curvature at the neck of the bud when it is inserted into the raft boundary. This leads to release of the budding virus (Figure 7C and D).

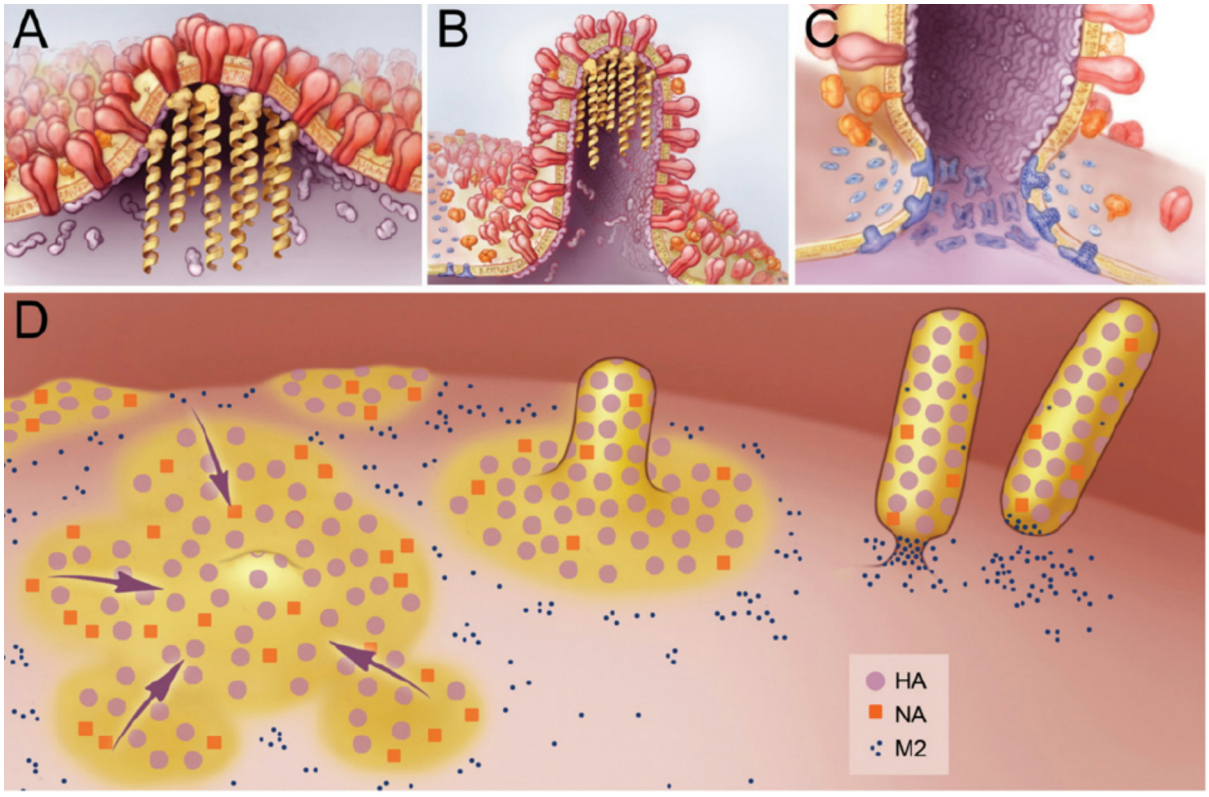

Figure 7 Model for influenza virus budding at the plasma membrane. (A) Initiation of the virus bud by clustering of HA (red) and NA (orange) in lipid raft domains. M1 (purple) binds to the cytoplasmic tails of HA and NA and cross-links the vRNPs (yellow) to the spike proteins. (B) Elongation of the bud by polymerization of M1. This leads to a perpendicular orientation of the vRNPs to the membrane. M2 (blue) is recruited to the periphery of the budding site through interactions with M1 and/or HA. (C) Insertion of the M2 amphipathic helix at the raft phase boundary alters membrane curvature at the neck of the bud and leads to release of the budding virus. (D) Overview of budding influenza viruses seen on the membrane. The sorting of HA and NA into lipid rafts (yellow), the formation of a filamentous virion, and membrane scission caused by M2, are depicted. Taken from [115].

A function of M1 as key organizer in the assembly of influenza virus can be derived from the M1 controlled formation of spherical or filamentous virions and its interaction with the three viral membrane proteins and the vRNPs. Even though the implications of the M1-HA/NA/M2 interaction for lateral lipid sorting and membrane shape changes have been analyzed to a great extent (reviewed in [51,62,115] it is still elusive how M1s intrinsic membrane binding capability fits into this model. Therefore it is essential to know what M1 does when it is attached to the membrane. GUVs and other artificial liposomes can provide a good starting point for examination of M1 membrane association. For instance, the appearance of HA and M2 was successfully visualized on this kind of vesicles [111,117].

1.2.5 Artificial liposomes as model membrane systems for protein interaction

Different membrane model systems have been established to approach protein-membrane interactions at the molecular level. The simplest are artificial liposomes. Such liposomes can be produced in different sizes by various methods.

Small unilamellar vesicles with a diameter below 100 nm were produced by ultrasonification of preformed multilamellar vesicles [125]. They can be used as drug delivery systems [126].

Large unilamellar vesicles (LUVs) were produced from multilamellar vesicles by extrusion through polycarbon membranes with defined pore sizes from 100 nm up to 400 nm [127,128]. Soluble molecules can be encapsulated into the lumen of the LUVs and later released in a controlled way [129]. LUVs cannot only harbor molecules; they can also provide a surface for attachment. ArfGAP1, a GTPase–activating protein (GAP) for ADP-ribosylation factor 1 (Arf1), could interact with lipid membranes. The curvature of the LUVs played a significant role, since binding of ArfGAP1 was stronger when smaller LUVs with a higher membrane curvature were used [130]. The membrane composition was shown to play a significant role for protein-membrane interaction beside the membrane curvature. Positively charged proteins bound to LUVs with negatively charged lipids through electrostatic interaction. This was shown for influenza M1. M1 was mixed with LUVs made of phosphatidylcholine, cholesterol, and negatively charged phosphatidylserine. This mixture was then adjusted to high density with a high concentrated sucrose solution. Sucrose solutions of lower concentrations were overlaid to form a gradient with the LUV-M1 mix at the bottom. Centrifugation was performed. M1 could be detected in the fractions from the low density region of the gradient [84]. It was not detected in the low density fractions when 500 mM NaCl, an inhibitor for

electrostatic interactions [131], was added to the initial LUV-M1 mix [27]. Thus, flotation with LUVs is a convenient method to analyze the parameters (like certain lipids as binding partners) that influence M1's membrane interaction.

GUVs are suitable for microscopic methods. They can be produced via induced electro-swelling from surface-attached preformed membranes [132,133]. These micrometer sized vesicles allow direct visualization of protein binding to membranes under the chosen experimental conditions. Suitable dyes for labeling both proteins and membranes are required for this purpose. During the last decades a plethora of fluorescent lipid analogues has been developed for membrane labeling [134]. Usually, they can be added directly to the mixture of the desired lipids in low concentrations (less than 1% of the total amount of lipids) and give well detectable signals [135]. Two strategies can be applied for protein labeling. The protein could be visualized via antibodies which carry a dye [136] or the dye is attached to the protein. A short tetracysteine stretch could be genetically engineered to the protein of interest. These tetracysteine motif was then specifically labeled by biarsenic dyes [137].

Another protein labeling method employs a chemical reaction between a reactive amino acid, for example lysine or cysteine, and the dye. A widely-used reaction couple is tetramethylrhodamine-6-maleimide and a cysteine of the protein [138].

2 Aims of this study

If M1 is a key organizer in the influenza assembly, it has to fulfill several functions. One of them is the binding to membranes. It is still elusive how this happens and whether specific lipids play a role in this process. Binding of M1 to liposomal membranes of different lipid compositions was investigated to address this question. The flotation assays as well as confocal fluorescence microscopy were chosen as methods for this analysis. Beside the affinity test to validate potential lipid specificity, structural information needs to be recorded. Nothing is known about the intraprotein dynamics upon membrane binding. CD spectroscopy offers the possibility for monitoring molecular rearrangements in presence of membrane material.

Secondary structure and membrane association of genetically engineered mutants were analyzed and compared with the wild type M1 to characterize the domain structure of M1 and domain specific function. Essentially, two questions can be answered by using such mutants. First, deletion mutants may unravel the location of membrane binding site(s) in M1. Second, site directed mutations in the PBS permit the elucidation of whether this sequence plays a significant role at the molecular level of the membrane interaction of the N-terminal M1 domain. Furthermore, it is possible to validate the molecular rearrangements of these mutants in comparison to the wild type. It may be possible to locate where molecular interactions take place. For instance, when rearrangements could only be detected in a deletion mutant lacking the N-terminal part but not in a mutant without the C-terminal part, the C-terminus of M1 could be identified as putative membrane interaction site of M1.

It is possible to study membrane association and lateral dynamics of M1 in real time by using GUVs of distinct composition as target membranes. Standard and confocal fluorescence microscopes and respective techniques, e.g. fluorescence recovery after photobleaching provide the technical and methodological equipment to monitor a possible self-oligomerization of the protein on membranes. Indeed, an M1-M1 interaction was proposed as the driving force for enrichment of all viral components at the assembly site in the plasma membrane.

Deeper insights into M1's function during the assembly of the influenza particle can be achieved when the lipid specificity, the membrane binding site and the lateral organization of M1 on the membrane are elucidated.

3 Materials and Methods

3.1 Instruments

AMINCO-Bowman Series 2 – Luminescence spectrometer (Thermo – Fisher Scientific, Schwerte, Germany)

Biophotometer plus (Eppendorf, Hamburg, Germany)

CD Spectrometer J-720 (Jasco, Gross-Umstadt, Germany)

Centrifuge Avanti J-20XP (Rotors JA 25.50 and JLA 10.500) (Beckmann Coulter, Krefeld, Germany)

Confocal microscope IX81 with FluoView-1000 scan head (Olympus, Tokyo, Japan)

Fluorescence microscope X100 (Olympus, Tokyo, Japan)

FluoroMax-4 (Horiba Yobin Yvon, Unterhaching, Germany)

FluoStar Optima (BMG Labtechnologies, Offenburg, Germany)

FUJIFILM FLA-3000 (Fujifilm, Düsseldorf, Germany)

Osmometer type 6 (Löser Messtechnik, Berlin, Germany)

Semi-Dry transfer cell “TransBlot SD” (Bio-Rad, Munich, Germany)

Thermal Cycler “MyCycler” (Bio-Rad, Munich, Germany)

Ultracentrifuge Optima L-100K (Rotors 45Ti, 70.1Ti, SW40Ti, SW60) (Beckmann Coulter, Krefeld, Germany)

Ultracentrifuge TL-100 (Beckmann Coulter, Krefeld, Germany)

UV-Vis Spectrometer Lambda 40 (Perkin Elmer Instruments, Waltham, USA)

Zetazizer Nano (Malvern, Herrenberg, Germany)

3.2 Materials

3.2.1 Enzymes, antibodies, kits, and other "ready-to-use" tools

Calf intestine phosphatase, T4 DNA ligase, Restrictionenzymes: DpnI, NdeI, XhoI (Fermentas, St. Leon-Rot, Germany)

Taq DNA polymerase (supplied with 10x PCR buffer) (Qiagen, Hilden, Germany or Peqlab, Erlangen, Germany)

Phusion™ DNA Polymerase Kit (supplied with 5x HF PCR buffer) (Finnzymes, Espoo, Finland)

QIAprep Spin Miniprep Kit, QIAquick Gel Extraction Kit (Qiagen, Hilden, Germany)

IgG from goat anti M1, IgG from goat anti H3N2 (Virostat, Portland (Ma), USA)

IgG from donkey anti goat, horseradish peroxidase conjugated (Santa Cruz Biotechnology, Heidelberg, Germany)

ECL™-Kit = Amersham ECL™ Advanced Western Blotting Detection Kit (GE Healthcare Life Science, München, Germany)

Micro BCA Protein Assay Kit (PIERCE, Rockford, USA)

Apoptest™ -*FITC* Kit, #A700 (VPS Diagnostics, Hoeven, Netherlands)

PIP Strips™ (Echelon Biosciences, Salt Lake City , USA)

3.2.2 Plasmids and Oligonucleotides

The plasmid pHH21-vM [139] was kindly provided by the group of PD Dr. Michael Veit (Free University, Berlin, Germany). pHH21-vM contains the viral genome fragment for M1 and M2. pET15b (Novagen – Merck, Darmstadt, Germany) was used as acceptor for all cloning procedures.

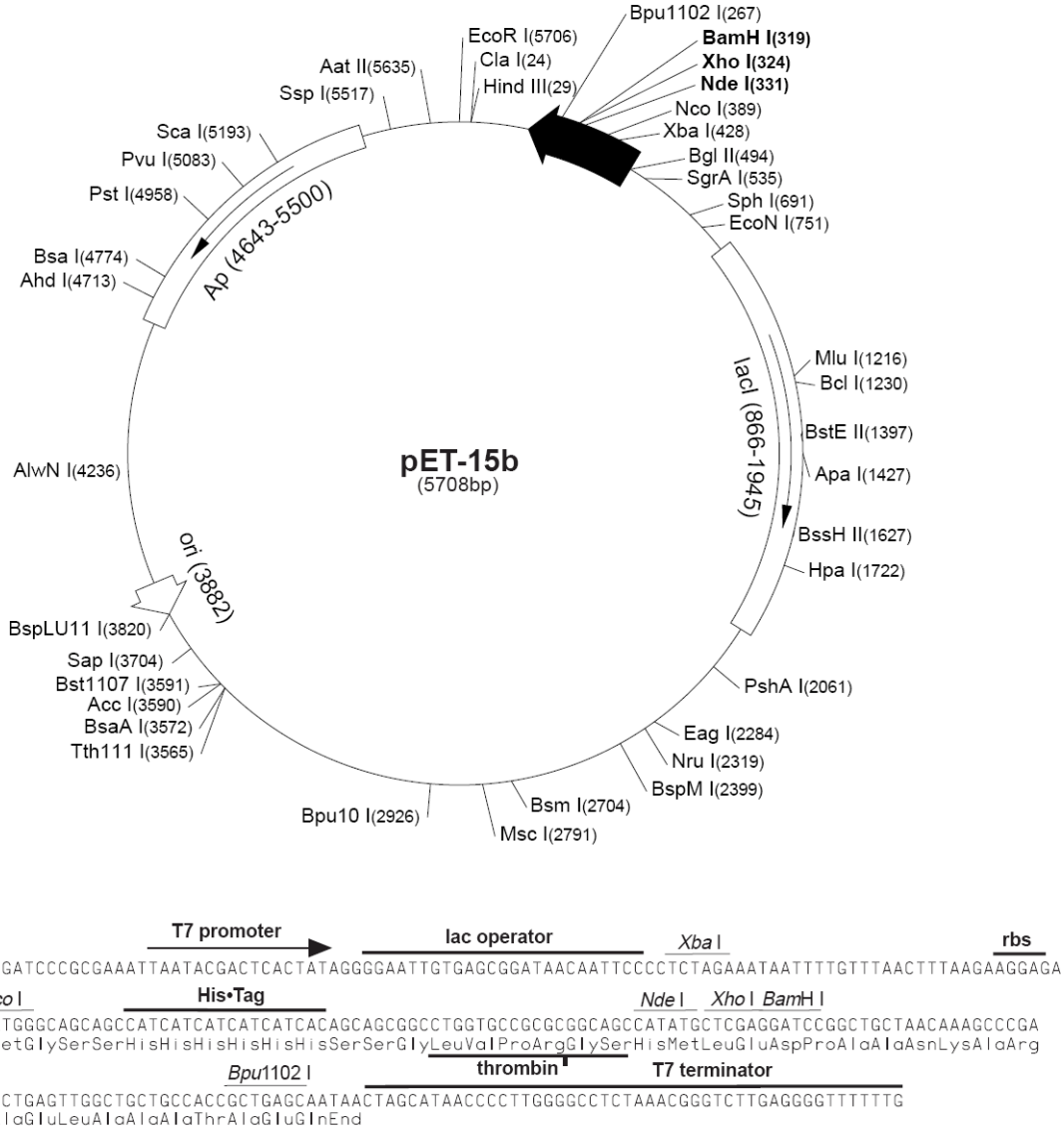

Figure 8 Map of the plasmid pET15b. The plasmid provides ampicillin resistance. It contains a lac operator for IPTG inducible protein expression behind the T7 promoter. The multiple cloning site includes a thrombin restriction site and the coding sequence for an His-tag. Open reading frames of proteins for recombinant expression were cloned between the restriction sites of NdeI and XhoI. The serine prior the NdeI restriction site was mutated to cysteine for CM1 labeling with fluorophors.

All PCR oligonucleotides listed below are shown in 5' – 3' orientation and were ordered from Invitrogen (Karlsruhe, Germany) in desalted purity. The final oligonucleotide concentration in the PCR mixture was 0.4 µM.

M1-NdeI-fw1	GGGAATTCCATATGAGTCTTCTAACCGAGGTTG (NdeI)
M1-XhoI-rev1	CCGCTCGAGTCACTTGAATCGTTGC (XhoI)
M1-fw	GACCACAGAGGTGGCATTTG
M1-rev	TCCCATCCGTTTCTGGTAGG
NP-fw	AAGAGCCCTTGTGCGTACTG
NP-rev	GCTCGTTGTGCTGCTGTTTG
M1-1-fw	GCCGTCAAACTATACGCGGCGTTGGCAGCTGAGATAACATTCTATGG
M1-1-rev	CCATAGAATGTTATCTCAGCTGCCAACGCCGCGTATAGTTTGACGGC
M1-2-fw	CCAAATAACATGGATGCAGCCGTCGCACTATACGCGGCGTTGGCAGC
M1-2-rev	GCTGCCAACGCCGCGTATAGTGCGACGGCTGCATCCATGTTATTTGG
NM1rev1	CCGCTCGAGTCACTGTCTGTGAGACCGATGC (XhoI)
CM1-for	GGGAATTCCATATGGTGGCTACCACCAATCC (NdeI)
M1Cy	GGTGCCGCGCGGCAGCCATATGTGTCTTCTAACCG
M1Cy rev	CGGTTAGAAGACACATATGGCTGCCGCGCGGCACC
CM1Cys	GGTGCCGCGCGGCTGCCATATGGTGGCTACCACC
CM1Cys–rev	GGTGGTAGCCACCATATGGCAGCCGCGCGGCACC
T7-promotor	TAATACGACTCACTATAGGG
T7-terminator	GCTAGTTATTGCTCAGCGG

3.2.3 Bacteria and culture media

DH5α (*E. coli*)	*F-, endA1, recA1, hsdR17 (rk- mk+), supE44, λ-, thi-1, gyrA(Na1), relA1, Φ80 lacZΔM15Δ (lacZY A-argF)*
Rosetta (*E. coli*)	*F–, ompT, hsdS$_B$ (r$_B$–, m$_B$–), dcm, gal, lacY1, λ (DE3), pLysS (Cm^R)*
BL 21 (*E. coli*)	*F–, ompT, hsdS$_B$ (r$_B$–, m$_B$–), dcm, gal, λ(DE3)*
LB + Amp	1 % [w/v] Bacto™ Tryptone; 0,5 % [w/v] Bacto™ Yeast Extract; 0,5 % [w/v] NaCl; 50 µg/ml Ampicillin in ddH2O
LB + Amp + Cm	LB + Amp + 50 µg/ml Chloramphenicol
Agar plates for DH5α	1 % [w/v] Bacto™ Tryptone; 0,5 % [w/v] Bacto™ Yeast Extract; 0,5 % [w/v] NaCl; 1,5 % [w/v] Agar; 50 µg/ml Ampicillin in ddH2O
Agar plates for Rosetta	1 % [w/v] Bacto™ Tryptone; 0,5 % [w/v] Bacto™ Yeast Extract; 0,5 % [w/v] NaCl; 1,5 % [w/v] Bacto Agar™; 50 µg/ml Ampicillin; 50 µg/ml Chloramphenicol in ddH2O
LB+G	1 % [w/v] Bacto™ Tryptone; 0,5 % [w/v] Bacto™ Yeast Extract; 0,5 % [w/v] NaCl; 50 µg/ml Ampicillin; 50 µg/ml Chloramphenicol; 0,4 % [w/v] Glucose in ddH2O

Bacto™ Tryptone, Bacto™ Yeast Extract, and Bacto Agar™ were ordered from BD (Becton, Dickinson and Company, Heidelberg, Germany). Ampicillin and Chloramphenicol were purchased from Sigma Aldrich (Taufkirchen, Germany) and Serva (Heidelberg, Germany). Sodium chloride was of analytical reagent grade. Glycerol for freezing of bacteria was delivered by Roth (Karlsruhe, Germany).

3.2.4 Buffers

All used chemicals in buffers were purchased in analytical reagent grade.

3.2.4.1 Buffers for protein purification

Lyses buffer	50 mM sodium phosphate; 250 mM NaCl; 10 mM EDTA, 20 mM DTT; pH 7.0 + 16 µg/ml DNase I; 300 µg/ml lysozyme; 1 mM PMSF was added shortly before use

Washing buffer	1 mg/ml desoxycholate; 20 mM DTT; 1 mM EDTA, pH 7.0; 0.2 mg/ml lysozyme was added directly before use
Unfolding buffer	100 mM sodium phosphate; 1 mM EDTA; 6 M guanidine hydrochloride; 50 mM reduced glutathione; pH 7.0
Refolding buffer	100 mM sodium phosphate; 1 mM EDTA; 0.5 mM oxidized glutathione; pH 7.5
Binding buffer	10 mM sodium phosphate, 120 potassium chloride, 20 mM imidazole, pH 7
Elution buffer	10 mM sodium phosphate, 120 mM potassium chloride, 250 - 500 mM imidazole; pH 7.0
NaP buffer	10 mM sodium phosphate; pH 7.0
NaPKCl buffer	10 mM sodium phosphate; 120 mM KCl; pH 7.0
Mops buffer	10 mM MOPS; pH 7.0 (KOH)

3.2.4.2 Buffers for SDS-PAGE, Coomassie-staining, and silver staining

4x non-reducing sample buffer	5 % [w/v] SDS; 0.05 % [w/v] bromine phenol blue; 25 % [v/v] glycerol; 12.5 % [v/v] 1M Tris/HCl buffer pH 6.8
4x reducing sample buffer	= 4x non-reducing sample buffer + 25 % [v/v] β-mercaptoethanol
1x running buffer	192 mM glycine; 25 mM Tris; 3.5 mM SDS

Table 1 Composition of stacking and separating gel

Components for 2 SDS-gels	**5 % Stacking gel**	**12 % Stacking gel**	**15 % Stacking gel**
ddH_2O	1.7 ml	3.3 ml	2.3 ml
30 % Acrylamide / Bisacrylamide ("Rotiphorese Gel 30" Roth, Karlsruhe, Germany)	0.5 ml	4.0 ml	5.0 ml
0.5 M Tris/HCl; pH 6.8	0.75 ml		
1.5 M Tris/HCl; pH 8.8		2.5 ml	2.5 ml
10 % SDS [w/v]	30 µl	100 µl	100 µl
10 % APS	30 µl	100 µl	100 µl
TEMED	3 µl	4 µl	4 µl

Coomassie staining solution	0.25 % [w/v] Coomassie Brilliant Blue R – 250, 45 % [v/v] ethanol, 10 % [v/v] acetic acid
washing solution	40 % [v/v] Ethanol, 7.5 % [v/v] acetic acid or 50 % [v/v] methanol; 10 % [v/v] acetic acid
Fixation solution	30 % [v/v] ethanol, 10 % [v/v] acetic acid
Cross-linking solution	30 % [v/v] ethanol, 0.5 % [v/v] glutaraldehyde, 0.2 % [w/v] sodium thiosulfate, 0.5 M sodium acetate
Silver solution	0.1 % [w/v] silver nitrate, 0.02 % formaldehyde
Developer	2.5 % [w/v] sodium carbonate, 0.01 % formaldehyde
Stop solution	0.05 M EDTA

3.2.4.3 Materials for preparation of large unilamellar vesicles (LUV)

The lipids 1,2-dioleoyl-*sn*-glycero-3-phosphocholine (DOPC), 1,2-dioleoyl-*sn*-glycero-3-phospho-L-serine (DOPS), 1,2-dioleoyl-*sn*-glycero-3-phosphoethanolamine (DOPE), 1,2-dioleoyl-*sn*-glycero-3-phosphate (DOPA), L-α-phosphatidylinositol-4-phosphate (PI4P), N-palmitoyl-D-*erythro*-sphingosylphosphorylcholine (SM), 1,2-dipalmitoyl-*sn*-glycero-3-phosphoethanolamine-N-(7-nitro-2-1,3-benzoxadiazol-4-yl) (N-NBD-DPPE), 1-oleoyl-2-6-[(7-nitro-2-1,3-benzoxadiazol-4-yl)amino]hexanoyl-*sn*-glycero-3-phosphocholine (C_6-NBD-PC), 1-oleoyl-2-6-[(7-nitro-2-1,3-benzoxadiazol-4-yl)amino]hexanoyl-*sn*-glycero-3-phosphoserine (C_6-NBD-PS), and 1,2-dioleoyl-*sn*-glycero-3-phosphoethanolamine-N-(lissamine rhodamine B sulfonyl) (LR-DOPE) were from Avanti Polar Lipids (Alabaster (Al), USA). Cholesterol (Chol), Dipalmitoyl-L-α-phosphatidylinositol-3-phosphate (PI4P), and Dipalmitoyl-L-α-phosphatidylinositol-4-phosphate (PI3P) were from Sigma Aldrich (Taufkirchen, Germany). 1,2-dioleoyl-*sn*-glycero-3-phosphoglycerol (DOPG) was ordered from Fluka (Buchs, Switzerland). The LUVs were produced in NaP, NaPKCl, NaP with 400 mM KCl or Mops buffer.

3.2.4.4 Flotation assay buffers

25 % Sucrose buffer	25 % [w/v] Sucrose in NaP or NaPKCl or NaP buffer with 400 mM KCl
75 % Sucrose buffer	75 % [w/v] Sucrose in NaP or NaPKCl or NaP buffer with 400 mM KCl

3.2.4.5 Buffers for PIP™ strips

TBST or TBS	10 mM Tris, 150 mM NaCl, pH 8.0, 0.1 % [v/v] Tween-20
TBST+BSA or TBS+BSA	10 mM Tris, 150 mM NaCl, pH 8.0, 3 % [w/v] fatty acid free BSA (Sigma-Aldrich) - (0.1 % [v/v] Tween-20) in TBST+BSA

3.2.4.6 Solutions for labeling of proteins

FM solution	2 mM fluorescein-5-maleimide (Invitrogen) in NaPKCl
TMR solution	0.5 mM 5/6-carboxy-tetramethylrhodamine ethyl-maleimide (emp Biotech GmbH, Berlin, Germany) in DMSO

3.2.4.7 Materials and buffers for GUV preparation and microscopy

The lipids DOPC, DOPS, 1,2-dioleoyl-*sn*-glycero-3-phosphate (DOPA), N-NBD-DPPE, C_6-NBD-PC, C_6-NBD-PS, Chol, PI4P, and PI3P were from Sigma Aldrich. 1,2-dioleoyl-*sn*-glycero-3-phosphoglycerol (DOPG) was ordered from Fluka (Buchs, Switzerland). The GUVs were produced in swelling buffer.

Swelling was carried out either on titanium slides or on indium tin oxide coated glass slides.

Swelling buffer	250 mM sucrose + 15 mM NaN_3, adjusted to 280 mosm
Microscopy buffer	5.8 mM NaH_2PO_4, 5.8 mM Na_2HPO_4, 250 mM glucose (300 mosm)
1x binding buffer	10 mM Hepes, 150 mM NaCl, 5 mM KCl, 1 mM $MgCl_2$, 1.8 mM $CaCl_2$ (part of the APOPTEST™-*FITC* Kit - VPS Diagnostics, Doeven, NL)

3.3 Methods

3.3.1 Cloning of M1

The M1 open reading frame was amplified in a standard PCR with Phusion DNA polymerase from the pHH21vM [139] with the oligonucleotides *M1-NdeI-fw1* and *M1-XhoI-rev1*. These oligonucleotides provided the restrictions sites for NdeI and XhoI in 3' and 5' overhanging sequences. The reaction condition in the 20 µl sample were 30 s at 98 °C initial denaturation, 30 cycles with 10 s denaturation at 98 °C followed by 45 s at a oligonucleotide melting tem-

perature (T_m) of 59 °C and 30 s at 72 °C extension, final extension step for 10 min at 72 °C and cooling to 4 °C until the sample was removed from the cycler. The fragments were doubly digested directly after amplification (5 u NdeI in buffer O for 2 h at 37 °C and after addition of 10 u XhoI another 2 h at 37 °C, volume 20 µl). The acceptor vector pET15b was digested in parallel and dephosphorylated. Purification of the fragments and vector occurred after gel electrophoresis using the QIAquick Gel Extraction Kit (Qiagen, Hilden, Germany). The M1 fragments were inserted into pET15b using T4 DNA ligase according to the manufacturer's manual. The resulting plasmid was named pET15b-M1. Five µl of the ligation were transfected into 50 µl chemical competent DH5α cells and they were cultivated on ampicillin plates. A part from one growing clone was added to a 25 µl Taq polymerase containing colony PCR mixture with the oligonucleotides *M1-fw* and *M1-rev* for M1 sequence detection and amplified (15 min at 95 °C, 25 cycles with 30 s at 95 °C + 45 s at T_m = 50 °C + 1 min at 72 °C, 10 min at 72 °C and cooling to 4 °C). Bacteria clones that contained the sequences of interest were cultured overnight and plasmids were purified with the QIAprep Spin Miniprep Kit (Qiagen, Hilden, Germany) and sent for sequencing (SMB – Services in Molecular Biology, Berlin, Germany). All plasmids were sequenced between the T7 promoter and T7 terminator region of pET15b using the *T7 promoter* + *T7 terminator* oligonucleotides. For long term storage 30 % glycerol [v/v] was mixed into the bacteria culture and frozen at -80 °C.

3.3.2 Cloning of the mutants M1m, NM1, NM1m, and CM1

For site-directed mutagenesis of the polybasic sequence (PBS) in M1 a double overlap extension PCR [140] approach was performed with Phusion polymerase. The principle of this method is based on a complementary oligonucleotide couple which carries the mutation (*M1-1-fw* + *M1-1-rev*, *M1-2-fw* + *M1-2-rev*) and two the fragment defining primers (*M1-NdeI-fw1* + *M1-XhoI-rev1*).

The first fragment amplification from pET15-M1 occurred in three parts. A PCR with *M1-NdeI-fw1* together with *M1-1-rev* amplified the 5' part of the fragment (T_m = 59 °C). In a parallel reaction the 3' part was amplified with *M1-1-fw* and *M1-XhoI-rev1*. The two fragments were analyzed electrophoretically, purified, mixed in equal volumes of the purified solution and used in a third subsequent PCR reaction containing only *M1-NdeI-fw1* + *M1-XhoI-rev1*. The resulting product functioned as matrix for amplification of the second mutagenesis step. This time *M1-NdeI-fw1* + *M1-2-rev* and *M1-2-fw* + *M1-XhoI-rev1*were used. The final PCR

product was digested with NdeI and XhoI as mentioned before, purified and ligated into pET15b. The resulting plasmid was named pET15b-M1m, transfected and checked via colony PCR with *M1-fw* and *M1-rev* (T_m = 50 °C).

The sequences of the N-terminal deletion mutants NM1 and NM1m with mutated PBS were amplified with *M1-NdeI-fw1* and *NM1rev1* from the plasmids pET15b-M1 for NM1 and pET15bM1m for NM1m (T_m = 59 °C) and cloned into pET15b giving the plasmids pET15b-NM1 and pET15b-NM1m.

The oligonucleotides for the C-terminal deletion mutant CM1 coded on the final plasmid pET15b-CM1 were *CM1-for* and *M1-XhoI-rev1* and used as described above.

3.3.3 Cloning of an additional cysteine into M1, M1m, NM1, NM1m, and CM1

For incorporation of an additional cysteine via S2C substitution into the open reading frames for M1, M1m, NM1, and NM1m, the oligonucleotides listed below were used in a quick change PCR reaction. This method was adapted from a procedure developed by Stratagene [141]. The plasmids pET15b-M1, pET15b-M1m, pET15b-NM1, and pET15b-NM1m functioned as matrices. These plasmids were amplified in a single PCR with the complementary mutagenesis oligonucleotides *M1Cy* and *M1Cy rev*. CM1 has no cysteine in its open reading frame. The serine located two amino acids ahead in the N-terminal overhang was therefore converted to cysteine in the plasmid pET15b-CM1 with *CM1Cys* and *CM1Cys-rev*. The plasmids with S→C conversion were named pET15b-M1-Cy, pET15b-M1m-Cy, pET15b-NM1-Cy, pET15b-NM1m-Cy and pET15b-CM1-Cys. Oligonucleotides, which did not define a fragment as it is the case in standard PCR, were the basis for this method. Here they in fact function as the origin for undetermined amplification with Phusion polymerase in both directions (30 s at 98 °C; 16 cycles with 10 s at 98 °C, 15 s at 69 °C and 3 min at 72 °C; 10min at 72 °C and cooling to 4 °C). To prevent transformation of non-mutagenized plasmids, the original methylated plasmid DNA was digested with DpnI (45 min, 37 °C, 1x buffer tango) and the remaining plasmids were transformed into DH5α cells. Selected clones were analyzed by colony PCR. The purified plasmids were sequenced, and stored at -20 °C

3.3.4 Expression of M1 and its mutants

For expression of the cloned proteins the respective plasmids were transformed into chemical competent *E. coli* BL21 or Rosetta cells. Several conditions were tested for the expression

optimum. The most efficient expression took place when cells were inoculated in 250 ml up to one liter LB+G medium in Erlenmeyer flasks to an optical density (OD_{600}) of 0.1 at 600 nm and precultivated until an OD_{600} of 0.7 ± 0.05 was achieved. Then protein production was induced with 0.1 – 1 mM IPTG for 3 h at 37 °C with rotational shaking at 200 rpm. Protein production was analyzed by SDS-PAGE of 18 µl bacteria lysates pre- and post-induction. For this purpose 1 ml culture was centrifuged (1 min at 10,000 x*g*) immediately and 3 h after induction. The optical densitiy of the culture was measured parallel to centrifugation. The supernatant was discarded and the pelleted cells were resuspended in ddH_2O. The volume of water was calculated using the following correlation: volume H_2O [µl] = OD_{600} · 100. The samples were frozen to -20 °C before gel separation.

3.3.5 Purification of M1 and the mutants

The protein expressing culture was centrifuged (10 min, 10000 rpm with JLA 25.50 rotor in the Avanti centrifuge, 4 °C). The pelleted cells were resuspended in lyses buffer (10 ml per litre original culture volume) and frozen to -80 °C. After thawing the volume was doubled with lyses buffer. Lysozyme and DNase I were added to final concentrations of 0.3 and 0.016 mg/ml. The suspension was shaken for 1 h on ice. The cells were lysed by ultrasonification. Cell debris and inclusion bodies were pelleted through centrifugation (20 min, 20000 rpm with JA 10.500 rotor in the Avanti centrifuge, 4 °C). M1, M1m, NM1, and NM1 as well as their homologues with additional cysteine were purified from pelleted inclusion bodies. The protocol is described in Chapter 3.3.5.1. Soluble CM1 was purified from the supernatant of bacterial lysates. Details can be found in Chapter 3.3.5.2. A summary scheme for the cloned proteins is presented in the Results section (see Figure 20).

3.3.5.1 Purification from inclusion bodies

To purify the proteins from inclusion bodies washing buffer with 0.2 mg/ml lysozyme (16 ml per 1 litre original culture volume) was added to the lysed cell pellet. The pellet was disrupted by stirring to flakes with a glass rod and centrifuged (20 min, 20,000 rpm with JA 10.500 rotor in the Avanti centrifuge, 4 °C). This procedure was repeated three times with washing buffer, thrice with lyses buffer containing 20 mM DTT and one final washing step with water to remove DTT. The washed inclusion bodies were dissolved with degassed unfolding buffer for 1 h at room temperature. Native protein was refolded by dilution of the solution with re-

folding buffer to the nine fold volume and incubated overnight at 4 °C. It was further purified as described in the next subchapter.

3.3.5.2 Purification of soluble proteins

The supernatant after lysate centrifugation (for CM1 purification) or the refolded solution (for purification of the other proteins) contained soluble protein. Four ml of this liquid were incubated with 1 ml Ni-NTA-agarose beads (Qiagen, Hilden, Germany) for 1 h at 4 °C. The mixture was placed onto polypropylene columns (Qiagen) with sealed exit. The agarose beads were allowed to form a homogeneous matrix. After opening of the outlet unbound protein was removed. Agarose with bound protein was washed twice with 4 ml of binding buffer. Elution buffer was added and eluted protein was collected in 0.5 ml fractions. Eighteen µl were analyzed by SDS-PAGE. Protein-rich fractions were pooled to 2.5 ml final volume and buffer exchange to NaP, NaPKCl or Mops buffer was performed on NAP™-25 columns (GE Healthcare Life Sciences, Freiburg, Germany) according to the manufacturer's manual. The protein concentration [µM] in the fractions was estimated by absorption measurement at 280 nm (A_{280}) using the Lambert-Beer and the extinction coefficients and molecular weights listed in Table 2 and equation (1). Extinction coefficients and molecular weight calculations were performed on the ORF of M1 and on the mutants including the N-terminal overhang with the His-tag using the ProtParam tool on the ExPASy Proteomics Server [142]. Samples were diluted in case the measured A_{280} exceeded a value of 0.8.

Table 2: Extinction coefficients for M1 and the mutants. Extinction coefficient and molecular weight of M1 and the mutants including the N-terminal His-tag were calculated using ProtParam. ProtParam can be found on the ExPASy Proteomics Server [142].

Protein	**Extinction coefficient [M^{-1} cm^{-1}]**	**Molecular weight [g/mol]**
M1 / M1-Cy	14502.5 / 14565	30088.6 / 30104.6
M1m / M1m-Cy	14502.5 / 14565	29690 / 29706
NM1 / NM1-Cy	13012.5 / 13075	20391.4 / 20407.5
NM1m / NM1m-Cy	13012.5 / 13075	19992.8 / 20008.9
CM1 / CM1-Cys	1490 / 1490	11878.5 / 11894.5

$$c = \frac{A_{280}}{\varepsilon_P} \cdot 10^6 \cdot DF \qquad (1)$$

c = protein concentration in µM

ε_P = extinction coefficient

DF = dilution factor

3.3.6 SDS-PAGE

Polyacrylamide gel electrophoresis (PAGE) in presence of sodium dodecyl sulfate (SDS) was performed for size-dependent separation of proteins according to Laemmli [143] in 1x running buffer. The Mini-PROTEAN 3 system with a PowerPac 1000 (Bio-Rad, Munich, Germany) was used for gel casting and electrophoresis. The sample for separation was mixed with 4x reducing sample buffer for reducing conditions or 4x non-reducing sample buffer for non-reducing conditions in a ratio of 3:1 to a final volume of 20 – 25 µl, boiled for 5 min at 95 °C, and centrifuged for 1 min at 10,000 x g. The supernatant was applied to the stacking gel using a Hamilton syringe. Electrophoresis ran for 40 min at 200 V. In case that the sample contained fluorescently labeled proteins or lipids, the glass plate stack including the gel was scanned for fluorescence with the FUJIFILM FLA-3000 (Fujifilm, Düsseldorf, Germany). The gels were afterwards removed and stained for protein using direct immersion in Coomassie staining solution. To remove background staining in Coomassie stained gels, these gels were rinsed in washing solution for at least 2 h. A silver staining procedure was used for protein amounts below the resolution of the Coomassie staining. Therefore the gels were first rinsed in fixation solution for 30 min, changed to cross-linking solution for another 30 min, washed thrice in ddH_2O, and stained with silver solution. The gels were washed shortly in ddH_2O prior to application of developer and incubation until proteins were visible and subsequently rinsed in stop solution. For long term storage gels were dried between cellophane films using a vacuum Gel Dryer 543 (Bio-Rad, Munich, Germany).

3.3.7 Preparation of large unilamellar vesicles (LUVs)

Large unilamellar vesicles were produced according to a published method [127,128]. In brief, lipids were mixed in solvent, and the solvent was evaporated under N_2 flow or vacuum until a dry film developed. NaP, NaPKCl, NaP with 400 mM KCl, or Mops buffer were added in the respective volume to reach the aimed concentration of lipids in solution. The suspension was homogenised by vigorous vortex motion. Five freeze-thaw cycles (-80 to 50 °C) followed to form multilamellar vesicles. The suspension was extruded 10 times through polycarbonate filters with 100 nm pore size (Millipore, Schwalbach Ts., Germany) under nitrogen atmosphere with a pressure between 10 to 30 bar at 50 °C or through a mini extruder (Avanti Polar Lipids, Alabaster (Al), USA) at room temperature. Lipid concentration was determined indirectly by measuring absorption spectra of the incorporated fluorescent lipids between 400

and 600 nm in a 1:10 dilution of the LUV suspension in methanol. The concentration of fluorescent lipids was calculated using the Lambert-Beer law from the absorption of N-NBD-DPPE at 463 nm and an extinction coefficient of 21000 M^{-1} cm^{-1} [144]. Lissamine Rhodamine DOPE was measured at 560 nm and ε = 75000 M^{-1} cm^{-1} [144] was used for concentration calculations. Fluorescent lipids were incorporated either as 1.5, 1, or 0.2 % of the total molar amount of lipids. From this ratio the final lipid concentration was derived.

3.3.8 Cryo- and transmission electron microscopy of purified M1 and LUVs

M1 (2.8 µM) in 10 mM Mops buffer was diluted 1:5 and 1:20 in Mops buffer. All three samples were negative stained for analysis by transmission electron microscopy. Negative staining was performed as follows. Grids (Quantifoil ® R 3/3, Quantifoil µ tools, Jena, Germany) were incubated 30 s at 0.3 mbar in the plasma cleaner (Harrick Plasma, Ithaca, USA). The RF-Level was set to high. Samples (3.5 µl) were placed on the prepared grids for 45 s. The liquid was removed with a filter paper. Staining solution (3.5 µl, 2 % sodium phosphotungstate in water, pH 7.4) was applied to the grid for 15 s. The staining solution was removed with filter paper. Images were acquired with the transmission electron microscope CM 100 - 100 kV (Koninklijke Philips Electronics, Amsterdam, Netherlands).

LUVs and LUVs with M1 were analyzed in cryo-electron microscopy. LUVs with 2 mM lipid were prepared as described above in Mops buffer. The suspension was diluted 1:1 with Mops buffer or M1 solution. Chloroform-washed grids (Quantifoil® R1.2/1.3) were incubated 30 s at 0.3 mbar in a plasma cleaner (Harrick Plasma, Ithaca, USA) before sample application. The RF-Level was set to high. The grid was fixed to forceps and placed for the semi-automated freezing procedure into the Vitrobot (FEI, Hillsboro, USA). Samples (3.5 µl) were placed on the prepared grids for approximately 45 s. The remaining liquid was removed by blotting with filter paper. The sample was frozen in liquid ethane immediately after blotting and stored in liquid nitrogen until image acquisition. Imaging was performed with the Tecnai G2 Spirit 120 kV (FEI) equipped with a 2k eagle CD (FEI) utilizing a single tilt liquid nitrogen cryo transfer holder model 626 (Gatan, Pleasanton, USA) for the transfer of the sample into the beam.

Electron microscopy was kindly performed by Jörg Bürger in the group of Thorsten Mielke (Ultra structure network, Max Planck Institute for Molecular Genetics, Ihnestr. 73, 14195 Berlin, Germany).

3.3.9 Flotation assay

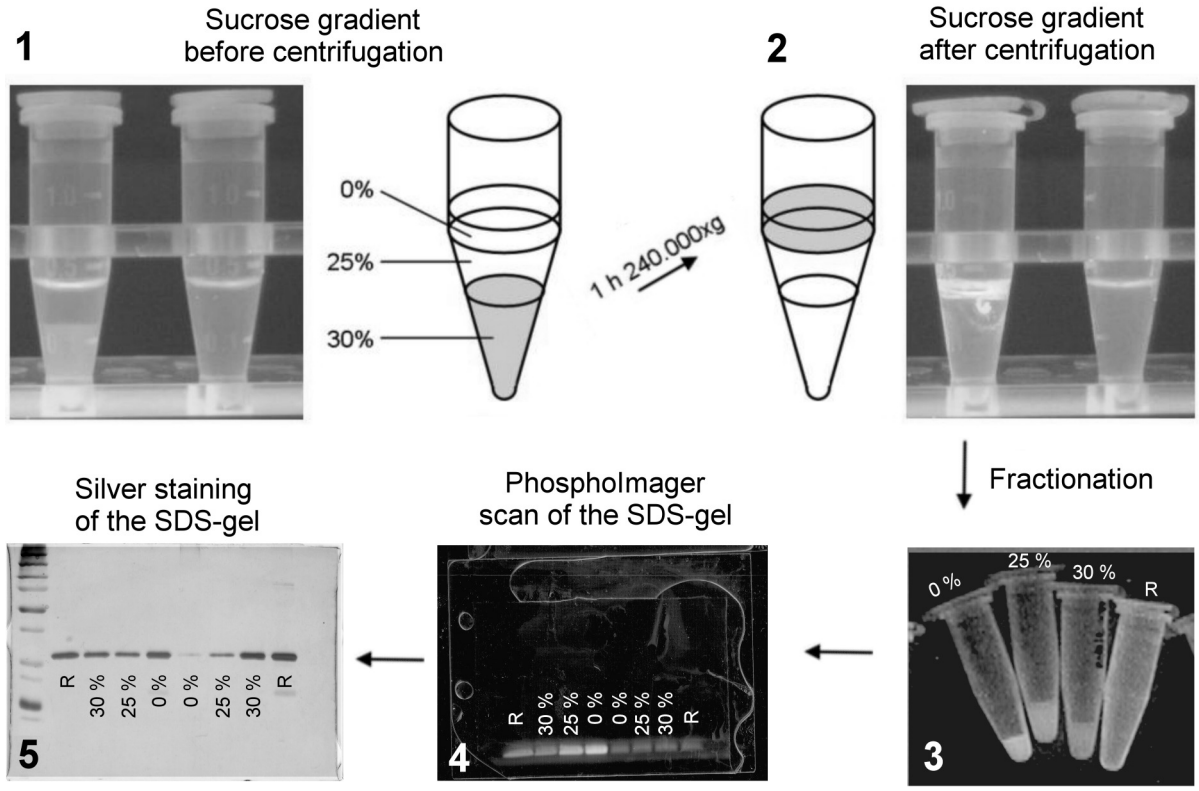

Figure 9 Flotation assay. (1) Sucrose gradients with and without LUVs. The left tube contained a gradient where NBD fluorescence can be seen in the 30 % sucrose fraction. The right tube did not contain vesicles. (2) The same sucrose gradients after centrifugation for 1 h at 240,000 x*g*. The NBD fluorescence was detected in the low density 0 % sucrose fraction of the gradient in the left tube. (3) Four samples were obtained after fractionation. 0 % = low density fraction, 25 % = fraction from the middle part of the gradient, 30 % = high density fraction from the bottom part of the gradient, R = water solubilized precipitates. These samples were size separated in SDS-PAGE. (4) PhosphoImager scan of the SDS-gel. Fluorescence of the lipid analogue N-NBD-DPPE was detected in the bottom line of the gel. Four samples (R, 0, 25, 30 %) of a gradient with LUVs (left side) and four samples (30, 25, 0 %, R) from a gradient without LUVs (right side) are shown here. (5) Silver staining of the same SDS-gel revealed the distribution of protein in the respective fractions.

The flotation method is based on a protocol developed by Bigay and colleagues [130,145]. In summary, purified protein in NaP or NaPKCl was mixed with the respective LUV suspension and buffer at room temperature to reach a final protein concentration of 1.5 µM and a final lipid concentration of 1 mM in 100 µl. 66.6 µl of 75 % sucrose buffer were added to adjust the solution to 30 % final sucrose concentration in the microfuge tube (Beckmann Coulter GmbH, Krefeld, Germany). 133 or 266 µl 25 % sucrose buffer were overlaid and 33 µl NaP or NaPKCl followed as final 0 % gradient step. The density gradient was centrifuged for 1 h at 4 °C in a TL-100 ultracentrifuge (Beckmann) at 240,000 x*g*. One 38 or 75 µl fraction was taken at room temperature from the top of the gradient. Three 38 or 75 µl fractions from the

middle part of the gradient followed, and one 165 µl fraction was taken from the bottom. The empty tube was washed with 50 µl ddH_2O with vigorous vortexing to remove pelleted precipitates. Aliquots of the fractions were size separated via SDS-PAGE. Gels were analyzed for fluorescence of the lipid analogues using the phosphoImager in fluorescence scan mode. The gels were silver stained to analyze the protein distribution.

3.3.10 PIP™ strips

Analysis of the interaction of M1 and its mutants with PIP™ strips (Echelon) was performed following the manufacturers manual. In brief, the PIP™ strip membrane was blocked in TBST+BSA or TBS+BSA for 1 h. M1 was diluted in TBST+BSA or TBS+BSA to a final concentration of 0.5 µg/ml. Incubation of the PIP™ strip with the protein took place for 2.5 h at 4 °C. The protein solution was removed and the membrane was washed three times in TBST+BSA or TBS+BSA. IgG from goat anti M1 (Virostat) was diluted 1:1000 in TBST+BSA or TBS-BSA and incubated with the membrane overnight at 4 °C. The membrane was washed three times in TBST+BSA or TBS+BSA. IgG from donkey anti goat (horseradish peroxidase conjugated, Santa Cruz Biotechnology, diluted 1:5000 in TBST or TBS) was added and incubated with the membrane for 1 h at room temperature. The membrane was washed three times in TBST or TBS. Signal detection was performed with the ECL-Kit (Amersham) according to the manufacturer's manual.

3.3.11 Circular dichroism measurements (CD)

Protein solutions in NaP, NaPKCl or Mops buffer were measured at concentrations between 2 and 10 µM in a quartz cuvette with 1 or 0.1 mm light path (Hellma, Mühlheim, Germany) in the CD spectrometer J-720 (Jasco, Gross-Umstadt, Germany) at 20 °C. Spectra from 5 – 9 accumulations were obtained between 185 and 260 nm without liposomes and between 205 and 260 nm with liposomes. The molar ratio between protein and lipids was 5 – 7 µM protein to 1.6 mM lipid.

$$\theta = \frac{\left(CD_{P(+L)} - CD_{B(+L)} - \text{offset}\right)}{d \cdot c \cdot N} \qquad (2)$$

Normalization of the spectra was conducted using equation (2) where θ is the normalized ellipticity in kdeg cm^2 $dmol^{-1}$, $CD_{P(+L)}$ the measured value for the protein ± liposomes, and $CD_{B(+L)}$ the measured value for buffer ± liposomes. The offset corresponds to the calculated

mean value from 258 to 260 nm, d to the light path length (1 mm or 0.1 mm), c is the protein concentration in µM, and N the number of amino acids in the protein. An UV spectrum between 200 and 340 nm was measured directly prior to CD acquisition to calculate the protein concentration. The protein concentration was computed according to Iersel *et al.* [146].

3.3.12 Measurement of dynamic light scattering (DLS)

Samples for DLS measurements were centrifuged 20 min at 36,000 xg. Forty µl were carefully pipetted under a constant air flow into the quartz cell (ZEN 2112 produced by Hellma, Mühlheim, Germany for Malvern Instruments, Herrenberg, Germany). The cuvette was sealed and inserted into the Zetasizer Nano ZS (Malvern), which was equilibrated for 2 min at 20 °C. LUV containing samples were measured three times with six 10 s long runs. Scattering profiles were fitted to hydrodynamic diameters applying the Size modus of the Zetasizer Software 6.01 (Malvern Instruments) taking solvent and temperature into account.

3.3.13 Fluorescent labeling of M1 and its mutants

FM solution was diluted in purified solutions of M1, M1m, NM1, NM1m, and CM1 in NaPKCl in a molar ratio of 1 FM : 1 protein. Protein concentration was determined as described in chapter 3.3.5. The mixture was incubated 30 min at room temperature. Unbound FM was removed by buffer exchange on NAP™-25 columns (GE). The amount of bound FM was derived from absorption measurements between 200 and 600 nm, calculating the protein concentration from the absorption at 280 nm (see 2.5.5) and the FM concentration from the absorption at 494 nm and ε_{494}^{FM} = 83000 M^{-1} cm^{-1} [144]. For labeling with TMR, proteins in 120 mM KF, 10 mM sodium phosphate, pH 7 were mixed with TMR solution to reach a ratio of protein to TMR of 1:1. The solution was incubated overnight at 4 °C and frozen to -80 °C until buffer exchange on NAP™-25 columns. The TMR amount was calculated with ε_{548}^{TMR} = 78000 M^{-1} cm^{-1}.

3.3.14 Measurement of Förster resonance energy transfer (FRET)

This method allows the analysis of local interactions between two molecules. Therefore a donor (D) fluorophor with an emission spectrum overlapping the excitation spectrum of an acceptor (A) fluorophor are used. This distance-dependent method allows estimations of the interaction probability of the two fluorophores and of the orientation of the fluorophores to

each other when the partners are well characterized (e.g. protein with a defined size on the membrane).

Samples for FRET measurements were prepared by mixing fluorescence donor and acceptor molecules in reaction vessels in a certain molar ratio (see Table 3). Incubation for at least 10 min followed. The mixture was pipetted into quartz glass fluorescence cuvettes (Hellma). Measurements were carried out using the AMINCO-Bowman Series 2 – Luminescence spectrometer (Thermo – Fisher Scientific, Schwerte, Germany) or the FluoroMax-4 (Horiba Yobin Yvon, Unterhaching, Germany). Energy transfer was measured between several different fluorescence donor and acceptor pairs (see table 3). For analysis of each FRET pair four spectra were recorded. First, a spectrum of the donor fluorophor emission was acquired in the wavelength interval [λ_{D1}–λ_{D2}] in absence of the acceptor. The donor fluorophor was excited at its excitation wavelength (λ_{ExD}). A buffer spectrum was recorded under same condition as second spectrum. The second spectrum was used for background correction of the first spectrum. Third, a spectrum of the donor fluorophor emission was acquired in the same interval [λ_{D1}-λ_{D2}] in presence of the acceptor to survey FRET events. Finally, a spectrum in the wavelengths [λ_{D1}–λ_{D2}] for unspecific acceptor excitation at the donor excitation wavelength (λ_{ExD}) was recorded in the absence of the donor fluorophor. The fourth spectrum was subtracted from the third spectrum for background correction. Fluorescence intensity was recorded in 1 nm steps for the different spectra.

Table 3: Donor and acceptor pairs for FRET measurements.

Fluorescence donor (c)	**Fluorescence acceptor (c)**	**λ_{ExD}**	**[λ_{D1}–λ_{D2}]**
Tryptophan of M1 (1.8 µM)	N-NBD-DPPE in LUVs (0.6 µM)	283 nm	300–550 nm
Tryptophan of Melittin (1.8 µM)	N-NBD-DPPE in LUVs (0.6 µM)	283 nm	300–550 nm
N-NBD-DPPE in LUVs (20 nM)	TMR labeled M1 and NM1 (22 nM)	469 nm	500–600 nm

Data procession for FRET between N-NDB-DPPE and TMR-M1 or TMR-NM1:

The fluorescence emission spectra for this FRET pair were recorded and corrected as described above (Figure 10 A and B) and processed as difference spectra. Normalization of the N-NBD-DPPE emission spectrum without TMR labeled protein was performed by setting the recorded fluorescence intensity of the N-NBD-DPPE emission maximum at 533 nm to 1. The same procedure was applied to the N-NBD-DPPE emission spectrum which was recorded when TMR was present (Figure 10 C and D). The normalized spectrum of N-NBD-DPPE

without TMR was then subtracted from the normalized N-NBD-DPPE spectrum in presence of TMR yielding a difference spectrum (Figure 10E).

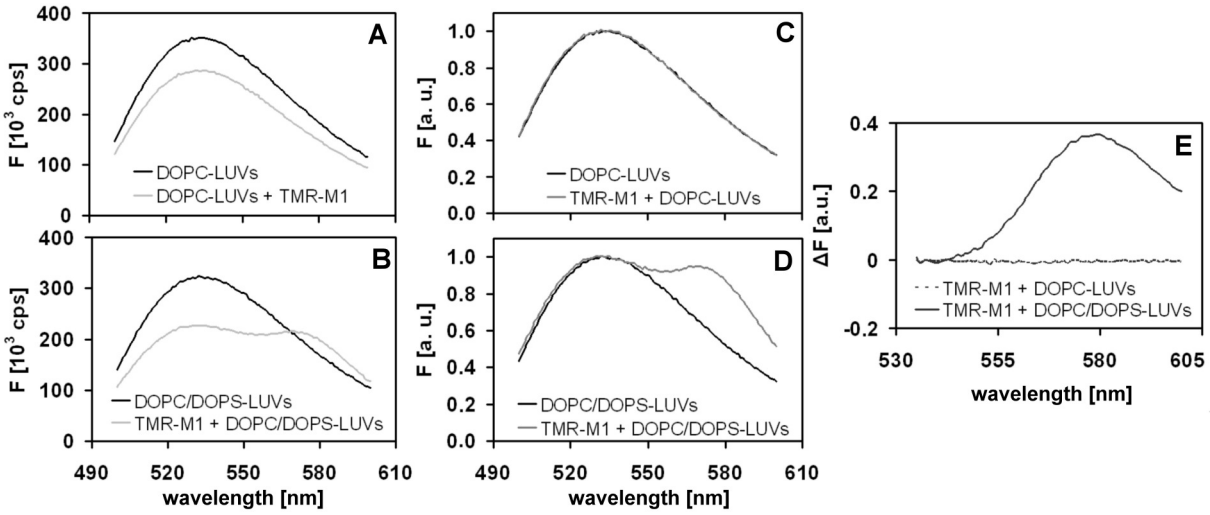

Figure 10 Data processing for N-NDB-DPPE in DOPC-LUVs or DOPC/DOPS-LUVs and TMR-M1. (A,B) Background corrected spectra of N-NBD-DPPE in absence (—) and in presence of TMR (—). (C,D) Normalized spectra. The intensity of the N-NBD-DPPE fluorescence emission at 533 was set to 1. The other intensity values of the spectrum were calculated using this correlation. (E) Difference spectra for the two FRET pairs. The normalized spectrum of N-NBD-DPPE was subtracted from the normalized spectrum of N-NBD-DPPE recorded in presence of TMR-M1.

3.3.15 Preparation of giant unilamellar vesicles (GUVs)

Giant unilamellar vesicles were prepared for microscopic visualization of protein-membrane interactions. Vesicles were produced by applying AC fields to hydrated lipid films on conducting surfaces [132,133,147,148].

In detail, 100 nmol lipids were mixed in chloroform in compositions suitable for the afterwards performed experiments. The liquid was spotted onto two heated (50 – 60 °C) glass slides coated with a conductive indium tin oxide (ITO) layer (Präzisions Glas & Optik, Iserlohn, Germany) or titanium plates. One of the titanium plates was shaped like a flat trough and a second functioned as lid. Removal of solvent traces was achieved by application of pressure below 10 mbar for at least 1 h. The ITO slides were assembled into a chamber by placing an insulating Teflon spacer between them and sealed with temperature stable plasticine. The rim of the titanium trough was laminated with parafilm at temperatures of 50 to 60 °C. Lipids in solvent were spotted and dried when titanium plates were used. Sealing of the titanium chamber was performed by a short heating pulse to 50 – 60 °C to the parafilm-lined plate and by pressing the lid onto it. The lipid films in the sealed chambers were hydrated

with swelling buffer and AC field application followed. An AC frequency of 10 Hz was applied. The voltage was raised stepwise (6 min per set voltage) from 20 mV to 1.1 V for at least three hours. Fission of GUV from the surface was induced by lowering the frequency to 4 Hz and changing the voltage to 1.3 V for at least half an hour.

3.3.16 Fluorescence microscopy

For examination of various samples two different microscopes were used. Standard fluorescence microscopy was performed with the inverted X100 fluorescence microscope (Olympus, Tokyo, Japan). Size bars were assigned to the images by the Metamorph (Olympus) software.

Confocal laser scanning fluorescence microscopy was carried out at the inverted IX81 fluorescence microscope (Olympus) equipped with a Fluoview 1000 scanning unit (Olympus) and a 60x oil immersion objective with a numerical aperture of 1.35. Beside phase contrast fluorescence images were recorded. NBD and FITC were excited with the 488 nm laser line of an Argon ion laser. Fluorescence was detected for NBD and FITC between 500 and 530 nm. TMR was excited with a 559 nm laser diode and the emission was recorded between 570 and 670 nm. Size bars were assigned to the images by the AS Viewer software (Olympus) that was calibrated to the camera and microscope setup.

For microscopic observation of GUVs, the vesicle solution in swelling buffer was diluted 50 to 100fold in microscopy buffer or in 1x binding buffer. Fifty µl of this dilution were placed on a cover slip (Roth). After settling of the GUVs, images were taken in the equatorial plane of the vesicle. For visualization of fluorescently labeled protein, the protein of interest was diluted in microscopy buffer or 1x binding buffer prior to addition of GUVs. Annexin V-FITC from the APOPTEST™-*FITC* kit (VPS Diagnostics, Doeven, Netherlands) was diluted 500fold and incubated for 10 min with the GUVs. TMR labeled M1 and NM1 were diluted in microscopy or 1x binding buffer to a final concentration of 0.1 µM, respectively. GUVs were added and the samples were examined after 30 min. TAMRA labeled α-Synuclein (kindly provided by Martin Stöckl [138]) was diluted to a final concentration of 1 µM in 1x binding buffer and incubated for 10 min with the GUVs.

3.3.17 Fluorescence recovery after photobleaching (FRAP)

The FRAP methodology was developed in the 1970s to estimate lateral diffusion of fluorescent molecules and subsequently improved [149,150]). Today it is a well established and

widely used method among microscopists. It was already used to study the dynamics of the influenza A ribonucleoproteins in cells [151]. Fluorescent molecules in (lipids) and on (e.g. M1) GUV membranes were examined microscopically during this study. Two different regions of interest (ROI) were assigned to a settled GUV. For data acquisition the FluoView software application *scan over time* was locked and collection of 400 to 1200 frames in free run modus (corresponds to 8 – 20 seconds observation time) was set for NBD-lipid and TAMRA labeled α-Synuclein diffusion. For observation of M1-TMR and NM1-TMR 800-1200 frames in 0.1 seconds intervals were acquired. In one region an additional ROI was assigned and bleached after collection of 5 (M1, NM1) or 20 (NBD, α-Synuclein) frames. Fluorescence intensity was monitored with 1 % laser intensity for TMR and TAMRA and 5 – 7 % for NBD and fluorescein. The photomultiplier voltage was adjusted to 600 – 800 mV. For bleaching the laser intensity was set to 100 % in tornado mode. The fluorescence intensity over time profile for bleached and unbleached ROI of at least six GUVs was recorded and normalized. Equation (3) was used for the calculation of the mobile fraction (MF_P) of fluorescent α-Synuclein, Annexin V, and NM1 according to [152]. F_i was the initial fluorescence intensity. F_0 was the intensity value that was recorded after the bleaching laser pulse. F_∞ was the fluorescence intensity in the bleached spot at the end of the experiment.

$$MF_P = \frac{(F_\infty - F_0)}{(F_i - F_0)} \tag{3}$$

The mobile fraction of the fluorescent lipid analogue C_6-NDB-PS (MF_L) was calculated for samples without any protein and with added NM1-TMR or α-Synuclein-TAMRA using equation (4). The averaged intensity values of the unbleached spot (F_u) and averaged intensity values of the bleached spot (F_b) were used. The average was calculated from the intensity values which were detected within the last second of the measurement.

$$MF_L = \frac{F_b}{F_u} \tag{4}$$

4 Results

4.1 M1 binding to lipids – a biochemical and biophysical analysis

Several studies showed membrane binding of M1, either in cellular [26,56,85] or in *in vitro* systems [27,84] (see chapter 1.1.3). This approach is based on recombinant expressed proteins and uses a membrane system where parameters like lipid composition and ionic strength can be fully controlled.

4.1.1 Expression and purification of M1

Recombinant expressed proteins provide a powerful tool to analyze a protein of interest for an intrinsic function in a defined system. They can be isolated in high purity and concentration. Tag-free M1 was expressed earlier for crystallization [68,82,83] and biochemical studies [27,84]. Elster *et al.* described a method where His-tagged M1 was purified from the soluble fraction of *Escherichia coli* lysate by affinity chromatography [153]. His-tagged M1 was also used during this study. The tag allowed the convenient purification of M1 (Figure 11) and its mutants under similar conditions.

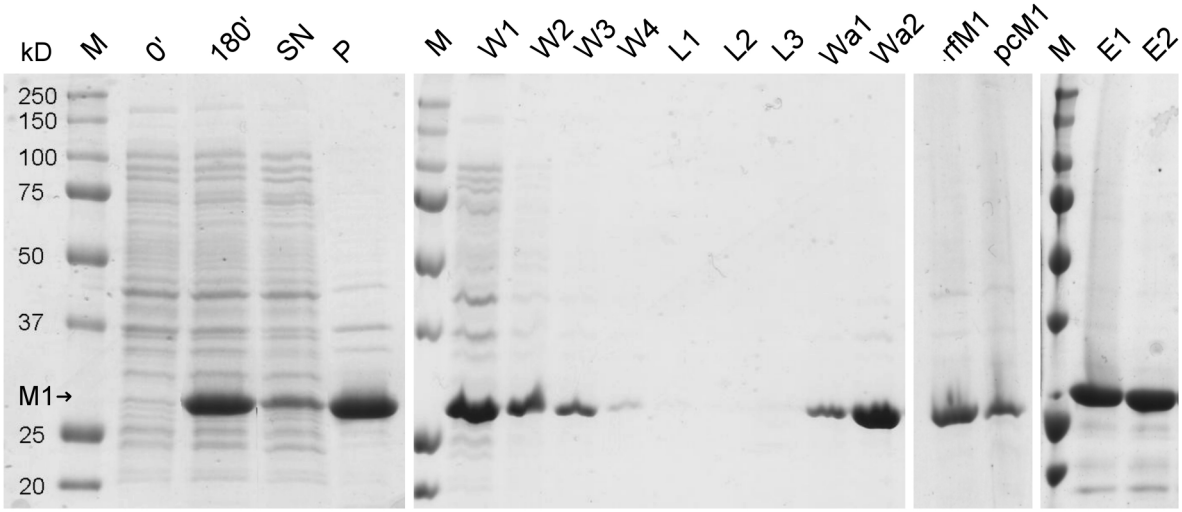

Figure 11 SDS-PAGE of aliquots taken throughout the purification of M1 from *E. coli* cells. Protein was expressed at 37°C and aliquots were taken immediately and 3 h after induction with IPTG (0' and 180'). Postlysis fractions of disrupted cells showed inclusion bodies in the pelleted debris (P). Only a minor fraction of M1 could be found in the supernatant (SN). M1 was therefore purified from inclusion bodies. M1 was found to be soluble in water during the washing procedure with washing buffer (W1-4), lysis buffer (L1-3), and water (Wa1-2). The aliquots taken from the washing step with water showed a significant amount of protein. The cleaned inclusion bodies were disrupted with unfolding buffer. Refolding was triggered upon dilution with refolding buffer yielding refolded M1 (rfM1). The solution was applied to Ni-NTA agarose and affinity chromatography performed. Samples were also taken after the refolded solution passed the column prior to elution (pcM1). These samples showed lower M1 content. Eluted fractions yielded high purified M1 (E1-2).

Expression of the His-tagged wild type M1 protein (see Material and Methods) led repeatedly to inclusion bodies. Since inclusion bodies consist mainly of the precipitated denatured recombinant protein [154,155], they allow high yield purification of the desired protein.

Refolded proteins need to be tested for the reconstitution of their secondary structure. An analytical tool to estimate the secondary structure of proteins is detection of circular dichroism [156]. The CD spectra of folded proteins show a distinct curve progression between 185 and 260 nm depending on the amount of α-helices, β-sheets, or loops in the backbone. A spectrum for M1 and the N-terminal mutant NM1 was published by Arzt *et al.* [82] (see Figure 12B). Contents of structure elements were calculated from these spectra using the CDnn software [157]. 58 % α-helical protein structure was estimated for M1. A crystal structure of the N-terminal domain was obtained in parallel. This CD spectrum and the calculated amount of amino acids were used as references for the recombinant expressed, purified, and refolded protein. Recombinant wild type M1 showed a clearly α-helical behavior (see Figure 12A). The obtained CD spectrum was congruent with the spectrum of M1 published by Arzt *et al*. Furthermore, the amount of α-helical structure was calculated with CDnn. Recombinant expressed M1 showed 48.0 ± 3.1 % (n = 6) α-helical organization. The difference in the calculated fractions of α-helical structure could have resulted from the additional 20 amino acids in the recombinant M1. These 20 amino acids contain the N-terminally attached His-tag. Analysis of this additional peptide with the protein structure prediction software ProteinPredict [158] revealed no helical organization (data not shown).

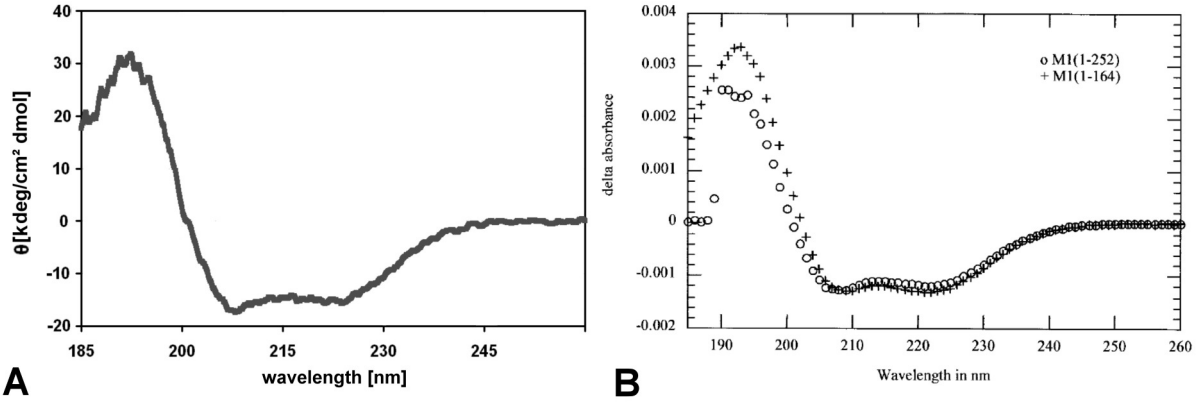

Figure 12 Circular dichroism spectra of purified M1. (A) The spectrum of M1 was obtained for a 7 µM solution of recombinant M1 in NaP buffer at 20 °C. It has α-helical character and is consistent with published data. (B) Published CD spectra of M1 (○ 1-252 amino acids) and M1 (+ 1-164), both at 0.25 mg/ml. Taken from [82].

4.1.2 M1 bound to DOPS and DOTAP

Flotation of vesicles in density gradients offers the possibility to separate vesicle-bound protein from unbound protein [130,145]. Proteins bound to vesicles float up in the gradient, whereas unbound protein stays in the high density fraction at the bottom of the gradient. In addition, the binding mechanism can be studied with this method. Ruigrok *et al*. [27] showed in a flotation study an electrostatically mediated binding of M1 to negatively charged vesicles. Therefore, lipid specificity of M1 was studied based on that to characterize M1s binding affinity to different lipids in more detail. Large unilamellar vesicles (LUVs) were used as model membranes. LUVs offer the opportunity to mimic lipid environments in a highly defined way. The preparation method used here enabled the choice of well characterized lipids and thereby the modulation of the membrane properties. Beside lipid composition, the conditions of the suspending medium can be varied over a broad range, including the pH, ionic strength, and by choosing specific lipids the fluidity and phase state of the membrane. Depending on the carbon filter used during extrusion of the LUVs the curvature of the membrane can be modified [127,130]. The vesicles used during this study were extruded through filters with a pore size of 100 nm.

Using DOPS containing LUVs as positive binding control and uncharged DOPC LUVs as negative control provided the basis for analyzing binding to other lipids. Purified M1 floated without liposomes was taken as a further control. The gradients were prepared, fractionated, and analyzed as described in the Method section 3.3.9. Figure 13A shows where LUV-bound protein is located in the post centrifugation gradient.

The samples were analyzed with SDS-PAGE (see Figure 13B). Lipid content of the respective fractions was recorded by scanning for fluorescence of the lipid analogue N-NBD-DPPE. N-NBD-DPPE was added to the lipid mixture to trace LUVs during the experiment. LUVs containing fractions showed a fluorescent signal after scanning in the bottom line of the SDS-gel (see Figure 9). Strong fluorescent signals were obtained in the 0 % fractions; weak signals were detected in the 25 % fractions, and the 30 % had no significant fluorescence signal. Protein content was assigned to the respective fractions after silver staining of the same gel.

A considerable amount of protein precipitated and remained in the test tube (R fractions) after fractionation of the gradient. No fluorescence of N-NBD-DPPE was observed in the PhosphoImager scan for these samples.

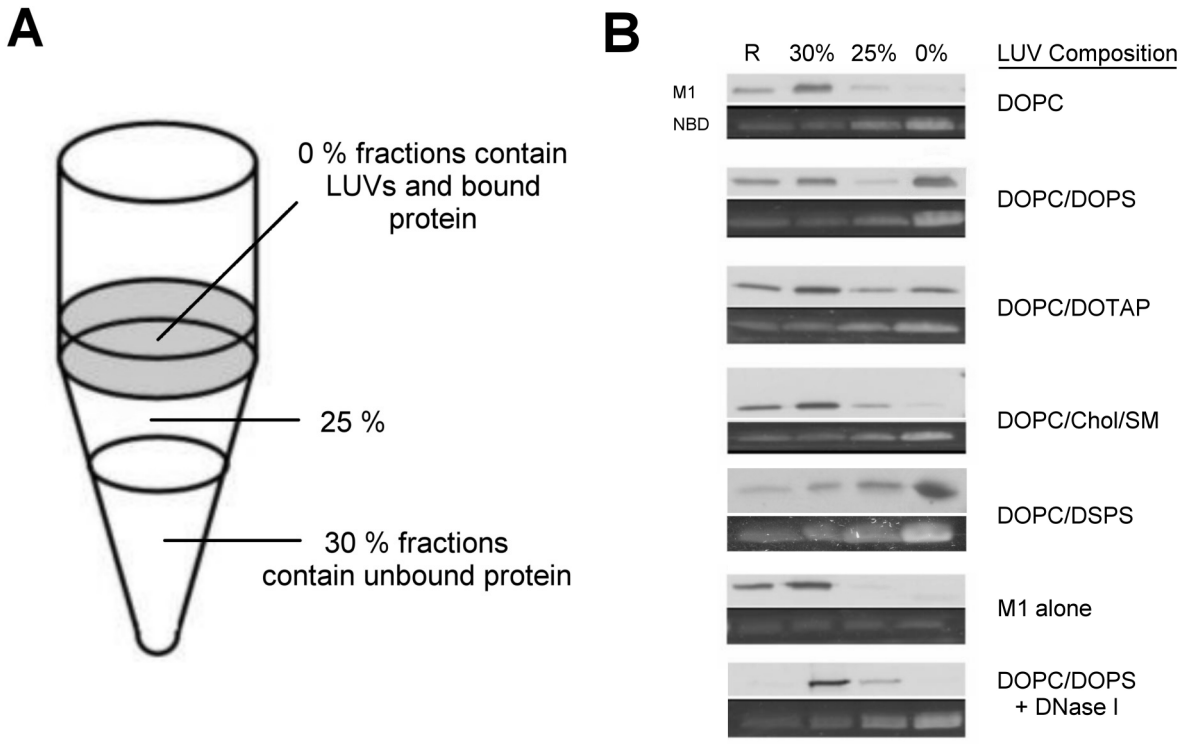

Figure 13 Flotation of M1 with different LUVs. (A) Scheme of the sucrose density gradient after centrifugation. (B) Results for flotation of M1 with anionic and cationic LUVs as well as LUVs with raft lipids. Vesicles and protein were mixed to final concentrations of 1.5 µM M1 and 0.5 mM lipid in the high density part of the gradient. Gradients were centrifuged and fractionated. Fractions from the low density (0 %), intermediate (25 %), and high density part of the gradient were analyzed. Pelleted protein lipid aggregates were removed after fractionation by washing with ddH_2O (R). For each sample two panels are depicted. The upper panel (M1) shows the results of the silver staining, where M1 was visible in the respective fractions. The lower panel (NBD) shows the PhosphoImager scan for N-NBD-DPPE fluorescence of LUVs. Molar lipid ratios in LUVs were: DOPC/DOPS = 4:1, DOPC/DSPS = 4:1, DOPC/DOTAP = 4:1, DOPC/Chol/SM = 1:1:1. Controls: M1 only = M1 floated without vesicles; DNaseI + DOPC/DOPS = DNase I floated with DOPC/DOPS-LUVs. Protein and vesicles were mixed at room temperature. Centrifugation was performed at 4 °C, Fractionation was done at room temperature. Flotation experiments were performed in NaPKCl buffer with the respective amounts of sucrose. All solutions were buffered at pH 7. For further details see Materials and Methods chapter 3.3.9.

M1 could only be detected in the R and the 30 % fraction when it was floated alone. The 25 and 0 % fraction of the DOPC control showed traces of M1. Based on this result, a second control was established to determine whether M1 interacted with DOPC membranes. DNase I was tested as non-floating protein. This protein showed similar traces in the 0 and 25 % fractions as M1 when it was floated with DOPC and DOPC/DOPS LUVs (see Figure 13B), even though this protein was shown to be soluble [159]. The traces in the 0 and 25 % fraction of M1 in the DOPC-LUVs containing gradient and the DNase I traces were the method based background.

Beside DOPC and DOPC/DOPS-LUVs, vesicles containing anionic DSPS, cationic DOTAP, as well as both sphingomyelin and cholesterol were tested. DSPS contains two saturated

stearyl chains. This lipid was chosen to examine the influence of the acyl chain on membrane binding of M1. DOTAP is an artificial lipid. The headgroup of this lipid harbors trimethylammoniumpropane which is positively charged at neutral pH. LUVs with sphingomyelin and cholesterol were produced to mimic raft lipid microdomains of the plasma membrane [108].

Significant M1 signals appeared only for liposomes with DOPS, DSPS and DOTAP. A signal comparable to DOPC was found for LUVs containing sphingomyelin and cholesterol (Figure 13B, central panel). An influence of the fatty acid chains of the lipids was not observed. DOPC/DOPS- and DOPC/DSPS-LUVs showed similar amounts of attached M1.

To test whether the here used system (see section 3.3.9, in brief: 5 min incubation of M1 with LUVs at pH 7, sucrose step gradient, 1 h centrifugation at 240.000 xg) was comparable to the method used by Ruigrok *et al.* [27] (over night incubation of M1 with LUVs at pH 4, linear sucrose gradient from 35 % at the bottom to 0 % on the top, 16 h centrifugation at 192.000 xg), the ionic strength was varied by removal and addition of KCl. The wild type protein showed strong binding to DOPC/DOPS-LUVs in NaP buffer (Figure 14 left panel), whereas the binding was slightly reduced in NaPKCl buffer (Figure 14 middle panel) and reduced to the level of binding to DOPC-LUVs in 400 mM KCl (Figure 14, right panel). Ruigrok *et al.* reported similar results.

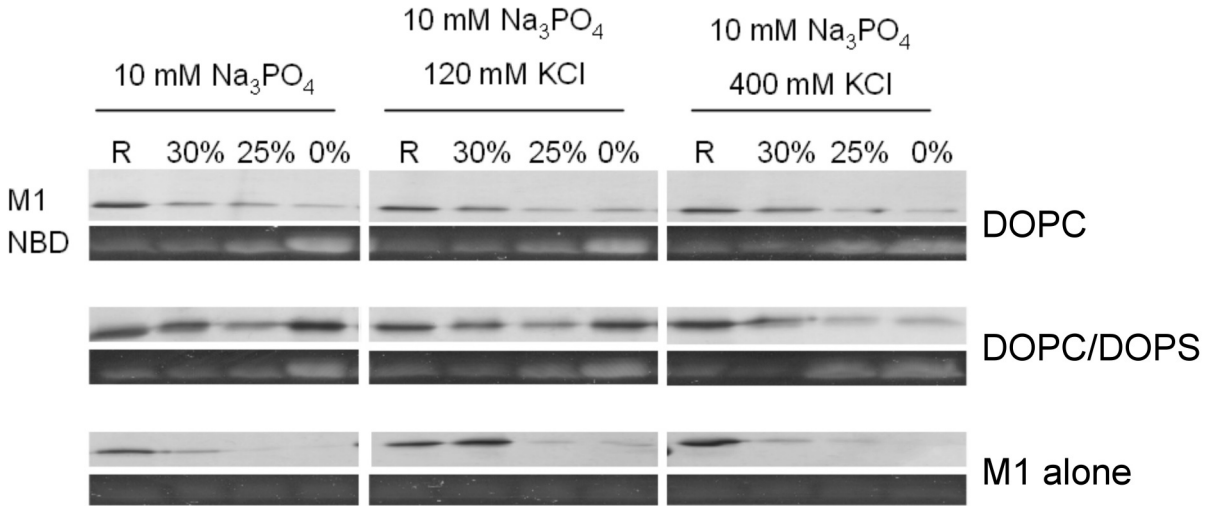

Figure 14 Flotation of M1 at low, medium and high salt conditions. LUVs were prepared in the corresponding buffers at pH 7. M1 solutions in NaP were adjusted to the respective salt condition by adding KCl. Preparation of the LUVs-M1-mixtures, gradient formation, centrifugation, fractionation, and sample analysis were performed as described above. The upper panel (M1) shows the silver stained M1. The lower panel (NBD) depicts fluorescence scans of N-NBD-DPPE. M1 was bound to DOPC/DOPS-LUVs under low and medium salt conditions. M1 binding to DOPC/DOPS-LUVS was reduced to the level of DOPC-LUVs in presence of 400 mM KCl. LUV composition: DOPC = pure DOPC, DOPC/DOPS = 4:1. Control: M1 alone = M1 floated without vesicles.

4.1.3 M1 changed its structure in presence of DOPC/DOPS-LUVs

Circular dichroism measurements were performed to analyze M1's structure when it was bound to LUVs. M1 (3 µM final concentration) was analyzed in presence of DOPC- and DOPC/DOPS-LUVs. Spectra were measured between 200 and 260 nm. Samples were prepared from mixtures of M1 (3 µM final concentration) with LUVs (1.6 mM final lipid concentration). No changes in the spectrum could be observed in presence of DOPC-LUVs. A narrower spectrum was recorded in presence of DOPC/DOPS-LUVs. This indicated a loss of α-helical content (see Figure 15).

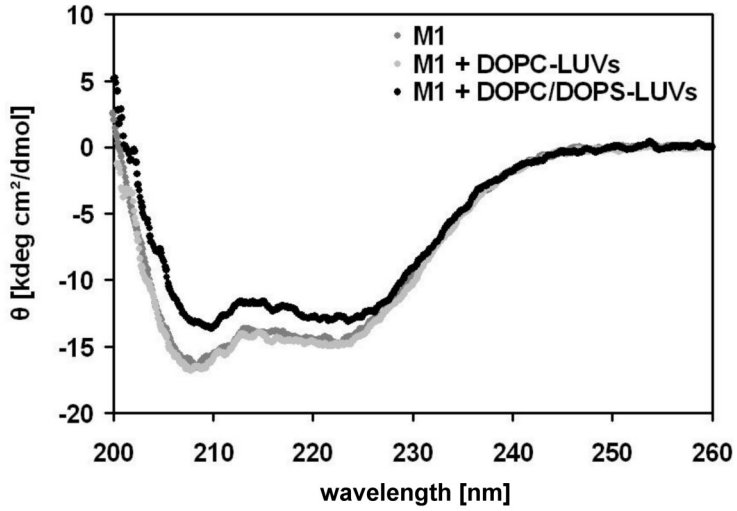

Figure 15 CD spectra of M1 and M1 in the presence of DOPC- and DOPC/DOPS-LUVs. M1 was mixed with LUVs to final concentrations of 3 µM M1 and 1.6 mM lipid. The samples were incubated for one hour at room temperature. Spectra from 200 to 260 nm were measured at 20 °C after 2 min equilibration in the spectrometer. The sample with DOPC-LUVs yielded a spectrum that was similar to M1 without LUVs. DOPC/DOPS-LUVs induced a change in the spectrum.

The presumed loss of α-helical structure was evaluated using the CDnn software. An α-helical content of 46.1 ± 7.2 % (n = 3) was calculated from the spectra when DOPC-LUVs were present in the sample. 33 ± 4.9 % (n = 2) was calculated when DOPC/DOPS-LUVs were added. Additional structural information could be derived from the local minima of the spectra at 208 and 222 nm. The ratio of the molar elipticity values at these wavelengths is an indicator for helix to helix orientations in the protein. Ratios ≥ 1 indicate an α-helical coiled coil secondary structure where the α-helices are closely packed. Ratios ≤ 1 indicate existence of loop regions [160,161]. The shift in the $\theta_{222}/\theta_{208}$ ratio from 0.89 ± 0.02 for M1 in buffer or 0.84 ± 0.07 in the presence of DOPC-LUVs to 0.98 ± 0.03 in presence of DOPC/DOPS-LUVs indicated no major helix rearrangements of helices in M1.

4.1.4 M1 bound to phohatidylinositol-4-phosphate (PI4P)

Another tool to examine lipid specificities are PIP™ strips. Different lipids including headgroup and their respective fatty acid chains were immobilized on nitrocellulose [162]. After incubation of these membranes with M1 in presence of Tween 20, M1 was immunological detected on spots corresponding to immobilized phosphatidic acid (PA), phosphatidylinositol-3,4-bisphosphate (PI34PP), phosphatidylinositol-3,5-bisphosphate (PI35PP), phosphatidylinositol-3-phosphate (PI3P), and phosphatidylinositol-4-phosphate (PI4P) (Figure 15A). When Tween 20 was not used in the buffers, M1 was detected at nearly all spotted lipids except lysophosphocholine (LPC), phosphatidylinositol (PI), phosphatidylethanolamine (PE), phosphatidylcholine (PC), and sphingosine-1-phosphate (S1P) (Figure 15B). This difference led to the conclusion that Tween 20 abolished M1 membrane interactions which have a low affinity. A different binding mechanism for the Tween 20 sensitive and the Tween 20 insensitive M1-lipid interaction seems likely.

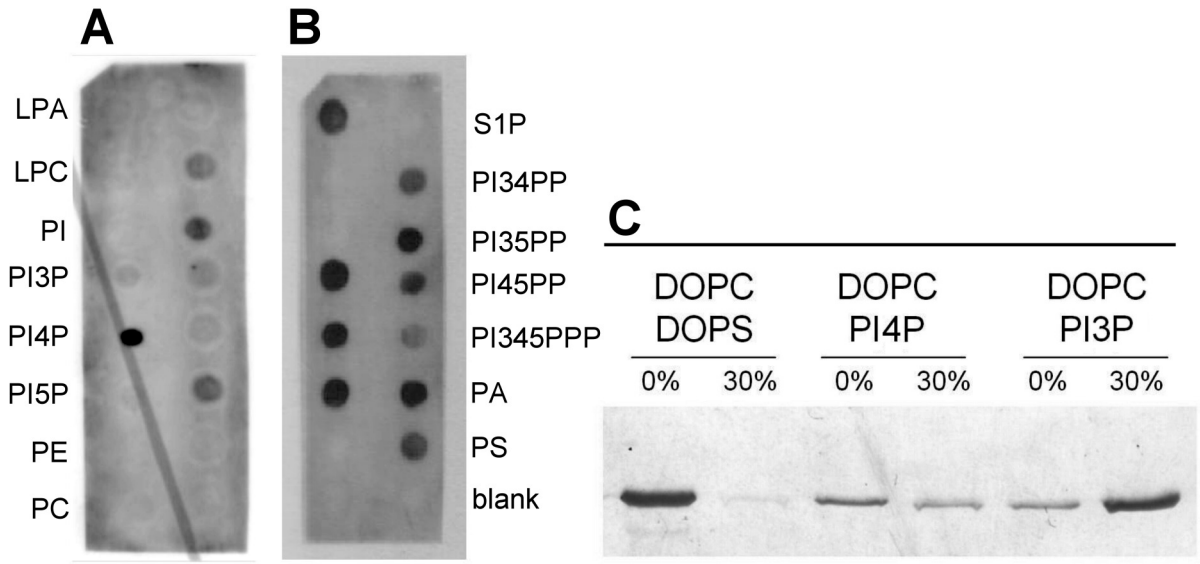

Figure 16 M1 visualized on the PIP™ strip with (A) and without Tween 20 (B) during membrane incubation. The spotted lipids on the membrane were (starting from the upper left): lysophosphatidic acid (LPA), lysophosphocholine (LPC), phosphatidylinositol (PI), phosphatidylinositol-3-phosphate (PI3P), phosphatidylinositol-4-phosphate (PI4P), phosphatidylinositol-5-phosphate (PI5P), phosphatidylethanolamine (PE), phosphatidylcholine (PC), sphingosine-1-phosphate (S1P), phosphatidylinositol-3,4-bisphosphate (PI34PP), phosphatidylinositol-3,5-bisphosphate (PI35PP), phosphatidylinositol-4,5-bisphosphate (PI45PP), phosphatidylinositol-3,4,5-triphosphate (PI345PPP), phosphatidic acid (PA), phosphatidylserine (PS), blank. When Tween 20 was absent during the binding reaction signals for all spotted lipids except LPC, PI, PE, PC, and S1P were detected. (C) Flotation assay in NaPKCl buffer with M1 and LUVs containing 5 mol% PI4P, or PI3P, and 20 mol% DOPS.

Another aspect, which needed to be taken into account, is the organization of the lipids on the PIP™ strip. It is not known that the spotted lipids form lipid layers on the strip or not. To test whether the weak and strong M1 signals can be reproduced in a system with lipid membranes,

LUVs with PI3P and PI4P were produced in NaPKCl buffer. Flotation in NaPKCl buffer of M1 with LUVs containing PI3P showed a weak band for the 0 % fraction (Figure 15 C). The signal for PI4P was stronger. The binding affinity of M1 to PI4P was not as prominent here as on the PIP strip, but M1 still bound much stronger to PI4P than to PI3P.

Circular dichroism measurements were performed to analyze structure rearrangements in M1 in presence of LUVs containing PI3P or PI4P. When DOPC/PI3P-LUVs were added to M1, no changes in the spectrum between 200 and 260 nm were observed. DOPC/PI4P-LUVs induced significant changes in the spectral properties of M1 (see Figure 17).

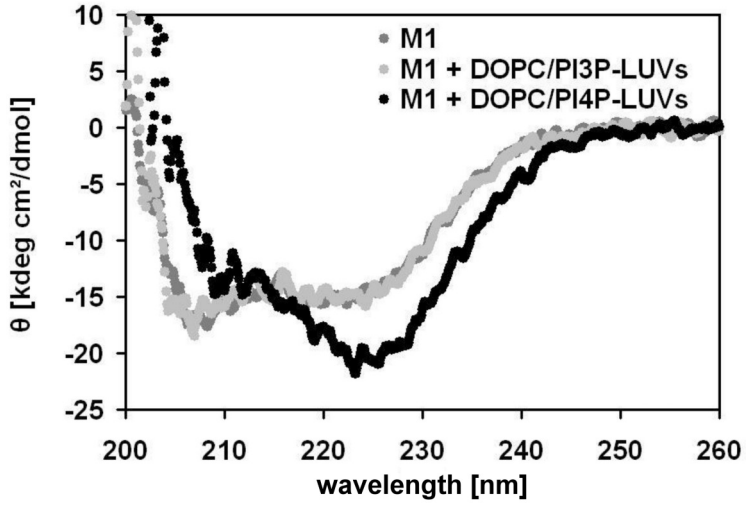

Figure 17 CD measurements for M1 with DOPC/PI3P- and DOPC/PI4P-LUVs. M1 (2.8 µM) and LUVs (1.6 mM) were mixed, incubated for one hour and measured at 20 °C.

The CDnn software was used to determine the α-helical content. An α-helical content of 50.9 ± 2.0 % (n = 2) was calculated when DOPC/PI3P-LUVs were in the sample, and 53.0 ± 2.0 % (n = 2) α-helical content was determined from the DOPC/PI4P-LUVs containing sample. The $\theta_{222}/\theta_{208}$ ratio for DOPC/PI3P-LUVs was 1.0 ± 0.1 and for DOPC/PI4P-LUVs 1.7 ± 0.1. The $\theta_{222}/\theta_{208}$ ratio of 1.7 indicated helix to helix rearrangements in M1. The observed changes in the M1 spectrum in presence of DOPC/PI4P-LUVs were different to those observed for DOPC/DOPS-LUVs. The calculated α-helical contents shifted to lower values for DOPC/DOPS-LUVs (33 ± 4.9 %) whereas higher values were calculated for DOPC/PI4P-LUVs. And the $\theta_{222}/\theta_{208}$ ratios changed in presence of DOPC/DOPS-LUVs to lower values (0.98) whereas higher values were observed with DOPC/PI4P-LUVs. These facts indicated a different rearrangement processes in M1 for DOPC/DOPS-LUVs and DOPC/PI4P-LUVs.

4.1.5 M1s surface exposed tryptophan did not interact with membranes

The Trp fluorescence of a small 26 amino acids long membrane binding peptide named melittin was studied in detail by other groups [163]. Upon binding to membranes a strong blue shift of its Trp emission could be observed. This change was even more prominent in presence of anionic lipids which interacted with the charged amino acids of melittin [164]. This peptide was chosen as positive control for membrane interactions involving tryptophan. The goal of this experiment was to determine whether membrane binding of M1 could be analyzed by examining the emission of the single Trp (W45) of M1. The crystal structure of the N-terminal part of M1 showed a surface location for this particular amino acid residue. Therefore, membrane interaction was analyzed by studying Trp fluorescence and Förster resonance energy transfer (FRET).

The experimental set up contained beside Trp a second fluorophor, the headgroup labeled lipid analog N-NBD-DPPE. This membrane incorporated fluorophor was used as acceptor for FRET from Trp. The NBD fluorophor has an absorption peak between 330 to 350 nm and could function as a FRET acceptor for Trp [165]. With this setup two different issues were addressed. First, a blue shift in the emission of the single Trp of M1 or melittin as control in presence of membranes would indicate that the environment of this Trp had become more hydrophobic. Second, FRET between the Trp of melittin or M1 and the N-NBD-PE in the LUVs would indicate an interaction of melittin or M1 with the membranes.

Spectra of M1 or melittin with and without LUVs were measured between 300 and 550 nm. The spectra were corrected for the background (buffer or buffer with unlabeled LUVs; see Materials and Methods Section 3.3.14). Adding DOPC-LUVs (final lipid concentration 60 µM) to melittin (1.8 µM) in NaPKCl buffer led to the described blue shift [164] of the Trp fluorescence emission. Also a stronger displacement of the emission peak was detected for DOPC/DOPS-LUVs (see Figure 18A and C). The very prominent blue shift of the Trp fluorescence indicated that melittin interacted strongly with the LUVs. This allowed the conclusion that melittin was indeed a valuable tool for comparison to the possible reactions of M1.

The behavior of the single Trp residue of M1 was monitored under equal conditions with DOPC- and DOPC/DOPS-LUVs. This experiment brought two results. No blue shift in the M1 Trp fluorescence was observed; neither with DOPC-LUVs nor with DOPC/DOPS-LUVs (see Figure 18B and D). The emission maximum of the M1 Trp did not change its wavelength in presence of DOPC- or DOPC/DOPS-LUVs.

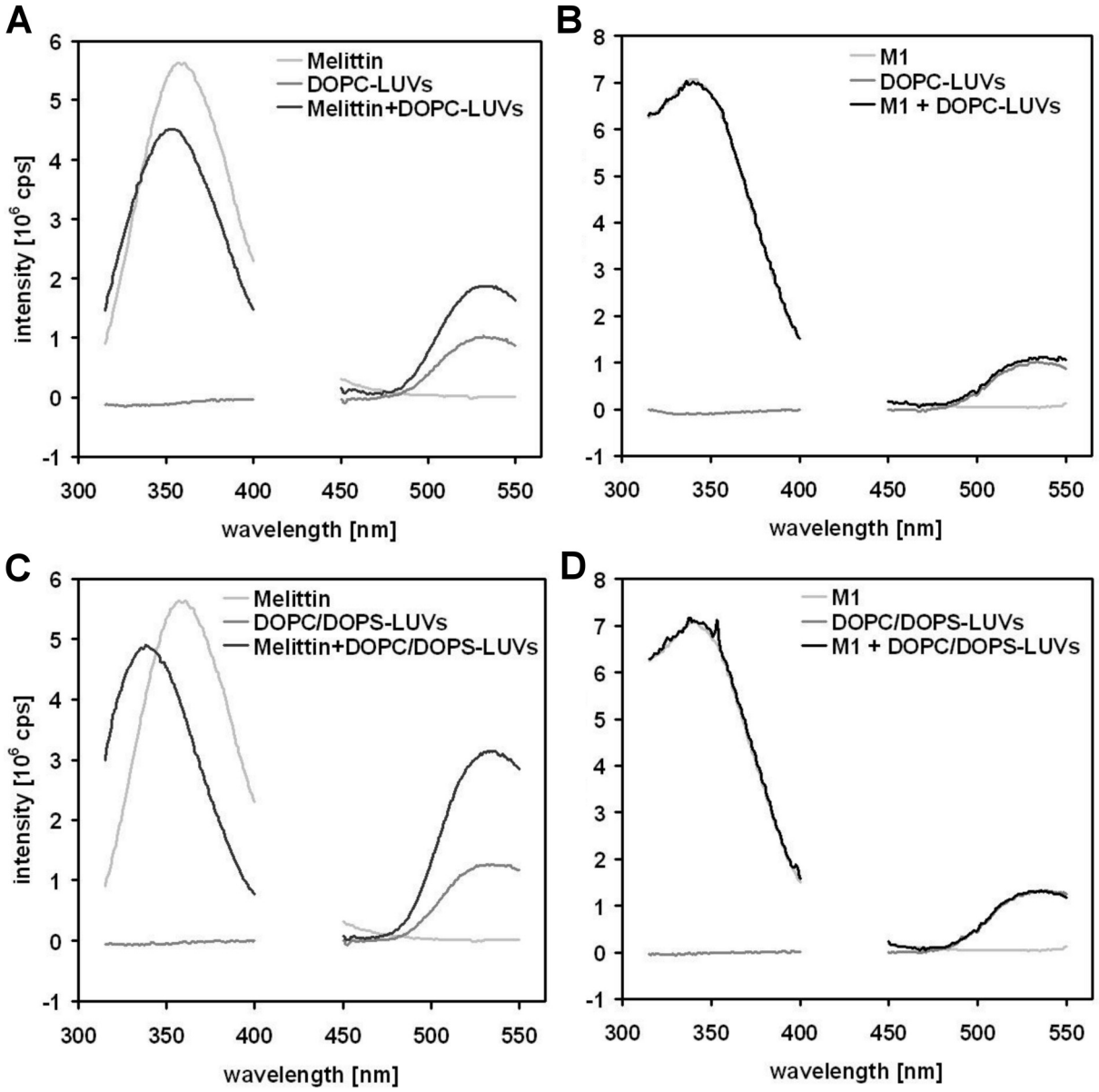

Figure 18 Emission spectra of melittin, M1, and N-NBD-DPPE from DOPC- and DOC/DOPS-LUVs. The excitation wavelength was 283 nm. (A) Spectra for melittin, DOPC-LUVs, and melittin with DOPC-LUVs. The emission maximum of the Trp residue of melittin was at 360 nm in absence of LUVs and 354 nm in presence of DOPC-LUVs. The intensities of these maxima were 5.6 10^6 counts per second (cps) at 360 nm and 4.5 10^6 cps at 354 nm. The NBD emission intensity at 530 nm of DOPC-LUVs alone was 1.0 10^6 cps. An intensity of 1.9 10^6 cps was measured in presence of melittin. (B) Spectra of M1, DOPC-LUVs, and M1 with DOPC-LUVs. (C) Spectra for melittin, DOPC/DOPS-LUVs, and melittin with DOPC/DOPS-LUVs. The emission maximum of the Trp residue of melittin was at 340 nm in presence of DOPC/DOPS-LUVs. The intensity at 340 nm was 4.9 10^6 cps. The NBD emission intensity of DOPC/DOPS-LUVs alone was 1.2 10^6 cps. An intensity of 3.1 10^6 cps was measured in presence of melittin. (D) Spectra of M1, DOPC/DOPS-LUVs, and M1 with DOPC/DOPS-LUVs. T= 20 °C. LUV composition: DOPC = pure DOPC, DOPC/DOPS = 4:1. The concentration of N-NBD-DPPE was 1 mol% of the total lipid.

Furthermore, the emission intensity of the M1 Trp did not change in presence of the FRET acceptor N-NBD-DPPE in DOPC- or DOPC/DOPS-LUVs. This indicated that the Trp residue of M1 did not interact with membranes even though it was exposed on the surface of M1. The

Förster radius between Trp and NBD was shown to be less than 6 nm [165], the thickness of a membrane. The diameter of M1 was given in [82] to be approximately 6 nm. Thus, M1 does not attach to membranes with the Trp containing region as no blue shift of its Trp fluorescence emission and no significant FRET could be measured.

4.1.6 M1-TMR bound to DOPC/DOPS-LUVs and DOPC/PI4P-LUVs

The red fluorescent dye tetramethylrhodamine (TMR) was covalently attached to M1 via a reaction between a cysteine of M1 and a reactive maleimide group of TMR for FRET measurements between fluorescently labeled liposomes and M1. The serine after the start methionine of M1 was substituted to cysteine to allow higher TMR-labeling efficiencies (see chapter 4.2 for more details).

The purpose of this FRET experiment was to show whether the result of flotation and PIP-strips can be analyzed in a system where the binding could be monitored upon occurrence and not indirectly by biochemical methods like flotation. Furthermore, the position of the attached TMR was known to be located at the N-terminus of M1 where the S2C substitution was introduced. N-NBD-DPPE was chosen as FRET partner for TMR-M1. N-NBD-DPPE was incorporated into DOPC-, DOPC/DOPS-, DOPC/PI3P-, and DOPC/PI4P-LUVs. The concentration of the FRET-donor fluorophore N-NBD-DPPE was kept at 20 nM (from LUVs which contained 1 mol% N-NBD-DPPE) in the cuvette. The final lipid concentration was 2 µM. These four versions of LUVs were incubated without TMR-M1 for one hour and the emission measured between 500 and 600 nm at an excitation wavelength of 469 nm. M1 was added in a subsequent measurement to a concentration of 0.1 µM (22.5 nM TMR-M1). The concentration of TMR-M1 was derived from the labeling efficiency of 28 %. Spectra were measured to acquire the intensity values for N-NBD-DPPE and TMR. The emission maximum (E_{max}) of N-NBD-DPPE was at 530 nm. The E_{max} of TMR was around 580 nm.

The intensity of N-NBD-DPPE at 530 nm was reduced in all samples where TMR-M1 was added (see Figure 10). The experiments were performed three times with similar intensity changes. The exemplary raw data for the FRET pairs TMR-M1 + N-NBD-DPPE in DOPC-LUVs and in DOPC/DOPS-LUVs are presented in Figure 10 A (page 37). The spectra from LUVs with and without TMR-M1 were normalized to the N-NBD-DPPE intensity maximum at 533 nm for better comparison. Difference spectra were calculated by subtraction of the N-NBD-DPPE emission spectrum in the absence of TMR from the N-NBD-DPPE

spectrum recorded in presence of TMR (see Figure 19). The difference spectra allowed the recognition of small changes in the spectral shape, especially around 580 nm. The difference spectra revealed spectral changes for samples containing DOPC/DOPS- and DOPC/PI4P-LUVs. The intensity at 580 nm increased significantly (Figure 19). Only minor changes could be observed for DOPC/PI3P-LUVs.

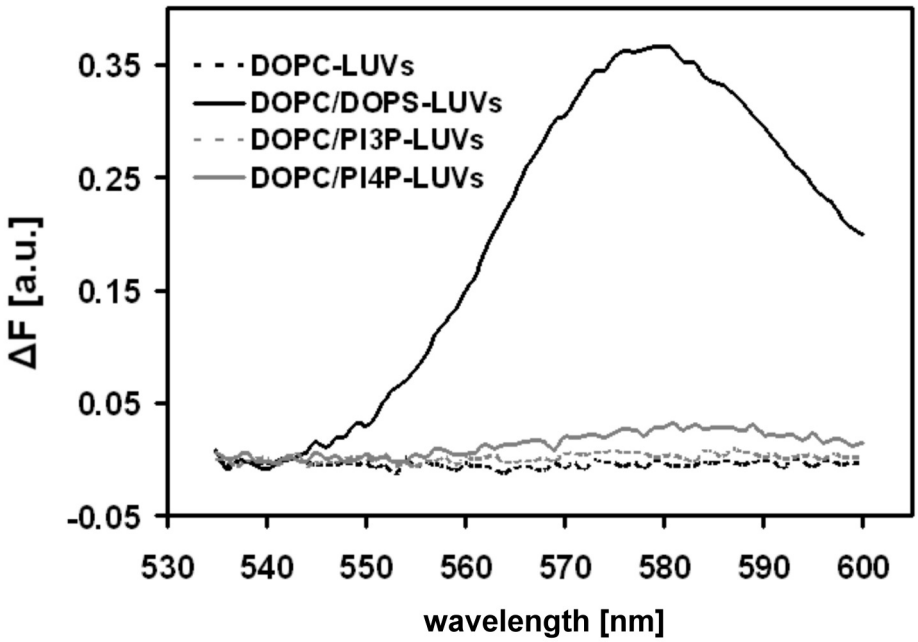

Figure 19 Difference spectra of N-NBD-DPPE from samples containing LUVs with and without TMR-M1. LUVs (final concentration of lipids 2 µM) were incubated without and with TMR-M1 (concentration of M1 0.1 µM, 28 % labeled with TMR) for one hour. Spectra of the respective LUVs and LUVs with TMR-NM1 were measured between 500 and 600 nm, after excitation of NBD at 469 nm. The spectra were normalized to the emission maximum at 533 nm. Difference spectra were calculated from these normalized spectra by subtraction of the N-NBD-DPPE emission spectrum in the absence of TMR from the N-NBD-DPPE spectrum recorded in presence of TMR. The difference spectra represent mean values from three different measurements. The composition of the LUVs was: DOPC = pure DOPC, DOPC/DOPS = 4:1, DOPC/PI3P = 19:1, DOPC/PI4P = 19:1. N-NBD-DPPE was added to the lipids at a final concentration of 1 mol % of total lipids. The measurements were performed at 20 °C.

It was possible to reproduce the results from the flotation and PIP-strip experiments for the affinity of M1 towards DOPS and PI4P. A specific interaction of M1 with these lipids was clearly visible by the increase of the TMR emission around 580 nm resulting from FRET. This could be observed for DOPC/DOPS- and DOPC/PI4P-LUVs.

The change in the NBD emission at 533 nm (Figure 10 A and B) resulted from another mechanism. It indicated an interaction of the two fluorophores NBD and TMR which could not be due to specific M1 membrane binding. This could be concluded from the fact that the NBD emission of all the differently composed LUVs showed a similar spectral change in

presence of TMR-M1. The strong spectral change of the NBD emission in presence of TMR-M1 was an unexpected result and TMR-M1 possibly could have influenced the quantum yield of the NBD emission with its presence. Flotation experiments, PIP-strips, and CD measurements suggested that only DOPS and PI4P containing LUVs should have been the target for M1 in this kind of experiment. DOPC and PI3P were ruled out as major binding partners in the three experiments mentioned above.

4.2 Fluorescent labeling of M1 needed protein modification

The amino acid sequence of M1 includes three cysteines and according to three published crystal structures none of these cysteines was coupled into a cystine [81,82,83]. A MALDI-TOF mass spectrometry study revealed a cystine bridge between C148 and C151 of M1 [166]. Several attempts were undertaken to attach cysteine-reactive fluorophores covalently to purified recombinant M1. The labeling efficiency was determined by absorption measurements. The highest labeling ratio for labeled M1 was 3 % of total protein. This was not suitable for FRET measurement or fluorescence microscopy.

An additional cysteine (S2C) was introduced at the N-terminal part of M1, M1m, NM1, and NM1m by site directed mutagenesis to enable a more efficient labeling. The sequence of CM1 did not harbor a cysteine. Serines for substitution were located within the peptide. Therefore, a mutation might have induced different folding or reaction behavior. The N-terminal His-tag could be used to introduce a cysteine for labeling without altering the CM1 core sequence. A serine in the linker sequence to the His-tag two amino acids prior the CM1 start methionine (see Figure 8) was substituted.

All proteins with S→C mutation were purified from inclusion bodies. After analysis of the proteins in SDS-gels under non-reducing conditions, additional bands at higher molecular weights were observed in distinct distances. This was not visible for the unmodified proteins. Deduced from the distance intervals, dimerization of the recombinant protein based on cystine formation was hypothesized. Size separation under reducing conditions proved this hypothesis, since no other bands beside the monomeric proteins were recognized (see Supplementary Figure 2). CD measurements in NaP buffer yielded spectra which were congruent to the spectra of the earlier described proteins without additional cysteine. This led to the conclusion that the modified proteins were comparable to the unmodified ones, even though they formed dimers and trimers. All five proteins could be labeled with significantly increased efficiency. After measurements of protein absorption and absorption of the fluorophores TMR or FM and calculation of the concentrations, the labeling efficiency was determined to be 17 % for FM labeled protein and 20 – 30 % of the proteins carried TMR. All labeled protein samples were analyzed in SDS-PAGE for free fluorophor and only a small amount was detected (Supplementary Figure 2). The labeled proteins were used in FRET measurements and predominantly for microscopy (see chapters 4.1.6, 4.3.4 and 4.4.2 to 4.4.4).

4.3 Membrane binding of M1 mutants

The identification of membrane binding domains or motifs of M1 was another aim of this study. Different mutants were expressed beside the wild type matrix protein and purified to enable the localization of membrane binding domains within M1. A full length mutant with substituted PBS (M1m), a truncated N-terminal fragment (NM1), the N-terminal fragment with substituted PBS (NM1m), and a C-terminal deletion mutant (CM1) were produced (Figure 20). The PBS was mutated to analyze the role of this particular motif in membrane binding. This sequence includes M1's NLS (101 – RKLKR – 105) and two additional basic amino acids that were shown to expose a positively charged patch on the surface of M1 [82]. This was proposed to be the interface for electrostatic interactions with negatively charged surfaces [27,84]. The flotation assay and CD measurement were used for mutant analysis.

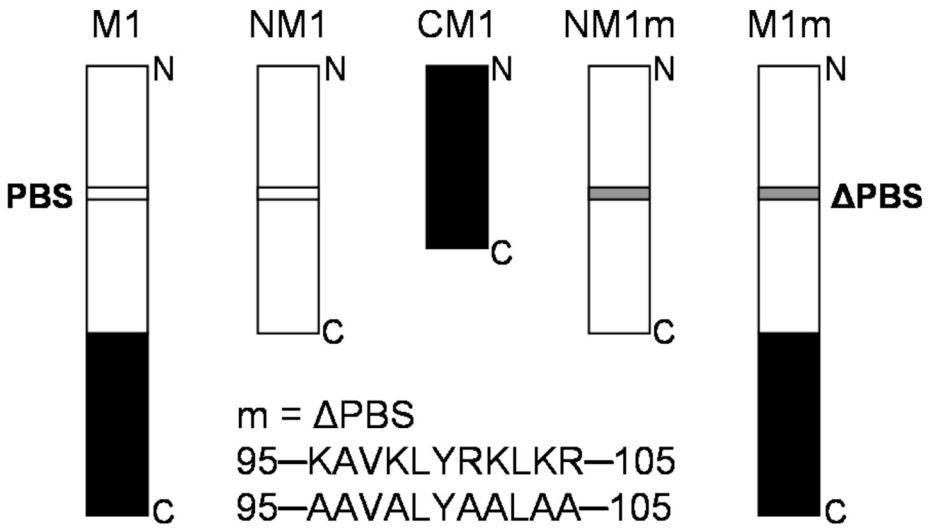

Figure 20 Mutants of M1. M1m contains a modified PBS sequence, with the basic amino acids being exchanged to alanines according to [83,153]. NM1 and CM1 reflect the 252 amino acid wild type protein cut in two pieces at amino acid 164. NM1m is the N-terminal part of M1 with substituted PBS.

4.3.1 Expression and purification of M1 mutants

All mutants containing the N-terminal part of M1 were purified from inclusion bodies. The only peptide that was not purified from inclusion bodies was CM1. All proteins yielded final concentrations of up to 20 µM after removal of imidazole on NAP™-25 columns. SDS-PAGE and Coomassie staining showed a purity of at least 95 % (see Supplementary Figure 1). CD spectra indicated mainly α-helical secondary structure for all proteins. The C-terminal part

was of heterogeneous secondary structure with low α-helical content according to the spectrum obtained from this polypeptide (see Figure 21).

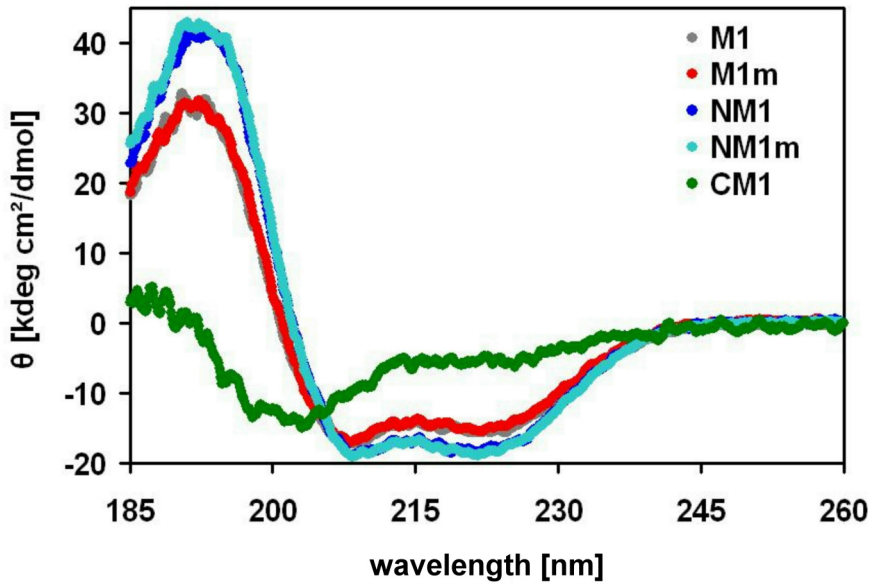

Figure 21 CD spectra of M1 and the purified mutants. Proteins were diluted in NaP buffer to a final concentration of 7 µM. CD spectra of the purified proteins were measured between 185 and 260 nm. The spectra were corrected for buffer background and normalized to molar elipticity θ. The spectrum of M1 was included for direct comparison to the mutants. The spectra were measured at T = 20 °C.

The fractions of the different structural components can be estimated based on computational algorithms. Applying the CDnn software [157] to the spectra of M1m, NM1 and CM1 resulted for M1m in 48.0 ± 3.1 % (131 ± 8 amino acids from 272), for NM1 in 56.4 ± 4.2 % (104 ± 8 amino acids from 184) and for CM1 in 22.3 ± 3.0 % (24 ± 3 from 108 amino acids) α-helical structured residues. The software predicted a low probability for β-sheets. Prediction with PredictProtein provided the evidence for an unfolded state of the additional N-terminal 20 residues which included the His-tag. Therefore, these 20 amino acids could be excluded as part of the α-helical elements. When this was taken into account, the percentage of α-helical structured residues changed to 51.8 ± 3.4 % (131 ± 8 amino acids from 252) for M1, 63.3 ± 4.8 % (104 ± 8 amino acids from 164) for NM1, and 27.4 ± 3.7 % (24 ± 3 from 88 amino acids) for CM1. Direct comparison with published data revealed only minor differences. The CDnn program gave a value of 58 % α-helix for M1 and 68 % for NM1 [82]. When measurement deviations (1.6 – 7.2 %, see Table 4) and given calculation accuracy (± 5 % average error) of the CDnn software [157] were taken into account, the acquired values were in the range of the α-helix contents that were previously reported [82].

An influence of the deletion on the secondary structure of the mutants could also be analyzed by utilizing the CDnn data. The α-helical organized amino acids of NM1 and CM1 (128 amino acids) and the α-helical content of full length M1 (131 amino acids) were not significantly different. This was used as indicator for the structural integrity of the mutants.

4.3.2 Flotation of the mutant proteins

The mutant proteins were tested for their membrane binding behavior using flotation experiments (see Figure 22). The LUVs contained the lipids DOPE, DOPC, and DOPS. DOPE was used because its headgroup represented another lipid that was found on the inner leaflet of the plasma membrane.

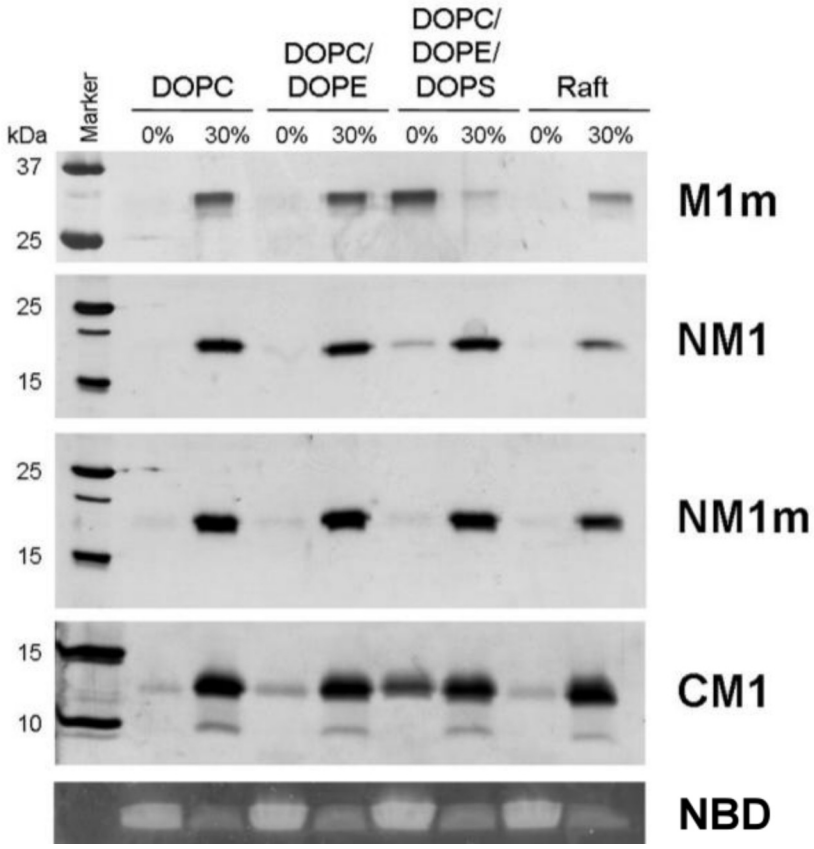

Figure 22 Flotation results for the M1 mutant proteins. Equal amounts of protein were floated with DOPC-, DOPC/DOPE-, DOPC/DOPE/DOPS- and Raft-LUVs. The gradient samples were analyzed electrophoretically and silver stained. The bottom panel shows NBD-fluorescence. Composition of LUVs: DOPC = pure DOPC, DOPC/DOPE = 9:1, DOPC/DOPE/DOPC = 7:1:2, Raft = SM/Chol/DOPC = 1:1:1. N-NBD-DPPE was added to the lipids at a final concentration of 1 mol % of total lipids.

M1m showed a binding pattern similar to the wild type protein (compare to Figure 13). M1m bound to DOPC/DOPE/DOPS-LUVs whereas no significant binding could be observed for

uncharged DOPC-, DOPC/DOPE-, and Raft-LUVs. Compared to M1 and M1m only a small fraction of NM1 bound to anionic DOPC/DOPE/DOPS-LUVs and nearly no binding was detected for uncharged vesicles. For NM1m no significant binding to any vesicle type was observed. CM1 bound to all types of vesicles, but with a significant higher extent to DOPC/DOPE/DOPS-LUVs.

In summary, the PBS played a role in membrane attachment of M1. The M1m mutant showed a similar binding pattern to the wild type M1 whereas the NM1 mutant of M1 showed a reduced binding capability for DOPC/DOPE/DOPS-LUVs. Since membrane binding was completely abolished for NM1m, it could be concluded that the PBS was able to link NM1 to membranes, although with a low affinity. The binding ability of the C-terminal part strongly suggests that this part is important for membrane interactions of M1 and might function as an additional membrane binding site.

4.3.3 CD measurements revealed structural changes upon binding to DOPC/DOPS-LUVs

CD measurements were undertaken to analyze potential changes in the secondary structure of the M1 mutant proteins in presence of lipid membranes. Therefore the proteins (3 – 7 µM final concentration) were mixed with buffer or DOPC- and DOPC/DOPS-LUVs (final lipid concentration 1.6 mM). CD spectroscopy was performed after one hour incubation. No differences in the spectra could be observed for proteins in buffer or in presence of DOPC-LUVs. For M1m and CM1 different spectra were measured when DOPC/DOPS-LUVs were added. The behavior of M1m was similar to the behavior of M1. The spectra were comparable in intensity of the signal and in curve progression. The spectra for CM1 in the presence of DOPC/DOPS-LUVs were shaped differently. These spectra were narrower. This indicated a loss in α-helical secondary structure in M1m and CM1. No significant spectral changes appeared for NM1 and NM1m in presence of DOPC/DOPS-LUVs (see Figure 23).

Additionally, the elipticity $\theta_{222}/\theta_{208}$ ratio was evaluated for the spectra of NM1, NM1m, and M1m in buffer and when DOPC- or DOPC/DOPS-LUVs were added. The $\theta_{222}/\theta_{208}$ ratios of NM1 and NM1m in buffer were 0.96 ± 0.02 and 0.97 ± 0.02. For samples where DOPC-LUVs were added ratios of 0.99 ± 0.01 and 1.03 ± 0.07 were calculated. These values did not differ from the ratios 0.98 ± 0.10 and 1.01 ± 0.10 that were derived from spectra in the presence of DOPS. These values support the conclusion, that NM1 and NM1m did not change their structure in presence of DOPC- or DOPC/DOPS-LUVs. A $\theta_{222}/\theta_{208}$ ratio of 0.84 ± 0.09

was calculated for M1m in buffer and 0.88 ± 0.04 in presence of DOPC-LUVs. These values were similar to the $\theta_{222}/\theta_{208}$ ratios of M1 in buffer (0.89 ± 0.02) or in presence of DOPC-LUVs (0.84 ± 0.07). A ratio of 0.92 ± 0.02 was calculated from the spectra taken in the presence of DOPC/DOPS-LUVs. This value was also comparable to the value that was obtained for M1 in presence of DOPC/DOPS-LUVs (0.98 ± 0.03). This indicated similar but no major rearrangements in M1m compared to M1. The $\theta_{222}/\theta_{208}$ ratios for CM1 in buffer and in the presence of LUVs could not be evaluated. The CD spectra of this protein did not show prominent minima at the appropriate wavelengths.

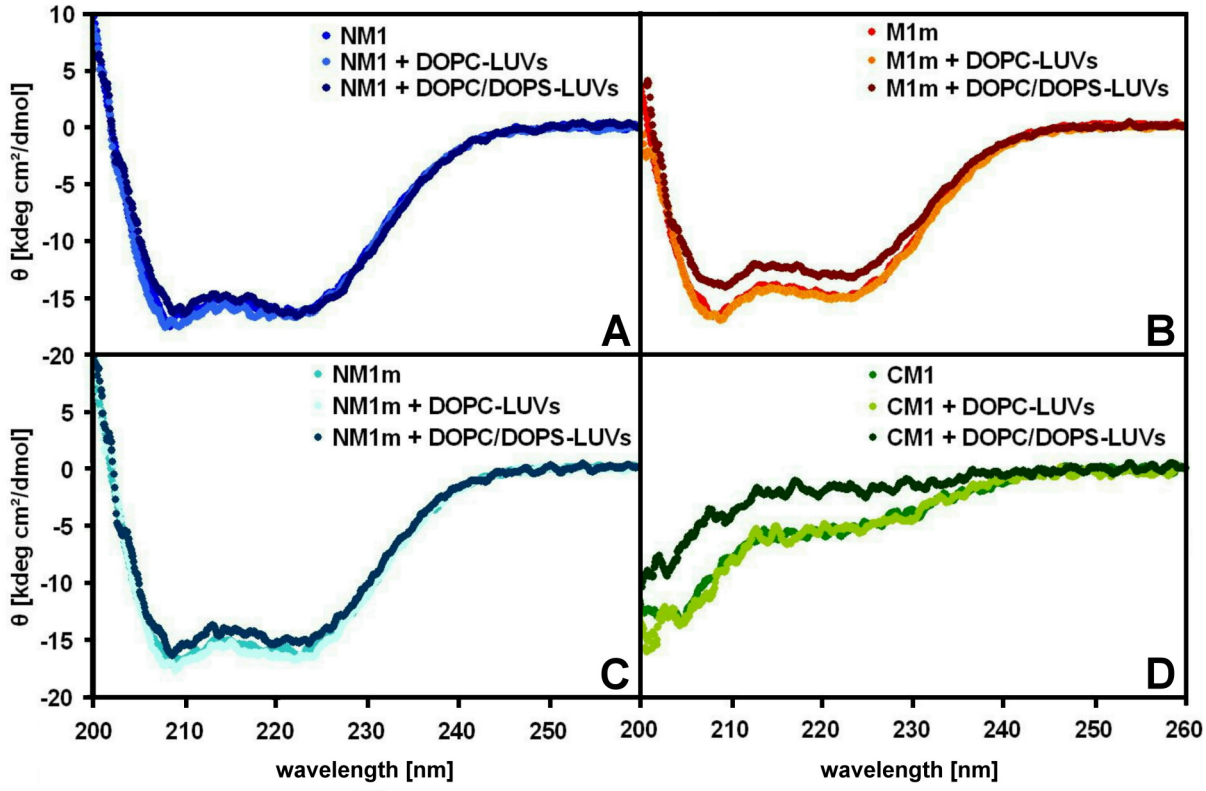

Figure 23 CD measurements for the M1 mutants. The purified proteins in NaP buffer (3 – 7 µM final concentration) were incubated with NaP buffer or DOPC-LUVs as well as DOPC/DOPS-LUV in NaP buffer (final lipid concentration 1.6 mM) for one hour, pipetted into the cuvette and measured between 200 and 260 nm. (A) and (C) depict the spectra that were measured for NM1 and NM1m. (B) shows the spectra for M1m. (D) represents the data obtained for CM1. The composition of the LUVs was: DOPC = pure DOPC, DOPC/DOPS = 4:1. T = 20 °C.

The CDnn algorithm was applied to spectra of M1m, NM1, NM1m, and CM1 in presence of LUVs to analyze the structural changes in detail. Table 4 contains the calculated values for all five proteins. M1 was included for direct comparison. No significant differences in the α-helical content could be observed for M1 and M1m or NM1 and NM1m in absence of LUVs. This led to the conclusion that M1 and M1m as well as NM1 and NM1m had a similar

structure. Crystal structures of NM1 and NM1m were obtained by Arzt *et al.* [83]. The projection of the two structures on each other was congruent. When the spectra, the calculated α-helical contents, the published spectra from [82], and the published crystal structures from [83] were taken into account, it is clear that structure of the proteins used in this study were similar to those published previously.

The α-helical content was also calculated for the mutant proteins in the presence of LUVs. The calculated α-helical content of all soluble and LUVs-associated mutant proteins was not significantly different. Only M1m and CM1 showed reduced α-helical content in presence of DOPC/DOPS-LUVs, as indicated by the spectra. The significant change in the spectra and α-helical content was limited to proteins that contained the C-terminal part. Derived from this, it was concluded that only the C-terminus of M1 showed structural rearrangements.

Table 4 Results from CDnn for M1, M1m, NM1, NM1m, and CM1 in buffer and in presence of DOPC- and DOPC/DOPS-LUVs. The CD Spectra [mdeg] of buffer or LUVs in buffer were subtracted. These corrected spectra were imported into the CDnn software in Milli-Degrees modus. Values for M1 were included for direct comparison of the mutants to the wild type protein.

	α-helical content [%] in presence of		
	Buffer	DOPC-LUVs	DOPC/DOPS-LUVs
M1	48.0 ± 3.1 (n = 6)	46.1 ± 7.2 (n = 3)	33.0 ± 4.9 (n =2)
M1m	49.0 ± 1.6 (n = 4)	48.1 ± 5.3 (n = 2)	38.6 ± 2.5 (n = 2)
NM1	56.4 ± 4.2 (n = 5)	51.6 ± 4.2 (n = 2)	56.5 ± 1.7 (n = 2)
NM1m	58.0± 4.2 (n = 3)	56.4 ± 1.6 (n = 2)	54.1 ± 2.0 (n = 2)
CM1	22.3 ± 3.0 (n = 3)	22.9 ± 2.1 (n = 2)	16.5 (n = 1)

4.3.4 NM1-TMR bound to DOPC/DOPS- and DOPC/PI4P-LUVs

FRET experiments between N-NBD-DPPE containing LUVs and TMR-NM1 (with S2C modification) were performed. Higher FRET efficiencies compared to TMR-M1 were assumed, because NM1 lacked the C-terminal part. The smaller size of NM1 (1.5 ± 0.3 nm [82,83]) should have increased the probability for FRET between NM1-TMR and N-NBD-DPPE in the membrane, since the maximal distance between the two fluorophores was shorter than for TMR on M1 and NBD. The PBS as membrane binding site of NM1 should have allowed FRET.

N-NBD-DPPE containing DOPC-, DOPC/DOPS-, DOPC/PI3P-, and DOPC/PI4P-LUVs were incubated without and with TMR-NM1 for one hour. Spectra were measured between 500 and 600 nm to acquire the intensity values for N-NBD-DPPE and TMR. The spectra were processed as described in Materials and Methods (see section 3.3.14).

E_{max} of N-NBD-DPPE was at 533 nm and of TMR around 580 nm. The intensity of N-NBD-DPPE at 533 nm was reduced in all samples where TMR-NM1 was added (data not shown). A TMR emission intensity increase around 580 nm could be observed for samples with DOPC/DOPS-LUVs, DOPC/PI4P-LUVs and additionally for DOPC/PI3P-LUVs (see Figure 24). Therefore, a similar interaction mode with DOPS containing LUVs could be concluded for M1 and NM1. Furthermore, the interaction was independent of the C-terminal part. The less pronounced difference in the spectra of TMR-NM1 with DOPC/PI4P- and DOPC/PI3P-LUVs compared to the obtained data for TMR-M1 (see Figure 19) might indicate a role of the C-terminal part in the binding of M1 to PI4P containing membranes.

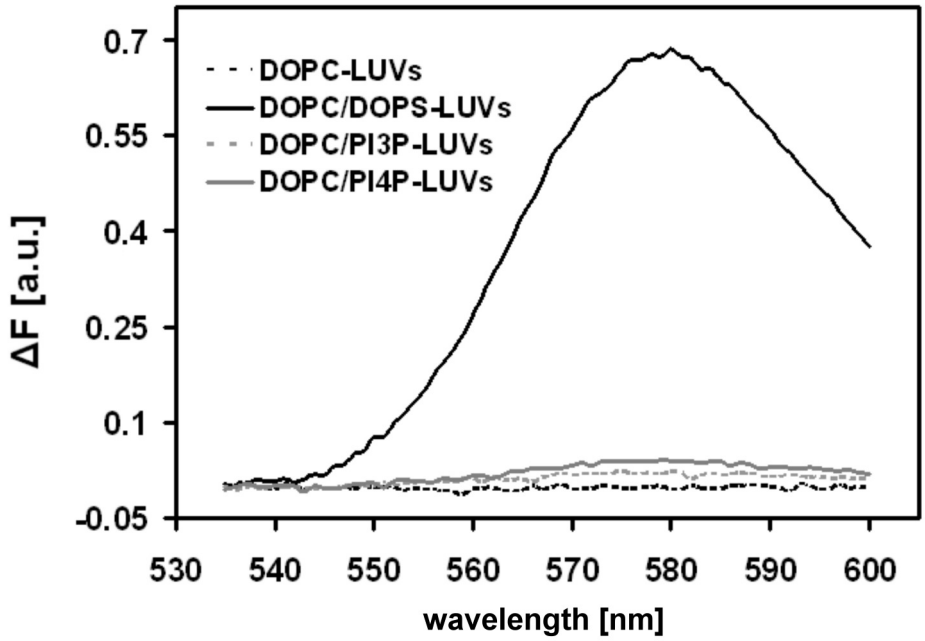

Figure 24 Difference spectra of N-NBD-DPPE containing LUVs in the absence and presence of TMR-NM1. LUVs (2 µM lipids) were incubated without and with TMR-NM1 (concentration of total NM1 0.1 µM, 21 % labeled with TMR) for one hour. Spectra of the respective LUVs and LUVs with TMR-NM1 were measured between 500 and 600 nm. The spectra were normalized to the emission at 533 nm to visualize possible differences and processed to difference spectra. Difference spectra of DOPC-LUVs and DOPC-LUVs with TMR-NM1, DOPC/DOPS-LUVs ± TMR-NM1, DOPC/PI3P-LUVs ± TMR-NM1 and DOPC/PI4P-LUVs ± TMR-NM1. The composition of the LUVs was: DOPC = pure DOPC, DOPC/DOPS = 4:1, DOPC/PI3P = 19:1, DOPC/PI4P = 19:1. The N-NBD-DPPE content was 1mol% of total lipid. T = 20 °C.

4.4 M1 organization on surfaces

The organization of M1 on membranes was approached so far only via electron microscopy in virus particles [20,34,123]. No electron microscopic data for M1 on membranes in a virus free system were available. M1 was analyzed during this study with dynamic light scattering to evaluate the possible size change that M1 might induce upon formation of M1-LUV-particles. Electron microscopy on LUVs in the presence of M1 was performed to reveal how M1 is organized on the LUV surface. Finally, micrometer sized GUVs were analyzed microscopically for bound fluorescent M1 and M1 mutants. The organization of M1 on these surfaces was approached by fluorescence recovery after photo bleaching (FRAP) experiments. These experiments were also suitable to analyze the influence of M1 on the lateral lipid diffusion.

4.4.1 DOPC/DOPS-LUV-M1 particles exhibited a considerably increased diameter

Size measurements were performed to validate the increase in the LUV diameter when M1 was bound. Dynamic light scattering was chosen for this purpose. Samples of DOPC- and DOPC/DOPS-LUVs were analyzed in the absence and presence of different concentrations of M1. The amount of protein was chosen in the following way: LUVs were provided with a fixed lipid concentration (80 µM). As membranes consist of two leaflets a maximum of 40 µM surface exposed lipids were available for interaction with M1. M1 was added to final concentrations of 30 nM, 0.3 µM, and 0.6 µM. These ratios were based on the assumption that M1 has a diameter of approximately 6 nm [82]. An area with a diameter of 6 nm on the LUV surface corresponds approximately to 73 lipids assuming a lipid diameter of 0.7 nm [167]. Therefore, a ratio of 600 nmol M1 to 40 µmol lipid (1 M1 to 67 lipids) will lead to maximal surface coverage, if all proteins bind. A size change of the LUVs of approximately 12 nm was expected under this circumstance. No differences in hydrodynamic diameter were observed for DOPC-LUVs with or without M1. When DOPC/DOPS-LUVs were analyzed without M1 and with the respective M1 concentrations a concentration-dependent change in particle diameter was observed. With increasing M1 concentration a significant larger diameter was measured. The expected size change of 12 nm was, however, not found. All DOPC/DOPS-LUVs had larger diameters in the presence of M1 (see Figure 25), even when the surface theoretically could not be completely covered by M1. This would have been the case for samples where 30 nM and 0.3 µM M1 were used. Two possible explanations could explain these

data. First, M1 induced vesicle clustering. Second, oligomers of M1 on the membrane could be responsible for the dramatic size change. Figure 25 summarizes the data obtained for the hydrodynamic diameter of the LUVs in presence of M1.

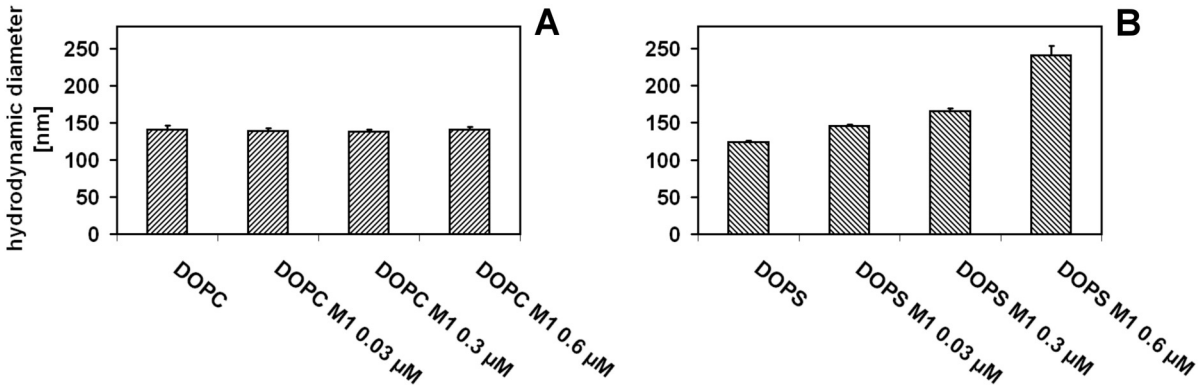

Figure 25 Dynamic light scattering measurements for LUVs in absence and presence of M1. DOPC- and DOPC/DOPS-LUVs were analyzed in presence of 0.03, 0.3, and 0.6 µM M1 (A) DOPC-LUVs showed no changes in diameter size when M1 was present. (B) DOPC/DOPS-LUVs in presence of M1. LUV composition: DOPC = pure DOPC, DOPC/DOPS = 4:1. The temperature in the samples was 20 °C.

Cryo-electron microscopy was performed on DOPC/DOPS-LUVs in absence and presence of M1. The samples were prepared at similar protein to lipid ratios that were used in the DLS experiments. The vesicles without M1 showed a size distribution of 123 ± 27 nm (Figure 26 A). The size was measured in the cryo-electron microscopic images. The thickness of the membrane was measured as well and the value was 7.1 ± 0.1 nm. The analysis of images where M1 was present showed no differences to images taken for samples without M1. M1 was not visible on the membrane (Figure 26 B). As a control for M1 association DOPC/DOGS-LUVs were employed. These LUVs contain a lipid analogue with a Ni-NTA equivalent headgroup. The N-terminal His-tag of M1 binds to this molecule with high affinity. This could be shown with GUVs (see Figure 27 J). DOPC/DOGS-LUVs also showed no visible M1 on the surface.

To check whether M1 alone could be observed, solutions of M1 were analyzed in absence of LUVs. For these experiments a negative staining procedure with phosphotungstic acid was performed to enhance the contrast for transmission electron microscopic imaging. The concentrations of M1 were 2.8, 0.6, and 0.2 µM. The acquired images revealed rod shaped particles (Figure 26 C and D). The amount of visible particles decreased when lower concentrated M1 solutions were analyzed. Thus, it could be concluded that these particles were formed by M1 oligomers.

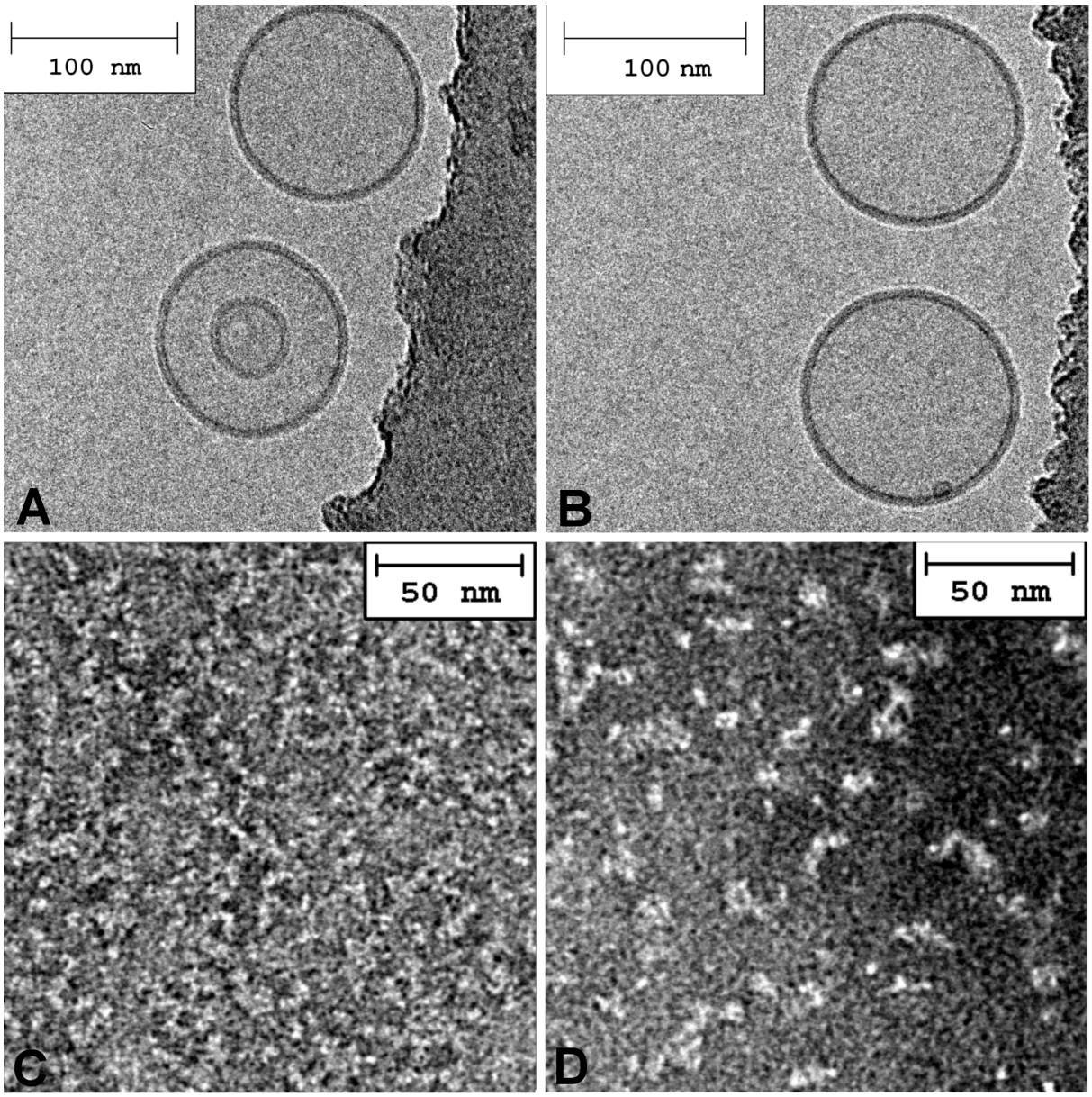

Figure 26 Cryo- and transmission electron microscopy of M1 and LUVs. (A) Cryo-electron microscopic images of DOPC/DOPS-LUVs in the absence and (B) in presence of M1. (C) Image of M1 oligomers. This image was derived from 2.8 µM M1 in Mops buffer. (D) M1 oligomers of a 0.6 µM dilution. LUV composition: DOPC = pure DOPC, DOPC/DOPS = 4:1

4.4.2 M1 clusters on anionic GUVs

GUVs were used as model membranes for the microscopic analysis of the lateral organization of M1 on membranes. GUVs were mixed with FITC-labeled Annexin V, TAMRA-labeled α-Synuclein and TMR-labeled M1 with C2S modification, incubated for 30 min and analyzed by confocal microscopy. The proteins Annexin V and α-Synuclein were used as controls for the presence of anionic lipids in the membrane of GUVs and as reference for membrane bind-

ing of labeled M1 and NM1. Homogeneous coverage of these two proteins on anionic GUVs was shown by Stöckl *et al.*[138]. No protein binding could be observed on DOPC-GUVs.

Annexin V and α-Synuclein bound to DOPC/PI3P-, DOPC/PI4P-, DOPC/DOPG-, DOPC/DOPA- (data not shown), and DOPC/DOPS-GUVs (Figure 27 K and L). The fluorescence of Annexin V and α-Synuclein was homogeneously distributed on the GUVs. GUVs that contained only DOPC showed no association of M1 (Figure 27 A). GUVs with the lipid analogue DOGS were used as positive binding control for M1 attachment in this system. DOGS carried a Ni-NTA headgroup which functioned as a binding site for the His-tag of the recombinant M1. A detectable amount of M1 bound to these GUVs. DOPC/DOPS-GUVs with a DOPS content of 30 % showed a significant amount of bound M1. DOPS at a concentration of 40 % and 50 % was also tested and showed similar binding of M1 (data not shown). DOPC/PI3P- and DOPC/PI4P-GUVs were also tested, but only small M1 clusters were observed on GUVs with PI3P (Figure 27 E) whereas significant amounts of M1 could be detected on DOPC/PI4P-GUVs (Figure 27 F). Small clusters and in rare cases faint homogeneous distributed M1 were observed for vesicles with 5 – 10 mol% PI4P. Furthermore, the negatively charged lipids DOPG and DOPA were tested in this system. An association of M1 to GUVs with these lipids was observed (Figure 27 C and D). DOPC/DOPG-GUVs showed mostly homogeneous distribution of M1 in addition to M1 clusters. Fluorescence of TMR-labeled M1 was only detected as patches on the GUVs' surface. Similar M1 clusters were observed for GUVs containing DOPS and DOPA.

Closer inspection of the morphology of these clusters revealed that the majority appeared as a layer of homogeneous thickness within the optical resolution of the used microscope. Flake like clusters or sometimes tubulated membranes with bound M1 were only rarely observed. M1 was not responsible for the formation of tubular membranes, since vesicles without bound M1 also exhibited similar membrane protuberances.

Binding of TMR-NM1 to DOPC- and DOPC/DOPG-GUVs was not observed (not shown). Clusters of TMR-NM1 comparable to those of M1 appeared on the surface of DOPC/DOPA-, DOPC/PI4P- (not shown), DOPC/DOGS-, and DOPC/DOPS-GUVs (Figure 27 I, J).

The data for M1 were consistent with data that were acquired with LUVs. Here, DOPG and DOPA could be identified as additional binding partners for M1 and NM1. The clustering of M1 and NM1 was a consistent phenomenon for several variants of GUVs. This indicated a lateral oligomerization process of M1 and NM1 on the membranes.

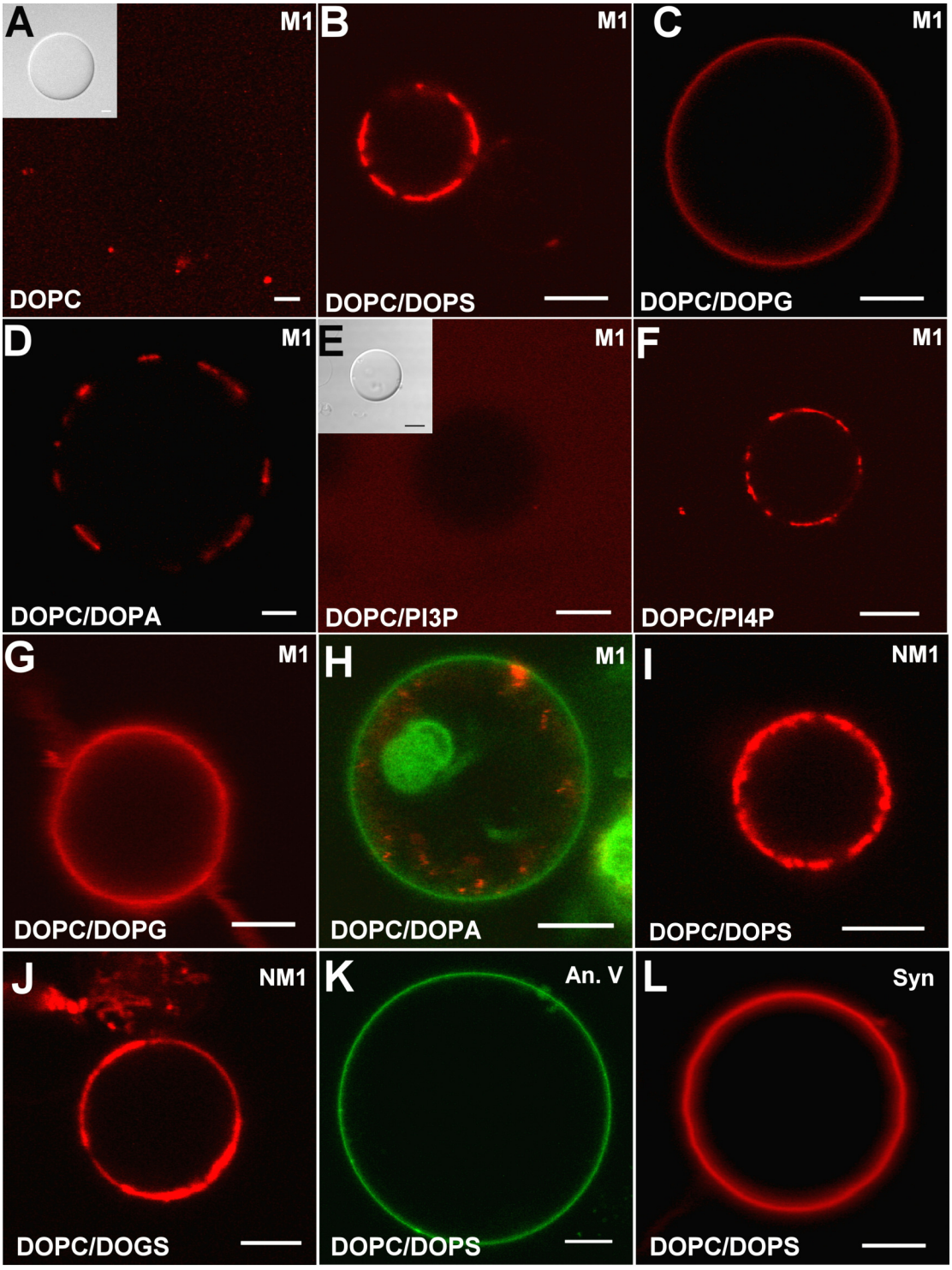

Figure 27 M1-clustering on anionic membranes. GUVs were prepared by electroswelling and harvested. TMR-M1 or TMR-NM1 were diluted to 0.1 µM in microscopy buffer or 1x binding buffer. Five µl GUVs and 45 µl of buffer with TMR-M1/TMR-NM1 were mixed, incubated for 30 min at 25 °C and analyzed microscopically. (A) M1 with DOPC-GUVs, (B) M1 with DOPC/DOPS-GUVs, (C) M1 with DOPC/DOPG-GUVs, (D) M1 with DOPC/DOPA-GUVs, (E) M1 with DOPC/PI3P-GUVs, (F) M1 with DOPC/PI4P-GUVs, (G) unusual M1 clusters perturbing from DOPC/DOPG-GUVs, (H) unusual M1 clusters within DOPC/DOPA-GUVs (in green: C_6-NBD-PS in the GUV membrane) (I) NM1 with DOPC/DOPS-GUVs (J) NM1 clusters on a DOPC/DOGS-GUV. FITC-Annexin V (K) and TAMRA-labeled α-Synuclein (L) were used as reference. The composition of the GUVs was: DOPC/DOPS = 7:3, DOPC/DOPG = 7:3, DOPC/DOPA = 7:3, DOPC/PI3P = 9:1, DOPC/PI4P = 9:1, DOPC/DOGS = 9:1. Calibration bar = 5 µm. T = 24 °C.

4.4.3 NM1 clusters consist of a rigid network

The organization of the NM1 clusters was assessed by FRAP. This method allows the monitoring of the organization of molecules on surfaces. It is based on the diffusion of fluorescent molecules. When a spot in the fluorescent sample is bleached and the fluorescent molecules are able to diffuse, then the fluorescence within the bleached spot recovers. The recovery is due to the diffusion of unbleached fluorescent molecules into the formerly bleached spot. FITC-labeled Annexin V as well as TAMRA-labeled α-Synuclein were used as controls in these FRAP experiments. When FRAP was applied to FITC-labeled Annexin V, a lateral movement of Annexin V was observed, since a fluorescence recovery was measured after bleaching of FITC-labeled Annexing V. α-Synuclein also showed fluorescence recovery on unlabeled vesicles. In addition, NM1-clusters on unlabeled GUVs were analyzed. No recovery of TMR fluorescence could be observed in the bleached spot after bleaching of the TMR-label on NM1 (see Figure 28) and monitoring of the fluorescence intensity for up to 2 min. Based on this and the microscopically recorded clusters of M1, the conclusion can be drawn, that M1 formed non-diffusible oligomers on the surface of the GUVs. This indicated an inhibition of lateral movement of the NM1 molecules.

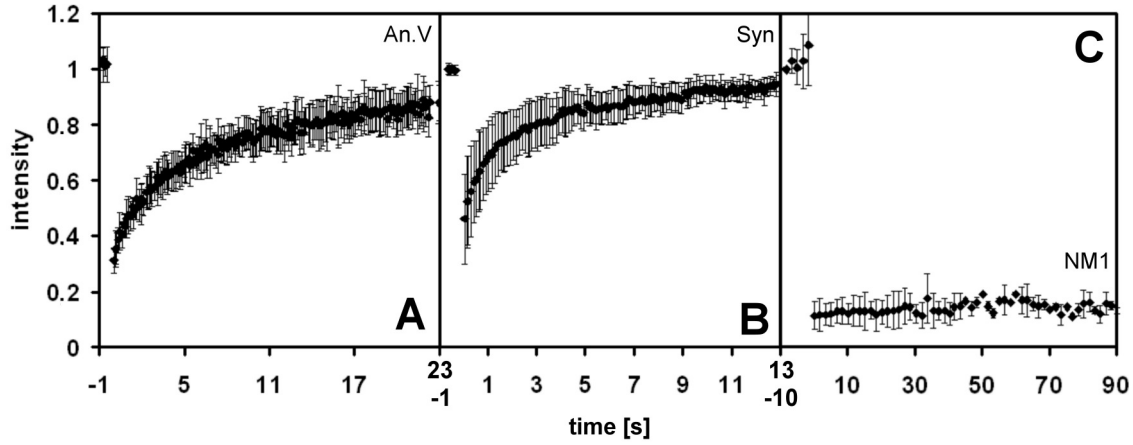

Figure 28 Normalized intensity profiles for the fluorescence recovery after photobleaching of FITC-labeled Annexin V (A), TAMRA-labeled α-Synuclein (B) and TMR-labeled NM1 (C). Annexin was diluted 500-fold in 1x binding buffer. Synuclein was used at a final concentration of 0.1 µM and NM1 also at 0.1 µM in 1x binding buffer or microscopy buffer. Forty-five µl of protein solution were mixed with 5 µl GUVs incubated for at least 10 min and analyzed. Two regions of interest were assigned. The intensity was recorded before bleaching of one region. The intensity was monitored for the indicated time period. Normalization was performed by defining the first recorded intensity value before bleaching as 1. Mean values and standard deviation of eight (Annexin V and α-Synuclein) and six (NM1) measurements are presented. The composition of GUVs was DOPC/DOPS = 7:3. The temperature in the microscopy room was set to 24 °C.

This indication was further supported by the calculated values for the mobile fractions (MF_P) of the proteins. MF_P was calculated according to equation (3). The calculated values allowed the approximation of the amount of mobile fluorophore. A MF_P of 0.82 ± 0.1 (n = 8) was calculated for FITC-Annexin V, 0.87 ± 0.06 (n = 8) for α-Synuclein and 0.02 ± 0.03 (n = 6) for TMR-NM1. Thus, at least 82 % of all fluorescent Annexin V and 87 % of the α-Synuclein were mobile within the measuring interval. In contrast, the MF_P value of NM1-TMR led to the conclusion that here only 2 % was freely mobile. In summary, the data prove the intrinsic clustering behavior of NM1 on the membrane.

4.4.4 The NM1 clusters do not influence lateral lipid movement

The direct interaction of the proteins with the lipids was analyzed by an alternative FRAP approach. The working hypothesis here was that protein bound lipids should have diffused slower than free lipids. Use of C_6-NBD-PS labeled vesicles allowed the surveillance of the lipid diffusion behavior in presence of NM1 and α-Synuclein. FRAP was performed on vesicles where no protein was added to estimate the lateral diffusion of the fluorescent lipid analogue C_6-NBD-PS. Therefore two different areas of one GUV were selected. One spot was bleached, the other was not. The fluorescence intensity was recorded for ten seconds after the bleaching pulse of the laser. When FRAP was performed in absence of protein the fluorescence intensity in the bleached spot recovered within ten seconds to at least 90 % of the intensity in the unbleached spot (Figure 29 A). FRAP on C_6-NBD-PS in the presence of a homogeneous distributed α-Synuclein revealed no significant effect of the bound protein on the lateral movement of the lipids. The recovery in the bleached spot was also at least 90 % compared to the unbleached spot (see Figure 29 D). The fluorescence recovery also reached 90 % when NM1-TMR was present (Figure 29 B and E). This indicated a free lateral diffusion of C_6-NBD-PS in the membranes of the GUVs, when NM1 was present on the surface of the GUV.

An additional FRAP experiment was performed to evaluate the influence of the NM1 clusters on C_6-NBD-PS in an area of the GUV were NM1 was visible and an area where no NM1 was detected. This was done to analyze the behavior of the lipids in the proximity of the protein cluster. The recorded intensity profiles of the area with protein cluster (Figure 29 E) showed no significant difference in the intensity profile compared to the area without protein cluster (Figure 29 B). Therefore, it could be concluded that NM1 had no effect on the lateral move-

ment of the C_6-NBD-PS in the area where a cluster was present. Nevertheless, the recorded fluorescent images revealed a lateral enrichment of C_6-NBD-PS in areas were NM1 clusters were present (Figure 29 C and F).

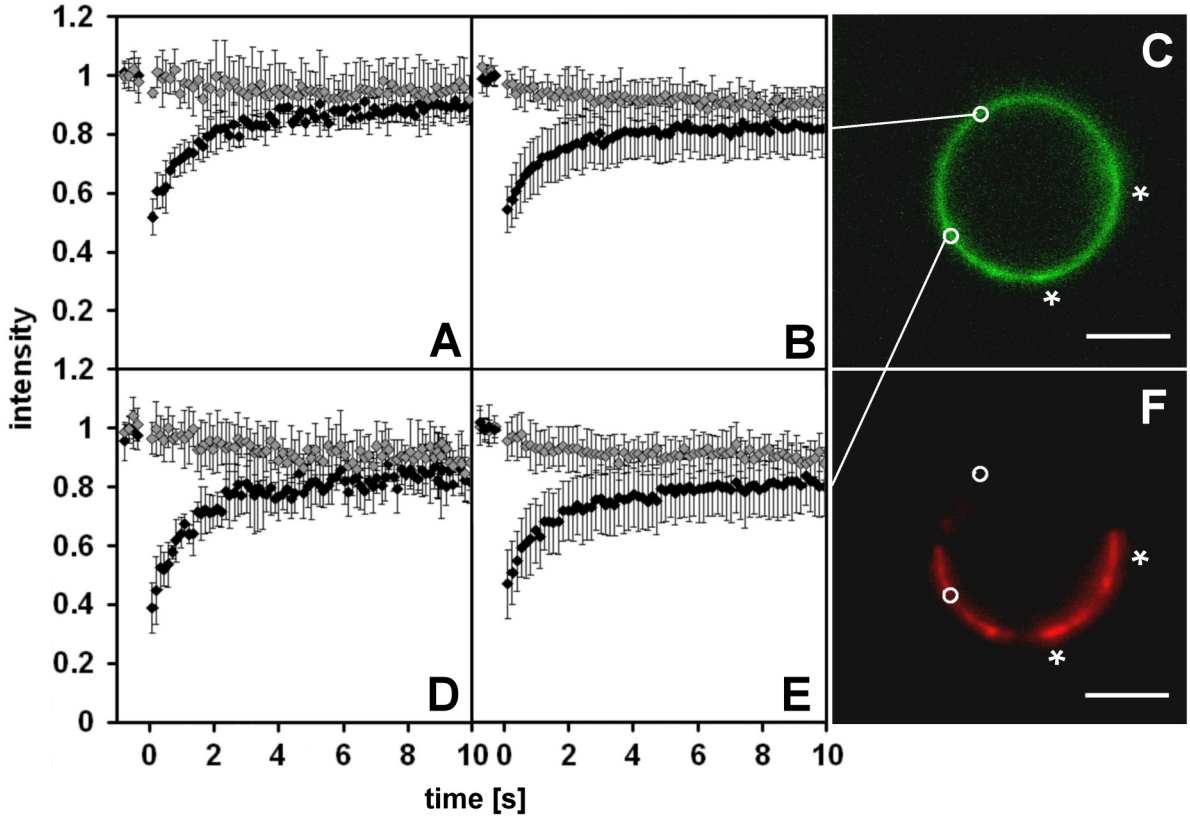

Figure 29 FRAP profiles of C_6-NBD-PS without protein (A) and in the presence of α-Synuclein (D), an area without NM1-cluster (B), and an area with NM1 (E). (C) Green fluorescence of C_6-NBD-PS (confocal fluorescence microscopy image). (F) Red fluorescence of NM1-TMR (confocal fluorescence microscopy image). ● = Intensity of the bleached spot, ● = Intensity of the unbleached spot. Asterisks highlight areas were C_6-NBD-PS was enriched and NM1-clusters were present. C_6-NBD-PS was added in 1mol% concentration to the lipids prior to lipid film formation and electroswelling of the GUVs. The calibration bar represents 5 µm. The composition of GUVs was DOPC/DOPS = 7:3. The temperature in the microscopy room was 24 °C.

The fluorescence intensity time curves were analyzed for the mobile fraction of fluorescent lipids (MF_L). Intensity values, taken in the last second of the measurement, from bleached (F_b) and unbleached spot (F_u) were averaged and used in equation (4) to calculate the mobile fraction (Table 5). F_u represents the maximal extent of recovery and could therefore be used as parameter for the total mobile fraction of fluorophores.

MF_L can be used to describe the extent of the recovery. Differences in the calculated values would indicate different lateral diffusion velocities of the lipids induced by the presence of

proteins. As controls, lipid movement was analyzed for samples without proteins and bound α-Synuclein. MF_L was also calculated for the motion of C_6-NBD-PS in an area where a protein cluster was present as well as without a cluster on the same GUV. MF_L showed no significant differences for all treatments. The visible enrichment of C_6-NBD-PS in an area where a NM1-cluster was present had not significant influence on the lateral diffusion behavior of this fluorescent lipid analogue.

Table 5 Summary of the calculated values for the approximation of mobile C_6-NBD-PS in presence of NM1 and α-Synuclein.

	MF_L
C_6-NBD-PS	0.93 ± 0.04 (n = 8)
C_6-NBD-PS + α-Synuclein	0.95 ± 0.03 (n = 7)
C_6-NBD-PS – NM1-cluster	0.91 ± 0.06 (n = 14)
C_6-NBD-PS + NM1-cluster	0.89 ± 0.09 (n = 11)

5 Discussion

5.1 The lipid binding of M1

New insights into the membrane binding of the matrix protein M1 of influenza were gained in this study. The hypothesis that M1 could use a specific lipid as binding partner was analyzed via binding assays to LUVs, GUVs, and spotted lipids. The results from these experiments revealed, that M1 was not capable of binding to membranes where no charged headgroups were present. A strong binding was observed for binding partners with positively and predominantly negatively charged headgroups.

Sha and Luo [81] presented a hypothetical model based on their crystal structure of M1 where conformational changes in M1's N-terminal domain exposed hydrophobic areas of M1 upon membrane binding. These exposed areas were considered as the driving force for hydrophobic interactions of M1 with membranes. Since M1 did not show a significant binding to DOPC vesicles and the secondary structure of M1 did not change in presence of DOPC-LUVs (Figure 13 to Figure 15), the hydrophobic interaction with phosphatidylcholine as a headgroup and the lipids' backbone with the fatty acids could be excluded as the major binding partners for M1.

The mixture of DOPC, cholesterol, and sphingomyelin was used to mimic lipid rafts. Such raft domains are the sites of specific protein attachment and clustering. This was shown for GPI-anchored proteins like CD 14 and lyn kinase [52,168,169] and membrane proteins like hemagglutinin with a special conformation of their transmembrane domain [53,170]. Little is known about proteins that attach to lipid domains without a lipid anchor or a specific transmembrane domain. It was shown in several studies that the influenza envelope contained liquid ordered lipid structures that were thought to be derived from lipids rafts [171,172]. Therefore, these microdomains needed to be tested as potential targets of M1 and the results of the flotation experiments indicated no specific targeting and clustering of M1 towards uncharged liquid ordered membrane domains consisting of typical raft lipids. Cholesterol and sphingomyelin were incapable to attract a significant amount of M1 (Figure 13). Furthermore, the saturated acyl chains of DSPS had no visible effect on the membrane binding of M1 compared to DOPS in the flotation assay. The appearance of the liquid ordered domains built of cholesterol and sphingomyelin in the influenza envelope is therefore not the result of direct

M1-lipid interaction. This finding fits into the current model, which is described in detail in the introduction (see chapter 1.2.4), that HA and NA recruit these lipids [115] to the viral membrane.

The finding of positively charged headgroups as binding partner indicated a so far unknown binding mechanism for the interaction of M1 with other cellular components. Positively charged lipid headgroups do not exist in cellular membranes. Other cellular molecules that own a local positive surface charge need to be considered as binding partners of M1. Proteins are the most likely candidates for this kind of interaction.

Representatives of naturally occurring negatively charged headgroups were used during this analysis. PS was a prominent binding partner during all experiments. This is consistent with published data. Ruigrok and coworkers [27,84] showed binding of M1 to PS containing membranes. Other lipids had not been reported for M1 binding yet. The data for M1 interaction with negatively charged lipids, which were collected during this study, revealed for the first time several different types of lipid headgroups as additional binding partners. Table 6 summarizes the negatively charged headgroups where binding of M1 was found.

Table 6 Summary for all negatively charged lipid headgroups which showed attachment of M1 in the different systems. + = binding, – = no binding, n. d. = not determined.

Headgroup	used system			
	PIP-strip – Tween 20	PIP-strip + Tween 20	LUVs	GUVs
Phosphatidylserine	+	–	+	+
Phosphatidylinositol-4-phosphate	+	+	+	+
Phosphatidylinositol-3-phosphate	+	-	+	+
Phosphatidylinositol-5-phosphate	+	-	n. d.	n. d.
Phosphatidic acid	+	+	n. d.	+
Lysophosphatidic acid	+	-	n. d.	n. d.
Phosphatidylinositol-3,4-bisphosphate	+	+	n. d.	n. d.
Phosphatidylinositol-3,5-bisphosphate	+	+	n. d.	n. d.
Phosphatidylinositol-4,5-bisphosphate	+	-	n. d.	n. d.
Phosphatidylinositol-3,4,5-triphosphate	+	-	n. d.	n. d.
Phosphatidylglycerol	n. d.	n. d.	n. d.	+

The binding of M1 to the different negatively charged lipids showed differences depending on the system used for investigation. Tween 20 abolished the M1 association to certain lipids on the PIP strip. Tween 20, as non ionic detergent, is used as emulsifier and solubilizer in biochemical experiments. The function of such a molecule is to reduce the unspecific binding of proteins to target molecules [173,174]. PS was among those lipids whose binding by M1 was

strongly inhibited in presence of Tween 20. A possible conclusion from this binding reduction was that the electrostatic interactions between M1 and PS were abolished. Deduced from this, all other lipids that showed similar binding reduction comparable to PS might have interacted with M1 in the same way. It was proposed earlier that M1 can bind through electrostatic interactions to membrane surfaces. Indeed, this interaction was significantly reduced when the salt concentration (Figure 14) or the pH [27] was changed. This interaction mechanism can now be proposed also for the other Tween 20-sensitive lipid interactions of M1 (see Table 6).

M1 binding was only observed for PI4P, PI34PP, PI35PP, and PA in presence of Tween 20 (Figure 16). This indicated a different interaction process of M1 towards these lipids. This assumption was further supported by the differences in CD spectra obtained with either DOPC/DOPS- or DOPC/PI4P-LUVs. The spectra change depended on the LUV composition in significantly different ways. Less α-helical organized M1 was present with DOPC/DOPS-LUVs compared to DOPC-LUVs whereas more α-helices and helix to helix rearrangements occurred in presence of DOPC/PI4P-LUVs (compare Figure 15 and Figure 17). The PI4P triggered conformational changes in M1 might have led to the detergent resistant binding to PI4P. Whether this binding mechanism is sensitive to salt needs verification.

Based on the results of the flotation experiments, the interaction of M1 with PIP-strips, and the by CD obtained structural information, it can be assumed that M1 binds PI4P in a specific way. This specific interaction goes beyond the electrostatic interaction, proposed earlier by Baudin *et al*. [84] and Arzt *et al.* [83], to the other negatively charged lipids tested.

The current model for the recruitment of M1 to the assembly site of the viral particle can be fine-tuned derived from the obtained data. PI4P might facilitate the association of M1 to the Golgi apparatus, since PI4P is locally enriched at the lipid membranes of the Golgi apparatus (see [175,176] and chapter 1.2.2 for details). M1 interacts there with the cytoplasmic tails of HA, NA, and M2. The transport pathway of HA and NA through the Golgi was shown before as well as the interaction of M1 with the cytoplasmic tails of the three proteins [28,58,75,85,112]. Its further transport might then be facilitated by hitchhiking with the spike proteins on transport vesicles during their passage through the Golgi apparatus to the plasma membrane. The data allow the assumption that a first step in the viral assembly happens at the Golgi membrane. Analysis of fluorescent proteins in a cellular context can provide further knowledge for this issue.

5.2 The lipid binding domain of M1

First attempts to localize the membrane binding domain of M1 were undertaken in the 1980s, where hydrophobic interaction of N-terminal M1 peptides were proposed as the driving force for association to and incorporation into membranes [177]. Sha and Luo [81] also proposed hydrophobic amino acids of the N-terminal part as binding mediators when the first crystal structures became available. Shishkov *et al.* revealed by tritium bombardment studies that N- and C-terminal parts of M1 are in close proximity to the membrane [178] in viral particles. Ruigrok and coworkers [84] performed flotation experiments with deletion mutants where either the 164 N-terminal amino acids or the 88 C-terminal amino acid containing C-terminal peptide were used. The applied liposomes were made of phosphatidylcholine, phosphatidylserine, and cholesterol. M1 and the truncated N-terminal part (1 – 164) showed similar flotation behavior. Both proteins bound to the vesicles and floated. The C-terminal part (165 – 252) could not be detected in the upper fraction of the gradient [84].

5.2.1 The C-terminal domain is a membrane binding domain

A similar flotation system utilizing two additional M1 mutant proteins was used in this study to analyze their membrane binding behavior. The PBS-mutant M1m was only present in significant amounts in the upper gradient fraction (0 %) when DOPC/DOPE/DOPS-LUVs were applied. This indicated that the mutated amino acids of the PBS had no significant influence on the ability of M1 to bind to negatively charged membranes. When NM1 (amino acids 1 to 164 of M1) was floated with DOPC/DOPE/DOPS-LUVs less NM1 was detected in the upper fraction in comparison to M1m. The initial concentration of M1m and NM1 in the high density fraction (30 %) of the gradient prior centrifugation was the same. Different protein amounts in the upper fraction after centrifugation should therefore be the result a reduced affinity of NM1 to lipid membranes. The PBS mutant of the N-terminal part NM1m was not detected in any upper gradient fraction. The mutation of the PBS also abolished the residual membrane binding that was found for NM1. This result is the first direct proof for the function of the PBS as a membrane anchor. The results for NM1 are consistent with published data, where this mutant was capable of binding to PS-containing membranes [84]. There are no data available for comparison of the *in vitro* membrane binding behavior of the PBS mutant M1m. But no difference between the membrane binding of M1 and its PBS mutant was

shown in floatation experiments utilizing disrupted mammalian cells [85]. This indicates further membrane binding sites in M1.

The C-terminal mutant, CM1, bound with significant affinity to DOPC/DOPE/DOPS-LUVs. CM1 was also detected to a small extent in the upper gradient fractions (0%) of the other LUVs tested (Figure 22). The hydrophobic interface in one of the α-helices might explain this behavior (Supplementary Figure 3). This interface could be shielded in the full length protein, since detectable binding to uncharged vesicle was only observed for CM1. The data reveal that the C-terminal part of M1 is also capable of associating with negatively charged membranes. The CD measurements further support an interaction of the C-terminus of M1 with negatively charged membranes. Only M1, M1m, and CM1 showed structural changes in presence of DOPC/DOPS-LUVs in comparison to DOPC-LUVs (Figure 23). Actually, the finding that CM1 binds to phoshatidylserine-containing membranes is indicated by its amino acid sequence. Ten basic amino acids can be found within the 88 amino acid peptide (Supplementary Figure 3). Although the structure of this M1 part is not yet known, it is reasonable that a peptide with a theoretical pI of 9.4 would interact with a PS-containing negatively charged membrane at pH 7.

The appearance of the C-terminal part of M1 in close proximity to the viral membrane was shown by tritium bombardment of viral particles [178,179] and by partial bromelain digestion of M1 [166]. The binding of CM1 to DOPC/DOPE/DOPS-LUVs conflicts with the published data of Baudin *et al*. [84]. Baudin and coworkers could not detect their C-terminal M1 mutant protein in the upper fractions of their used gradient system. The difference in the experimental setup could be the reason because in the presented work a system based on silver staining was used which is much more sensitive compared to Coomassie as it was used by Baudin *et al*.

Based on these new insights into the membrane binding of mutant M1, it can be concluded that the PBS as well as the C-terminal part of M1 enable membrane association (see Figure 30). This was shown when the PBS mutant M1m was found at the membrane but not the N-terminal PBS mutant NM1m. In addition, the C-terminal part alone was also capable of binding to LUVs.

In summary, these data additionally emphasize the role of the NLS in the reproduction cycle of the influenza virus. The essential function of this amino acid sequence was shown before. The production of infectious viral particles was significantly reduced when this motif was mutated [79,180]. Two functions have been postulated for the NLS. First, the transport of

newly synthesized M1 into the nucleus of the infected cell [32,181] and second, the association to negatively charged membranes via electrostatic interaction [27,83,84]. A mutation of the PBS including the substitution of the NLS would abolish both functions in the N-terminal part of M1. This study revealed precisely the membrane binding function of the PBS as it clearly showed that NM1m was not able to bind DOPC/DOPS-LUVs.

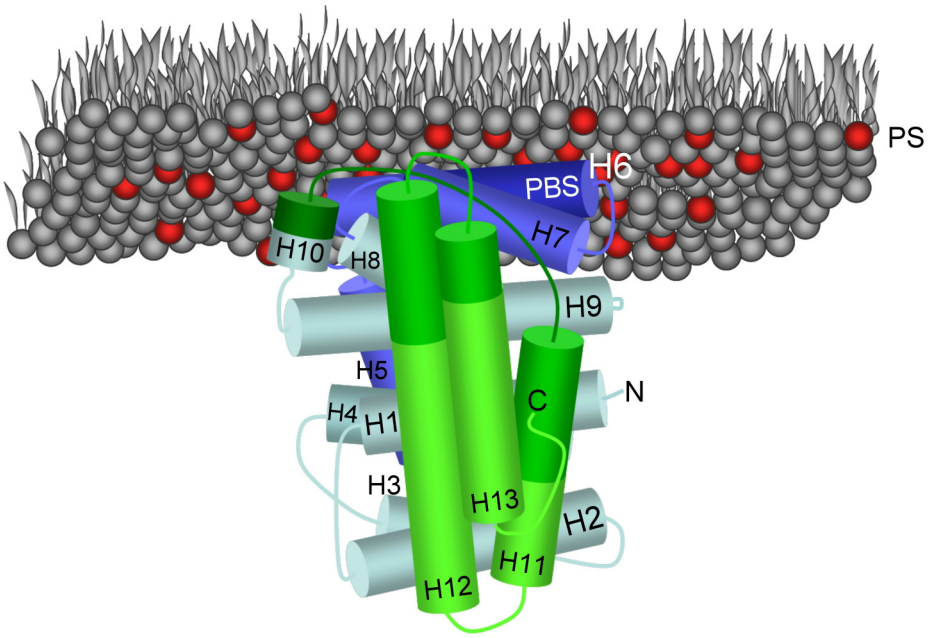

Figure 30 Model of the M1 interaction with PS containing membranes. The presented protein structure is based on data published by Shishkov *et al.*[179]. The tubes represent the α-helices of M1. The N-terminal part of M1 (blue) contains the PBS on helix 6. The C-terminal part is shown in green. As darker the color as higher is the probability of membrane association of the respective M1 part.

The role of the C-terminal part needs further analysis since structural changes occur here upon membrane association. The calculation of the α-helical content revealed a loss of helical organized amino acids in the bound state that was not seen when uncharged vesicles were present. NMR studies on CM1 could elucidate the helical organization of the peptide and the orientation of particular amino acids towards the membrane. The C-terminal part of M1 contains several additional basic amino acids. The structure of this part was not yet crystallized. CD measurements [82] and modeling based on tritium bombardment [178,179] revealed that this M1 part consists of α-helical and unstructured regions (Supplementary Figure 3). The potential of this part of M1 for membrane interaction is not yet fully understood but the reported experiments on negatively charged LUVs prove that the C-terminal part of M1 is involved in membrane binding of M1 (Figure 30).

5.2.2 NM1 has a PI4P binding site

The FRET measurements of NM1 in presence of DOPC/PI4P- and DOPC/PI3P-LUVs showed results equivalent to the FRET measurements with M1 (Figure 19 and Figure 24). This result indicates a function of NM1 in the recognition and binding of M1 to PI4P. The C-terminal part of M1 alone seems to be not essential for efficient binding to PS and PI4P. The PBS might drive membrane binding mediated by electrostatic interactions. But when only electrostatic interactions play a role, a FRET signal for PI3P- and PI4P-containing vesicles should be detected to similar extents. This was not the case. Clearly, a higher FRET signal for M1 as well as NM1 in presence of DOPC/PI4P-LUVs was detected (Figure 19 and Figure 24). A similar binding behavior could be shown in flotation and PIP strip experiments for M1 (Figure 16).

The physiologic relevance for this interaction can be discussed in close connection to the published data, where the N-terminal part of M1 was identified as a membrane binding domain [27,84]. The involvement of the PBS in PI4P binding of M1 and NM1 is not clear. However, the published data for other PI binding proteins [175,182,183,184] (see chapter 5.2.3) indicate an involvement of the polybasic sequence of NM1. Further experiments including the N-terminal PBS mutant NM1m could clarify this issue. If the NLS was also responsible for the PI4P binding of M1 and particularly NM1, the effects of its mutation will result in a further loss of function. Beside the deletion of the nuclear localization and the electrostatic interaction site a disruption of the PI4P binding site might also lead to misrouting of M1 in the cell and thereby to nonviable viral particles.

5.2.3 PI binding proteins – a comparison to M1

We do not know the precise mechanism of the interaction of M1 with PI4P. Therefore it might be helpful to look at other proteins. Binding to PI was also shown for other viral matrix proteins. The HIV Gag protein interacts specifically with PI45PP. PI45PP is anchored to the N-terminal matrix domain of Gag by electrostatic interactions between the PI45PP headgroup to a basic surface patch of the matrix domain and the insertion of the 2'-fatty acid chain of PI45PP into a hydrophobic groove of the protein [182]. Conformational changes occur in Gag upon PI45PP binding. These rearrangements lead to the exposure of the sequestered myristyl group [182,185] which incorporates into the plasma membrane of the infected host cell. The myristate is a result of posttranslational acylation of Gag [186]. A similar membrane associa-

tion was proposed for the Gag protein of murine leukemia virus [187]. This so-called myristyl switch cannot explain the association of M1 to membranes since M1 is not acylated [166], and M1 bound with highest affinity to PI4P in presence of Tween 20.

Analysis of other cellular PI binding proteins without acylations revealed that two structural elements were present in proteins with specific interaction to PI. The PI binding protein Pf1 contains the poly basic sequence –**RRKKR**EQ**KK**– [188]. A similar patch of positively charged amino acids was found with the polybasic sequence 95-**K**AV**K**LY**RK**L**KR**–105 in M1 (basic amino acid residues in bold letters, see Figure 20 and Figure 32).

A zinc finger motif was published to be the second structural element in Pf1 which is necessary for membrane binding [188]. A similar zinc finger motif was present in the amino acid sequence 148-**C**AT**C**EQIADSQ**H**RS**H**-162 (amino acids of the zinc finger in bold letter, see Figure 32) of M1 [79]. This strongly indicated that these two elements were responsible for the PI binding in both proteins. Specificity to PI3P was shown for Pf1. This specificity was mediated by the polybasic sequence [188]. Since the polybasic sequences differ between Pf1 and M1, this could explain the preference of M1 for PI4P.

Proteins with binding to specific PIs localize in defined intracellular membranes. Early endosome antigen 1 (EEA1) was localized preferentially at early endosomal membranes. The early endosomal membranes were found to be enriched in PI3P [189] and specific binding of EEA1 to PI3P was shown. The FYVE domain of EEA1 was identified as binding site for PI3P [190]. This domain showed a zinc finger motif as a prominent feature [191]. It needs to be investigated, whether the zinc finger motif of M1 has a similar function towards PI4P as the FYVE domain of EEA1 has towards PI3P.

EpsinR was specifically recruited to the Golgi by its interaction with PI4P [175]. PI4P was shown to be enriched in the Golgi membranes [176]. The ENTH domain of EpsinR mediated the specific binding of the protein to PI4P. Mutation of the ENTH domain led to a significant reduced PI4P binding [175]. Analysis of the surface electrostatic potential of the ENTH domain revealed a local enrichment of positively charged amino acid residues on the protein surface. This area was proposed to be the binding pocket for PI4P [175]. Comparison of the global structure of the first 164 amino acids of epsinR to the first 164 amino acids of M1 revealed that both proteins share structural similarities (Figure 31). They are composed of α-helices which build a compact brick shaped structure. Furthermore, both proteins show surface exposed positively charged areas.

Differences can be seen beside these similarities. For instance, the positively charged areas differ in composition and size. The proposed PI4P binding site of epsinR consists of densely packed basic amino acids that build a binding grove. The polybasic patch of M1 is not only less densely packed, but it also forms a convex structure rather than a grove. These differences can result from the absence of PI4P as binding partner during the crystallization of the published M1 part.

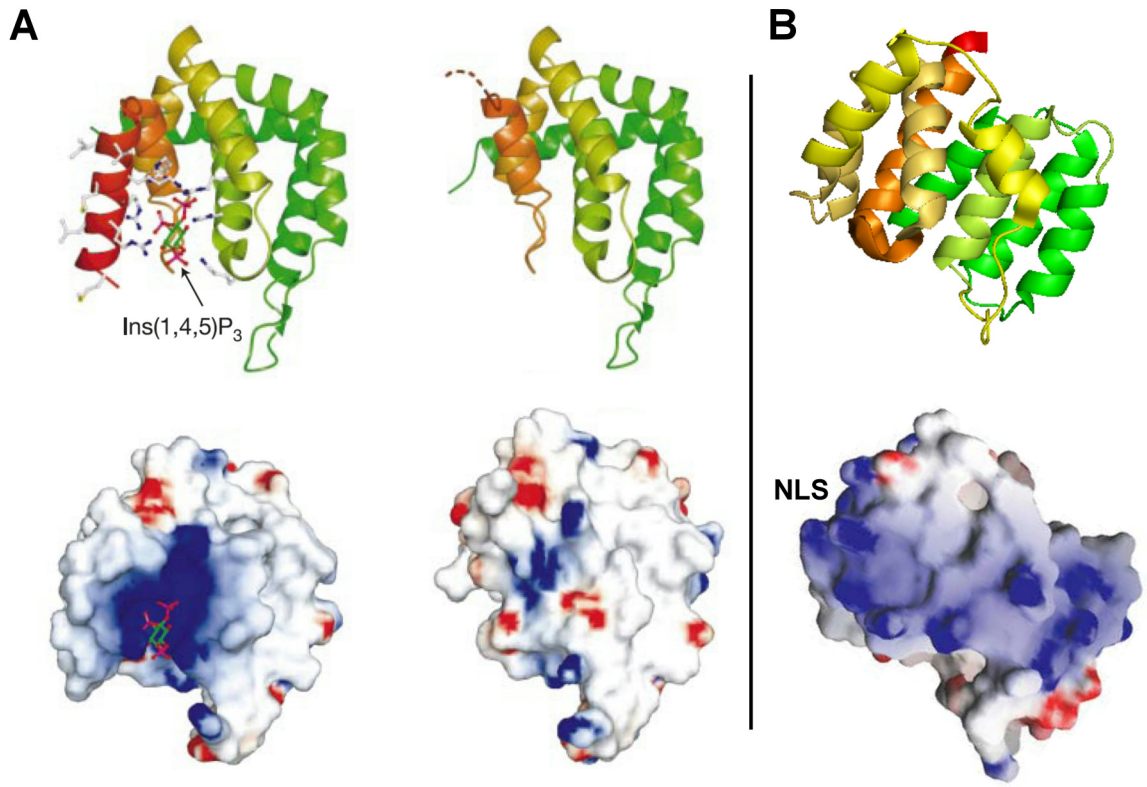

Figure 31 Surface structures of epsin1 and M1. (A) Epsin1 with and without phosphatidylinositol-1,4,5-triphosphate. (B) Surface model of M1. The figure shows the putative structures of epsin1 and M1 in the upper panel. The lower panel depicts the surface potential maps of epsin1 and M1. Negatively charged amino acids are depicted in red (-10 kT e^{-1}) and positive charges are shown in blue (10 kT e^{-1}). The epsin structures were taken from [183]. The structures of M1 were computed from the pdb file 1EA3 of M1 that was published in [82].

A two-step process was shown for the binding to PI145PPP of the epsinR homologue epsin1 [183]. This protein binds to the membrane via electrostatic interactions in the first step. The formation of an additional α-helix comprises the second step. This rearrangement leads to the specific binding groove for PI145PPP (see Figure 31) and insertion of an amphipathic helix into the membrane [184]. The complex inserted into the membrane was visualized by electron microscopy [184]. M1 also showed rearrangements in its secondary structure when it bound to PI4P containing vesicles. The analysis of the CD measurement revealed a gain of α-

helically organized amino acids. This finding is similar to the rearrangement in epsin1 upon its interaction with PI145PPP containing vesicles, even though it is not known yet which amino acids rearrange in M1. First measurements revealed that the Trp (W45, see Figure 32) containing region of M1 does not interact with membranes. For this region can be assumed that insertion of M1 parts into a lipid membrane do not occur, as it was the case for the epsins. This was shown experimentally when FRET was not acquired between M1s Trp and N-NBD-DPPE in LUVs. Furthermore, the fluorescence emission maximum of M1s Trp was not altered. This indicates that at least this region of the N-terminal M1 part is not attached to or inserted into the membrane (see Figure 18).

Taken together, all these facts allow the hypothesis of a comparable binding mechanism between M1 and the an ENTH domain containing epsins. Crystallization of M1 with bound PI4P could provide proof for this speculation. The interplay of PI4P with parts of M1 especially the PBS and the zinc finger motif needs to be analyzed in more detail by usage of the M1 mutant proteins NM1m and CM1. It can be hypothesized that the NLS and the zinc finger motif of M1 play a significant role during membrane binding to PI4P.

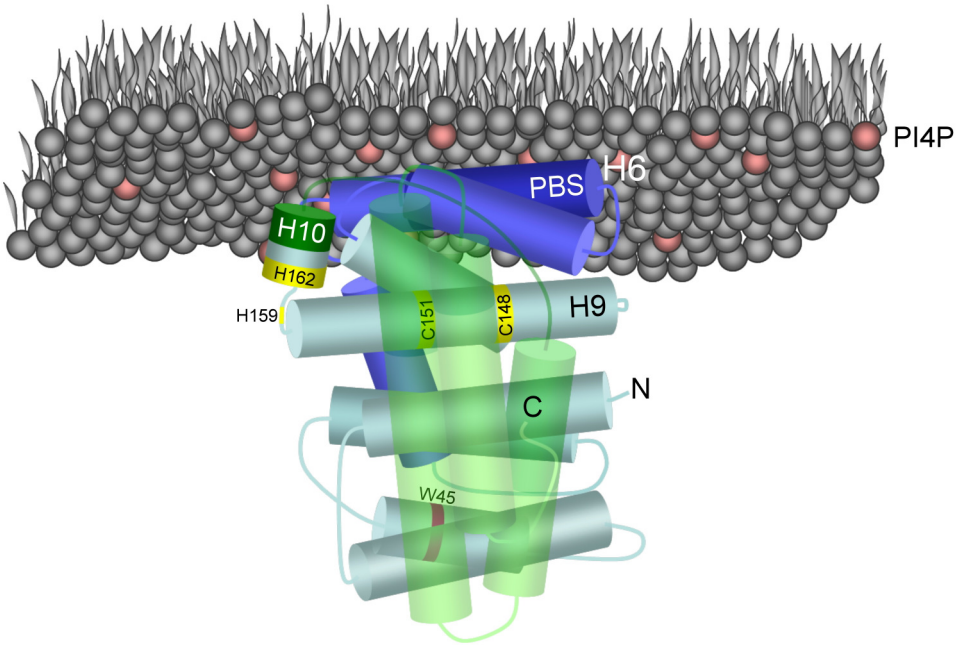

Figure 32 Model of M1's interaction with PI4P containing membranes. The N-terminal domain of M1 (blue) with the PBS (dark blue) and the residues of the zinc finger motif (yellow). H10 forms a linker helix between N-terminal and C-terminal (green) part of M1. At least the helices H6, H9, and H10 have to rearrange for the formation of the specific binding site for PI4P. The single Trp of M1 (W45, purple) is located at the part of M1 that does not interact with the membrane.

5.3 The lateral organization of M1 on membranes

The organization of M1 on the membrane was assessed by cryo-electron microscopy already in the early 1980s. It revealed a spot-like distribution of 8 nm particles on artificial vesicles [192]. Later on fluorescently labeled M1 was analyzed in the cellular context. These experiments provided information about the inner cellular localization of M1 in the nucleus and indicated membranes of ER and Golgi apparatus as targets [58,85]. M1 was not yet analyzed by fluorescence microscopy on artificial membranes that mimic the plasma membrane.

5.3.1 M1 can form viral assembly platforms on membranes

The use of LUVs provided a tool to measure the size of the membrane attached M1 layer by dynamic light scattering (Figure 25). Based on the assumption of homogeneous M1 distribution a size increase of approximately 12 nm should have been measured for model vesicles containing the M1 target phosphatidylserine. The measured values significantly exceeded this approximation and indicated the attachment of M1 structures larger than 12 nm or vesicle clustering. Cryo-electron microscopy of DOPC/DOPS-LUVs in presence of M1 showed no vesicle aggregation (Figure 26 B). But M1 was also not visible. The reason for this invisibility of M1 might have been the low contrast of the protein in this method. Staining methods [193], especially designed for cryo-electron microscopy, can circumvent this issue. Electron microscopy of negative stained purified M1 revealed pearl chain-like M1 oligomers up to 50 nm length in the preparation (Figure 26 C and D). Attachment of these oligomers might have induced the increased particle size in the DLS samples.

Oligomerization of M1 without other viral components has been shown [27,84]. 3D modeling based on the crystal structure of the N-terminal part of M1 assumed a sheet formation of the oligomers [82] or a structure similar to a compressed corkscrew made from a ribbon of pearl chain like organized M1 [68]. Similar oligomers might have been the reason for the size increase of the analyzed DOPC/DOPS-LUVs.

GUVs were also analyzed for the recruitment of M1. Fluorescently labeled M1 could be detected on the surface of all negatively charged unilamellar liposomes. The attached M1 was not homogeneously distributed. It formed clusters with lateral diameters in the micrometer range which did not spread over the complete GUV surface. The extension of the clusters was limited but not restricted to a particular shape or size. Similar clusters were recorded for fluo-

rescently labeled NM1 (Figure 27). These M1 and NM1 clusters were not able to initiate membrane tubules. The clusters showed a predominantly flat laterally restricted constitution. Clusters with an inbound extension were rarely observed. These extensions did not colocalize with fluorescently labeled membrane components (Figure 27H).

A hypothetical model (see Figure 33) for the organization of the M1 oligomers on the surface of the GUVs can be developed based on the reported data on M1 oligomerization and the attachment to negatively charged membranes. It can be assumed that the observed clusters are composed of M1 arranged into a helical oligomer. This assumption is based on electron micrographs where such structures were found in preparations of M1 from disrupted virus [27] and 3D-modeling of the crystal structure [68].

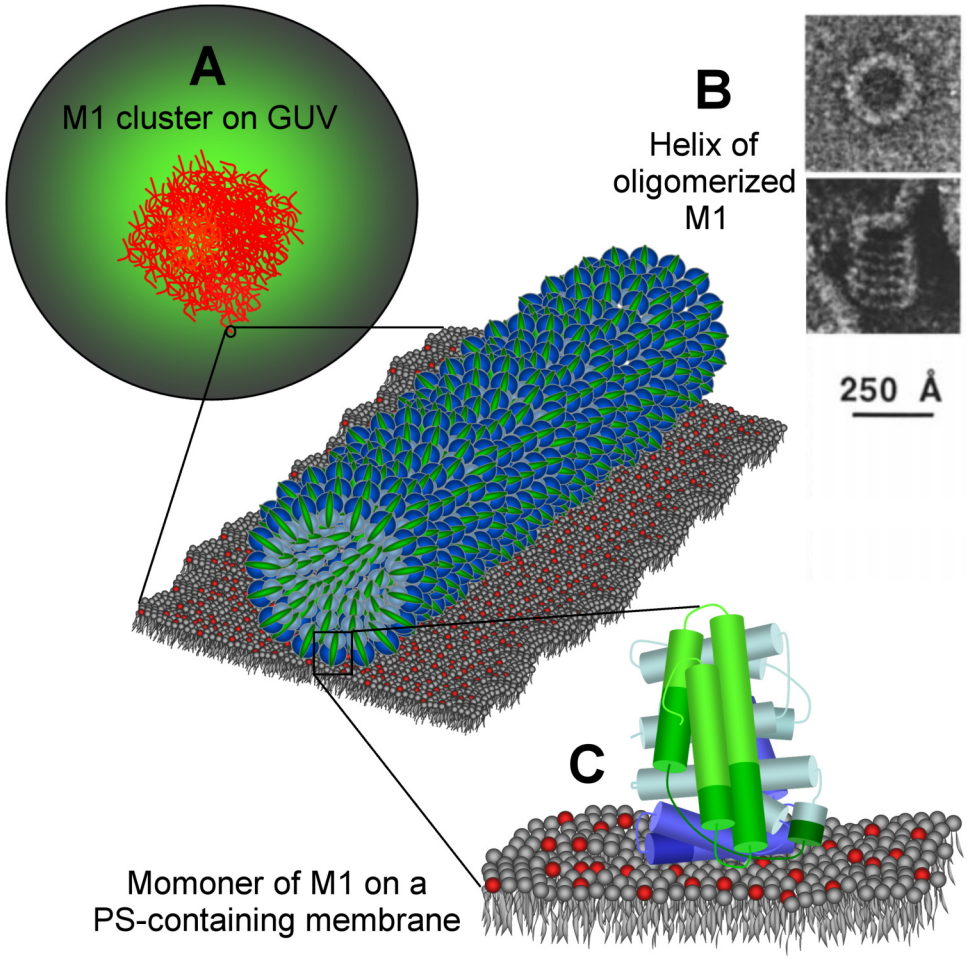

Figure 33 Hypothetical organization of the M1 clusters on the surface of GUVs. (A) Cluster of M1 on the surface of a GUV. The subunits of the cluster are not to scale. Single oligomers could not be resolved. (B) Helical arrangement of oligomerized M1. The model of the helix is based on the electron micrographs presented in [27]. The N-terminal part of M1 is presented in blue and the C-terminal part in green. (C) M1 monomer attached to a PS-containing membrane.

The inability of M1 alone to induce formation of VLPs from the host membrane has been published. No sufficient budding of M1 containing particles was observed when M1 was expressed alone in the cell in a nontoxic system [69,75]. The interaction with cytoplasmic tails of HA, NA, and the M2 protein was necessary for the incorporation of M1 into the VLPs [26,28,75].

The composition of the NM1 clusters was assessed by FRAP experiments. The results revealed a rigid network of NM1 molecules as a cluster fundament, since there was no fluorescence recovery observed in the bleached spot. Such a rigid molecule meshwork can also be assumed for the full length protein M1, since the observed clusters had a similar constitution on the membranes (Figure 27).

An hypothesis has been proposed that M1-HA or M1-NA heterodimers are brought together by homooligomerization of M1 [51,62,115,194]. The results from the confocal microscopy studies on M1 and NM1 give the first experimental data that show that M1 and its N-terminal domain are indeed capable of oligomerizing on target membranes. M1 interacts specifically with the cytoplasmic tails of the viral membrane proteins HA, NA, M2. A lateral oligomerization of M1, as it was shown on the surface of GUVs, could cross-link the spike proteins at a specific place on the membrane. The appearance of the resulting membrane-protein particles was shown by electron microscopy of viruses and VLPs. A spherical structure was always observed when virus-like particles were produced, either with or without M1 [75,76]. The oligomerization status of M1 was not assessed. Recently, a highly ordered helical M1 oligomer was shown to be the structural fundament for filamentous influenza particles [20].

5.3.2 M1s N-terminal domain does not assemble the viral lipids

The direct interaction of M1 or its proposed N-terminal membrane interaction site with lipids was so far not directly analyzed. FRAP was used earlier to reveal the diffusion characteristics of the influenza polymerase complex in the cytoplasm [151] and of HA on membranes [52]. The presented approach for M1 applied two fluorophores, TMR covalently bound to M1 or NM1 and C_6-NBD-PS in the membrane. They offered the opportunity to acquire data for the membrane-bound M1 (see above) and its influence on the lipids that are in close proximity to the protein. The result of the FRAP experiments with the N-terminal domain of M1 indicated unrestricted movement of phosphatidylserine underneath of the NM1 clusters. The recovery curves for the C_6-NBD-PS lipid analogue showed similar progressions for all analyzed sce-

narios (Figure 29). C_6-NBD-PS moved freely without protein and in presence of α-Synuclein. Free C_6-NBD-PS movement was also observed in areas where NM1 clusters were detected.

An uneven distribution of C_6-NBD-PS fluorescence was observed in some cases when NM1 clusters were present (Figure 29C and Supplementary Figure 4). This leads to the assumption of a specific C_6-NBD-PS accumulation beneath the NM1 clusters. This accumulation had no effect on the lateral movement of C_6-NBD-PS. Analysis for immobile lipid fractions was performed and revealed no significant differences between C_6-NBD-PS free of NM1 clusters and C_6-NBD-PS with NM1 clusters (Table 5).

For the case that NM1 did not influence the lateral movement of the underlying lipids it is possible to conclude that NM1 is not capable of fixing phosphatidylserine below the cluster. Thus, an influence on the other lipids can be excluded. It has to be analyzed in further studies whether this concept can be extended to the full length M1. The CD measurements revealed structural changes of the C–terminal domain in presence of DOPC/DOPS-LUVs. Although the observed clusters of M1 and NM1 were similar in their constitution on the membrane it cannot be excluded that full length M1 might influence the lateral movement of phosphatidylserine.

In summary, the interaction of the N-terminal domain of M1 with phosphatidylserine is flexible and not contributive to membrane lipid sorting or membrane bending as it was described for HA and NA [115,195]. The inability of NM1 to influence the lateral movement of PS and the finding that M1 does not interact with raft lipids in flotation experiments is consistent with published data concerning the essential proteins HA and NA. These two proteins induced formation of VLPs, M1 alone not [75]. M1 can only work as accumulator and cross-linker of these proteins at the assembly site at the plasma membrane. Although M1 can attach to the membrane independently it might not be capable of fixing certain lipids or bending the membrane when it is not specifically linked to the membrane by a membrane inserted anchor [195].

5.4 Conclusion and outlook

Research on influenza matrix protein M1 covers a wide area. M1 is found throughout the whole cell during the infection with the influenza virus. It is visible in the nucleus and spotted in the cytosol where it colocalized with intracellular membranes [58,69,76,195]. M1 was found at the plasma membrane when the viral membrane proteins were present or M1 itself was equipped with a plasma membrane targeting peptide [26,195] in huge amounts and in smaller amounts when it was expressed alone [58,85]. This overall appearance suggests several different functions of M1 during the influenza replication cycle. While focusing on M1 membrane binding alone three aspects for analysis were addressed in this study:

1. The association of M1 to specific lipids was assessed by different methods. The results revealed a precise set of negatively charged lipids that are targeted by M1 (Table 6). Association to these lipids explains the appearance of M1 at the intracellular membranes as well as the plasma membrane. PI4P was found to be a new potentially specific target of M1. This lipid induced different secondary structural changes in M1 compared to PS. Uncharged lipids could be excluded as direct binding partners for M1.

2. The evaluation of the structural basis for the membrane attachment of M1 was undertaken. A single membrane binding domain was not found in M1. Rather the protein showed dual binding with its N- and C-terminal domain.

3. The organization of M1 on membranes was examined. It formed flat oligomers with a lateral extension on negatively charged lipids containing giant unilamellar vesicles of various compositions. Clusters that were made up from a protein which consisted only of the N-terminal part of M1 showed loose interaction to the underlying lipids. This interaction had no significant influence on the lateral movement of the lipids.

It is possible to fine tune the current model for influenza virus assembly based on these findings. An interaction of M1 with the spike proteins was shown to mediate the transport of M1 to the plasma membrane [26,58]. The place where M1 is coupled to the spike proteins is not

known. If M1 targets PI4P specifically, M1 is localized at the Golgi apparatus, since PI4P is a Golgi marker [175,176]. The initial connection between M1 and the spike proteins could occur at the Golgi apparatus. Golgi-bound M1 could change its binding partner from PI4P to the cytoplasmic tails of HA and NA. From there HA-M1 and NA-M1 heterodimers could be transported towards the plasma membrane. Support of this hypothetical pathway could be obtained by affinity binding assays like surface plasmon resonance. This method was already used with M1 to reveal its affinity for phosphatidylserine containing membranes [179]. A PI4P-containing membrane could be used as a binding matrix for M1. The addition of LUVs with reconstituted HA or perhaps only the cytoplasmic tail of HA could release M1 from the membrane matrix. The fact that M1 builds oligomers on surfaces might make these experiments difficult to accomplish.

The analysis of GUV-bound M1 showed for the first time a lateral multi-molecular oligomerization of M1 on a membrane that mimics the plasma membrane in a simple way. M1 oligomerization was not triggered by interaction with other viral proteins. This was proposed in a recent review [115]. It happened spontaneously. This ability of M1 to organize spontaneously to higher molecular structures gives the molecular basis for the viral assembly at the budding site. The incorporation of the cytoplasmic tails of HA and NA into the clustered M1 would fix HA and NA at the budding site. The transmembrane domains of both proteins are incorporated into lipid raft microdomains which are enriched in sphingomyelin and cholesterol. When M1 cross-links HA and NA, it would also cross-link the protein-associated microdomains at the plasma membrane. The clustering of HA on the plasma membrane of mammalian cells was examined by FLIM-FRET and FRAP in detail [52,53]. The impact of M1 could be analyzed by coexpression of M1 in this context.

Literature

[1] Statistisches_Bundesamt (2010): Gesundheit - Todesursachen in Deutschland 2008.

[2] Cunha, B. A. (2010): Swine Influenza (H1N1) pneumonia: clinical considerations, Infect Dis Clin North Am 24 [1], pp. 203-28.

[3] Martin, P. M. and Martin-Granel, E. (2006): 2,500-year evolution of the term epidemic, Emerg Infect Dis 12 [6], pp. 976-80.

[4] Kuszewski, K. and Brydak, L. (2000): The epidemiology and history of influenza, Biomed Pharmacother 54 [4], pp. 188-95.

[5] Taubenberger, J. K. and Morens, D. M. (2006): 1918 Influenza: the mother of all pandemics, Emerg Infect Dis 12 [1], pp. 15-22.

[6] Tumpey, T. M.; Basler, C. F.; Aguilar, P. V.; Zeng, H.; Solorzano, A.; Swayne, D. E.; Cox, N. J.; Katz, J. M.; Taubenberger, J. K.; Palese, P. and Garcia-Sastre, A. (2005): Characterization of the reconstructed 1918 Spanish influenza pandemic virus, Science 310 [5745], pp. 77-80.

[7] Smith, G. J.; Bahl, J.; Vijaykrishna, D.; Zhang, J.; Poon, L. L.; Chen, H.; Webster, R. G.; Peiris, J. S. and Guan, Y. (2009): Dating the emergence of pandemic influenza viruses, Proc Natl Acad Sci U S A 106 [28], pp. 11709-12.

[8] Kilbourne, E. D. (2006): Influenza pandemics of the 20th century, Emerg Infect Dis 12 [1], pp. 9-14.

[9] Sturm-Ramirez, K. M.; Hulse-Post, D. J.; Govorkova, E. A.; Humberd, J.; Seiler, P.; Puthavathana, P.; Buranathai, C.; Nguyen, T. D.; Chaisingh, A.; Long, H. T.; Naipospos, T. S.; Chen, H.; Ellis, T. M.; Guan, Y.; Peiris, J. S. and Webster, R. G. (2005): Are ducks contributing to the endemicity of highly pathogenic H5N1 influenza virus in Asia? J Virol 79 [17], pp. 11269-79.

[10] Olsen, B.; Munster, V. J.; Wallensten, A.; Waldenstrom, J.; Osterhaus, A. D. and Fouchier, R. A. (2006): Global patterns of influenza a virus in wild birds, Science 312 [5772], pp. 384-8.

[11] Shoham, D. (2006): Review: molecular evolution and the feasibility of an avian influenza virus becoming a pandemic strain--a conceptual shift, Virus Genes 33 [2], pp. 127-32.

[12] Naffakh, N.; Tomoiu, A.; Rameix-Welti, M. A. and van der Werf, S. (2008): Host restriction of avian influenza viruses at the level of the ribonucleoproteins, Annu Rev Microbiol 62, pp. 403-24.

[13] Garten, R. J.; Davis, C. T.; Russell, C. A.; Shu, B.; Lindstrom, S.; Balish, A.; Sessions, W. M.; Xu, X.; Skepner, E.; Deyde, V.; Okomo-Adhiambo, M.; Gubareva, L.; Barnes, J.; Smith, C. B.; Emery, S. L.; Hillman, M. J.; Rivailler, P.; Smagala, J.; de Graaf, M.; Burke, D. F.; Fouchier, R. A.; Pappas, C.; Alpuche-Aranda, C. M.; Lopez-Gatell, H.; Olivera, H.; Lopez, I.; Myers, C. A.; Faix, D.; Blair, P. J.; Yu, C.; Keene, K. M.; Dotson, P. D., Jr.; Boxrud, D.; Sambol, A. R.; Abid, S. H.; St George, K.; Bannerman, T.; Moore, A. L.; Stringer, D. J.; Blevins, P.; Demmler-Harrison, G. J.; Ginsberg, M.; Kriner, P.; Waterman, S.; Smole, S.; Guevara, H. F.; Belongia, E. A.; Clark, P. A.; Beatrice, S. T.; Donis, R.; Katz, J.; Finelli, L.; Bridges, C. B.; Shaw, M.; Jernigan, D. B.; Uyeki, T. M.; Smith, D. J.; Klimov, A. I. and Cox, N. J. (2009): Antigenic and genetic

characteristics of swine-origin 2009 A(H1N1) influenza viruses circulating in humans, Science 325 [5937], pp. 197-201.

[14] Gordon, S. M. (2009): Update on 2009 pandemic influenza A (H1N1) virus, Cleve Clin J Med 76 [10], pp. 577-82.

[15] Gibbs, A. J.; Armstrong, J. S. and Downie, J. C. (2009): From where did the 2009 'swine-origin' influenza A virus (H1N1) emerge? Virol J 6, p. 207.

[16] Gao, Q. and Palese, P. (2009): Rewiring the RNAs of influenza virus to prevent reassortment, Proc Natl Acad Sci U S A 106 [37], pp. 15891-6.

[17] Presti, R. M.; Zhao, G.; Beatty, W. L.; Mihindukulasuriya, K. A.; da Rosa, A. P.; Popov, V. L.; Tesh, R. B.; Virgin, H. W. and Wang, D. (2009): Quaranfil, Johnston Atoll, and Lake Chad viruses are novel members of the family Orthomyxoviridae, J Virol 83 [22], pp. 11599-606.

[18] Modrow, Susanne and Falke, Dietrich (1997): Molekulare Virologie, Spektrum Akademischer Verlag, Heidelberg Berlin Oxford, ISBN: 3-86025-274-7.

[19] Ruigrok, R. W.; Andree, P. J.; Hooft van Huysduynen, R. A. and Mellema, J. E. (1984): Characterization of three highly purified influenza virus strains by electron microscopy, J Gen Virol 65 (Pt 4), pp. 799-802.

[20] Calder, L. J.; Wasilewski, S.; Berriman, J. A. and Rosenthal, P. B. (2010): Structural organization of a filamentous influenza A virus, Proc Natl Acad Sci U S A 107 [23], pp. 10685-90.

[21] Alexander, D. J. (2007): An overview of the epidemiology of avian influenza, Vaccine 25 [30], pp. 5637-44.

[22] Gamblin, S. J. and Skehel, J. J. (2010): Influenza hemagglutinin and neuraminidase membrane glycoproteins, J Biol Chem 285 [37], pp. 28403-9.

[23] Stevens, J.; Blixt, O.; Tumpey, T. M.; Taubenberger, J. K.; Paulson, J. C. and Wilson, I. A. (2006): Structure and receptor specificity of the hemagglutinin from an H5N1 influenza virus, Science 312 [5772], pp. 404-10.

[24] Sunstrom, N. A.; Premkumar, L. S.; Premkumar, A.; Ewart, G.; Cox, G. B. and Gage, P. W. (1996): Ion channels formed by NB, an influenza B virus protein, J Membr Biol 150 [2], pp. 127-32.

[25] Betakova, T. and Hay, A. J. (2007): Evidence that the CM2 protein of influenza C virus can modify the pH of the exocytic pathway of transfected cells, J Gen Virol 88 [Pt 8], pp. 2291-6.

[26] Enami, M. and Enami, K. (1996): Influenza virus hemagglutinin and neuraminidase glycoproteins stimulate the membrane association of the matrix protein, J Virol 70 [10], pp. 6653-7.

[27] Ruigrok, R. W.; Barge, A.; Durrer, P.; Brunner, J.; Ma, K. and Whittaker, G. R. (2000): Membrane interaction of influenza virus M1 protein, Virology 267 [2], pp. 289-98.

[28] Chen, B. J.; Leser, G. P.; Jackson, D. and Lamb, R. A. (2008): The influenza virus M2 protein cytoplasmic tail interacts with the M1 protein and influences virus assembly at the site of virus budding, J Virol 82 [20], pp. 10059-70.

[29] Noda, T.; Sagara, H.; Yen, A.; Takada, A.; Kida, H.; Cheng, R. H. and Kawaoka, Y. (2006): Architecture of ribonucleoprotein complexes in influenza A virus particles, Nature 439 [7075], pp. 490-2.

[30] Portela, A. and Digard, P. (2002): The influenza virus nucleoprotein: a multifunctional RNA-binding protein pivotal to virus replication, J Gen Virol 83 [Pt 4], pp. 723-34.

[31] Hale, B. G.; Randall, R. E.; Ortin, J. and Jackson, D. (2008): The multifunctional NS1 protein of influenza A viruses, J Gen Virol 89 [Pt 10], pp. 2359-76.

[32] Boulo, S.; Akarsu, H.; Ruigrok, R. W. and Baudin, F. (2007): Nuclear traffic of influenza virus proteins and ribonucleoprotein complexes, Virus Res 124 [1-2], pp. 12-21.

[33] Karlsson Hedestam, G. B.; Fouchier, R. A.; Phogat, S.; Burton, D. R.; Sodroski, J. and Wyatt, R. T. (2008): The challenges of eliciting neutralizing antibodies to HIV-1 and to influenza virus, Nat Rev Microbiol 6 [2], pp. 143-55.

[34] Harris, A.; Cardone, G.; Winkler, D. C.; Heymann, J. B.; Brecher, M.; White, J. M. and Steven, A. C. (2006): Influenza virus pleiomorphy characterized by cryoelectron tomography, Proc Natl Acad Sci U S A 103 [50], pp. 19123-7.

[35] Varki, Ajit; Cummings, Richard D.; Esko, Jeffrey D.; Freeze, Hudson H.; Stanley, Pamela; Bertozzi, Carolyn R.; Hart, Gerald W. and Etzler, Marilynn E. (2008): Essentials in Glycobiology, Second Edition. ed., Cold Spring Harbor Laboratory Press, Cold Spring Harbor, ISBN: 978-087969770-9.

[36] Kasson, P. M. and Pande, V. S. (2008): Structural basis for influence of viral glycans on ligand binding by influenza hemagglutinin, Biophys J 95 [7], pp. L48-50.

[37] Wang, C. C.; Chen, J. R.; Tseng, Y. C.; Hsu, C. H.; Hung, Y. F.; Chen, S. W.; Chen, C. M.; Khoo, K. H.; Cheng, T. J.; Cheng, Y. S.; Jan, J. T.; Wu, C. Y.; Ma, C. and Wong, C. H. (2009): Glycans on influenza hemagglutinin affect receptor binding and immune response, Proc Natl Acad Sci U S A 106 [43], pp. 18137-42.

[38] Neumann, G.; Noda, T. and Kawaoka, Y. (2009): Emergence and pandemic potential of swine-origin H1N1 influenza virus, Nature 459 [7249], pp. 931-9.

[39] Lakadamyali, M.; Rust, M. J. and Zhuang, X. (2004): Endocytosis of influenza viruses, Microbes Infect 6 [10], pp. 929-36.

[40] Rust, M. J.; Lakadamyali, M.; Zhang, F. and Zhuang, X. (2004): Assembly of endocytic machinery around individual influenza viruses during viral entry, Nat Struct Mol Biol 11 [6], pp. 567-73.

[41] Whittaker, Gary R. and Digard, Paul (2006): Entry and intracellular transport of influenza virus, Kawaoka, Yoshihiro, Influenza Virology: Current Topics pp. 37-64, Caister Academic Press, Norfolk.

[42] Cooper, Geoffrey M. and Hausmann, Robert E. (2009): The Cell - a molecular approach, Fifth Edition. ed., Palgrave Macmillan, ISBN: 087893300X.

[43] Gruenke, J. A.; Armstrong, R. T.; Newcomb, W. W.; Brown, J. C. and White, J. M. (2002): New insights into the spring-loaded conformational change of influenza virus hemagglutinin, J Virol 76 [9], pp. 4456-66.

[44] Cross, K. J.; Langley, W. A.; Russell, R. J.; Skehel, J. J. and Steinhauer, D. A. (2009): Composition and functions of the influenza fusion peptide, Protein Pept Lett 16 [7], pp. 766-78.

[45] Compans, R. W.; Content, J. and Duesberg, P. H. (1972): Structure of the ribonucleoprotein of influenza virus, J Virol 10 [4], pp. 795-800.

[46] Bui, M.; Whittaker, G. and Helenius, A. (1996): Effect of M1 protein and low pH on nuclear transport of influenza virus ribonucleoproteins, J Virol 70 [12], pp. 8391-401.

[47] Wu, W. W. and Pante, N. (2009): The directionality of the nuclear transport of the influenza A genome is driven by selective exposure of nuclear localization sequences on nucleoprotein, Virol J 6, p. 68.

[48] Cros, J. F.; Garcia-Sastre, A. and Palese, P. (2005): An unconventional NLS is critical for the nuclear import of the influenza A virus nucleoprotein and ribonucleoprotein, Traffic 6 [3], pp. 205-13.

[49] Ruigrok, R. W.; Crepin, T.; Hart, D. J. and Cusack, S. (2010): Towards an atomic resolution understanding of the influenza virus replication machinery, Curr Opin Struct Biol 20 [1], pp. 104-13.

[50] Elton, Debra; Digard, Paul; LaurenceTiley and Ortin, Juan (2005): Structure and function of the influenza virus RNP, Kawaoka, Yoshihiro, Influenza Virology: Current Topics pp. 1-36, Caister Academic Press, Norfolk.

[51] Nayak, D. P.; Hui, E. K. and Barman, S. (2004): Assembly and budding of influenza virus, Virus Res 106 [2], pp. 147-65.

[52] Engel, S.; Scolari, S.; Thaa, B.; Krebs, N.; Korte, T.; Herrmann, A. and Veit, M. (2009): FLIM-FRET and FRAP reveal association of influenza virus hemagglutinin with membrane rafts, Biochem J.

[53] Scolari, S.; Engel, S.; Krebs, N.; Plazzo, A. P.; De Almeida, R. F.; Prieto, M.; Veit, M. and Herrmann, A. (2009): Lateral distribution of the transmembrane domain of influenza virus hemagglutinin revealed by time-resolved fluorescence imaging, J Biol Chem 284 [23], pp. 15708-16.

[54] Leser, G. P. and Lamb, R. A. (2005): Influenza virus assembly and budding in raft-derived microdomains: a quantitative analysis of the surface distribution of HA, NA and M2 proteins, Virology 342 [2], pp. 215-27.

[55] Schroeder, C.; Heider, H.; Moncke-Buchner, E. and Lin, T. I. (2005): The influenza virus ion channel and maturation cofactor M2 is a cholesterol-binding protein, Eur Biophys J 34 [1], pp. 52-66.

[56] Kretzschmar, E.; Bui, M. and Rose, J. K. (1996): Membrane association of influenza virus matrix protein does not require specific hydrophobic domains or the viral glycoproteins, Virology 220 [1], pp. 37-45.

[57] Zhang, J. and Lamb, R. A. (1996): Characterization of the membrane association of the influenza virus matrix protein in living cells, Virology 225 [2], pp. 255-66.

[58] Ali, A.; Avalos, R. T.; Ponimaskin, E. and Nayak, D. P. (2000): Influenza virus assembly: effect of influenza virus glycoproteins on the membrane association of M1 protein, J Virol 74 [18], pp. 8709-19.

[59] Zamarin, D.; Garcia-Sastre, A.; Xiao, X.; Wang, R. and Palese, P. (2005): Influenza virus PB1-F2 protein induces cell death through mitochondrial ANT3 and VDAC1, PLoS Pathog 1 [1], p. e4.

[60] Marjuki, H.; Alam, M. I.; Ehrhardt, C.; Wagner, R.; Planz, O.; Klenk, H. D.; Ludwig, S. and Pleschka, S. (2006): Membrane accumulation of influenza A virus hemagglutinin triggers nuclear export of the viral genome via protein kinase Calpha-mediated activation of ERK signaling, J Biol Chem 281 [24], pp. 16707-15.

[61] Takizawa, N.; Kumakura, M.; Takeuchi, K.; Kobayashi, N. and Nagata, K. (2010): Sorting of influenza A virus RNA genome segments after nuclear export, Virology 401 [2], pp. 248-56.

[62] Nayak, D. P.; Balogun, R. A.; Yamada, H.; Zhou, Z. H. and Barman, S. (2009): Influenza virus morphogenesis and budding, Virus Res 143 [2], pp. 147-61.

[63] Murti, K. G.; Webster, R. G. and Jones, I. M. (1988): Localization of RNA polymerases on influenza viral ribonucleoproteins by immunogold labeling, Virology 164 [2], pp. 562-6.

[64] Akarsu, H.; Burmeister, W. P.; Petosa, C.; Petit, I.; Muller, C. W.; Ruigrok, R. W. and Baudin, F. (2003): Crystal structure of the M1 protein-binding domain of the influenza A virus nuclear export protein (NEP/NS2), Embo J 22 [18], pp. 4646-55.

[65] Fornerod, M.; Ohno, M.; Yoshida, M. and Mattaj, I. W. (1997): CRM1 is an export receptor for leucine-rich nuclear export signals, Cell 90 [6], pp. 1051-60.

[66] Martin, K. and Helenius, A. (1991): Nuclear transport of influenza virus ribonucleoproteins: the viral matrix protein (M1) promotes export and inhibits import, Cell 67 [1], pp. 117-30.

[67] Momose, F.; Kikuchi, Y.; Komase, K. and Morikawa, Y. (2007): Visualization of microtubule-mediated transport of influenza viral progeny ribonucleoprotein, Microbes Infect 9 [12-13], pp. 1422-33.

[68] Harris, A.; Forouhar, F.; Qiu, S.; Sha, B. and Luo, M. (2001): The crystal structure of the influenza matrix protein M1 at neutral pH: M1-M1 protein interfaces can rotate in the oligomeric structures of M1, Virology 289 [1], pp. 34-44.

[69] Zhao, H.; Ekstrom, M. and Garoff, H. (1998): The M1 and NP proteins of influenza A virus form homo- but not heterooligomeric complexes when coexpressed in BHK-21 cells, J Gen Virol 79 (Pt 10), pp. 2435-46.

[70] Noton, S. L.; Medcalf, E.; Fisher, D.; Mullin, A. E.; Elton, D. and Digard, P. (2007): Identification of the domains of the influenza A virus M1 matrix protein required for NP binding, oligomerization and incorporation into virions, J Gen Virol 88 [Pt 8], pp. 2280-90.

[71] Simpson-Holley, M.; Ellis, D.; Fisher, D.; Elton, D.; McCauley, J. and Digard, P. (2002): A functional link between the actin cytoskeleton and lipid rafts during budding of filamentous influenza virions, Virology 301 [2], pp. 212-25.

[72] Ozawa, M.; Maeda, J.; Iwatsuki-Horimoto, K.; Watanabe, S.; Goto, H.; Horimoto, T. and Kawaoka, Y. (2009): Nucleotide sequence requirements at the 5' end of the influenza A virus M RNA segment for efficient virus replication, J Virol 83 [7], pp. 3384-8.

[73] Marsh, G. A.; Hatami, R. and Palese, P. (2007): Specific residues of the influenza A virus hemagglutinin viral RNA are important for efficient packaging into budding virions, J Virol 81 [18], pp. 9727-36.

[74] Marsh, G. A.; Rabadan, R.; Levine, A. J. and Palese, P. (2008): Highly conserved regions of influenza a virus polymerase gene segments are critical for efficient viral RNA packaging, J Virol 82 [5], pp. 2295-304.

[75] Chen, B. J.; Leser, G. P.; Morita, E. and Lamb, R. A. (2007): Influenza virus hemagglutinin and neuraminidase, but not the matrix protein, are required for assembly and budding of plasmid-derived virus-like particles, J Virol 81 [13], pp. 7111-23.

[76] Latham, T. and Galarza, J. M. (2001): Formation of wild-type and chimeric influenza virus-like particles following simultaneous expression of only four structural proteins, J Virol 75 [13], pp. 6154-65.

[77] Gottschalk, A. (1957): Neuraminidase: the specific enzyme of influenza virus and Vibrio cholerae, Biochim Biophys Acta 23 [3], pp. 645-6.

[78] Xu, X.; Zhu, X.; Dwek, R. A.; Stevens, J. and Wilson, I. A. (2008): Structural characterization of the 1918 influenza virus H1N1 neuraminidase, J Virol 82 [21], pp. 10493-501.

[79] Liu, T. and Ye, Z. (2002): Restriction of viral replication by mutation of the influenza virus matrix protein, J Virol 76 [24], pp. 13055-61.

[80] Bourmakina, S. V. and Garcia-Sastre, A. (2005): The morphology and composition of influenza A virus particles are not affected by low levels of M1 and M2 proteins in infected cells, J Virol 79 [12], pp. 7926-32.

[81] Sha, B. and Luo, M. (1997): Structure of a bifunctional membrane-RNA binding protein, influenza virus matrix protein M1, Nat Struct Biol 4 [3], pp. 239-44.

[82] Arzt, S.; Baudin, F.; Barge, A.; Timmins, P.; Burmeister, W. P. and Ruigrok, R. W. (2001): Combined results from solution studies on intact influenza virus M1 protein and from a new crystal form of its N-terminal domain show that M1 is an elongated monomer, Virology 279 [2], pp. 439-46.

[83] Arzt, S.; Petit, I.; Burmeister, W. P.; Ruigrok, R. W. and Baudin, F. (2004): Structure of a knockout mutant of influenza virus M1 protein that has altered activities in membrane binding, oligomerisation and binding to NEP (NS2), Virus Res 99 [2], pp. 115-9.

[84] Baudin, F.; Petit, I.; Weissenhorn, W. and Ruigrok, R. W. (2001): In vitro dissection of the membrane and RNP binding activities of influenza virus M1 protein, Virology 281 [1], pp. 102-8.

[85] Thaa, B.; Herrmann, A. and Veit, M. (2009): The polybasic region is not essential for membrane binding of the matrix protein M1 of influenza virus, Virology 383 [1], pp. 150-5.

[86] Gennis, Robert B. (1989): Biomembranes, Cantor, Charles R., Ed, Springer Advanced Texts in Chemistry, Springer-Verlag, New York, ISBN: 0387967605.

[87] van Meer, Gerrit; Voelker, Dennis R. and Feigensen, Gerald W. (2008): Membrane lipids: where they are and how they behave, Nat Rev Mol Cell Biol. 9 [2], pp. 112-124.

[88] Sampaio, J. L.; Gerl, M. J.; Klose, C.; Ejsing, C. S.; Beug, H.; Simons, K. and Shevchenko, A. (2011): Membrane lipidome of an epithelial cell line, Proc Natl Acad Sci U S A 108 [5], pp. 1903-7.

[89] Pomorski, T. and Menon, A. K. (2006): Lipid flippases and their biological functions, Cell Mol Life Sci 63 [24], pp. 2908-21.

[90] Pomorski, T.; Lombardi, R.; Riezman, H.; Devaux, P. F.; van Meer, G. and Holthuis, J. C. (2003): Drs2p-related P-type ATPases Dnf1p and Dnf2p are required for phospholipid translocation across the yeast plasma membrane and serve a role in endocytosis, Mol Biol Cell 14 [3], pp. 1240-54.

[91] Tuuf, J.; Kjellberg, M. A.; Molotkovsky, J. G.; Hanada, K. and Mattjus, P. (2011): The intermembrane ceramide transport catalyzed by CERT is sensitive to the lipid environment, Biochim Biophys Acta 1808 [1], pp. 229-35.

[92] Peretti, D.; Dahan, N.; Shimoni, E.; Hirschberg, K. and Lev, S. (2008): Coordinated lipid transfer between the endoplasmic reticulum and the Golgi complex requires the

VAP proteins and is essential for Golgi-mediated transport, Mol Biol Cell 19 [9], pp. 3871-84.

[93] Kirchhausen, T. (2009): Imaging endocytic clathrin structures in living cells, Trends Cell Biol 19 [11], pp. 596-605.

[94] Schmid, S. L. (1997): Clathrin-coated vesicle formation and protein sorting: an integrated process, Annu Rev Biochem 66, pp. 511-48.

[95] Kirchhausen, T. (2000): Clathrin, Annu Rev Biochem 69, pp. 699-727.

[96] Nickel, W.; Brugger, B. and Wieland, F. T. (2002): Vesicular transport: the core machinery of COPI recruitment and budding, J Cell Sci 115 [Pt 16], pp. 3235-40.

[97] Pucadyil, T. J. and Schmid, S. L. (2009): Conserved functions of membrane active GTPases in coated vesicle formation, Science 325 [5945], pp. 1217-20.

[98] Jensen, D. and Schekman, R. (2011): COPII-mediated vesicle formation at a glance, J Cell Sci 124 [Pt 1], pp. 1-4.

[99] Singh, I.; Doms, R. W.; Wagner, K. R. and Helenius, A. (1990): Intracellular transport of soluble and membrane-bound glycoproteins: folding, assembly and secretion of anchor-free influenza hemagglutinin, Embo J 9 [3], pp. 631-9.

[100] Zachowski, A. (1993): Phospholipids in animal eukaryotic membranes: transverse asymmetry and movement, Biochem J 294 (Pt 1), pp. 1-14.

[101] Silva, L. C.; Futerman, A. H. and Prieto, M. (2009): Lipid raft composition modulates sphingomyelinase activity and ceramide-induced membrane physical alterations, Biophys J 96 [8], pp. 3210-22.

[102] Kaiser, H. J.; Lingwood, D.; Levental, I.; Sampaio, J. L.; Kalvodova, L.; Rajendran, L. and Simons, K. (2009): Order of lipid phases in model and plasma membranes, Proc Natl Acad Sci U S A 106 [39], pp. 16645-50.

[103] Munro, S. (2003): Lipid rafts: elusive or illusive? Cell 115 [4], pp. 377-88.

[104] Kierszniowska, S.; Seiwert, B. and Schulze, W. X. (2009): Definition of Arabidopsis sterol-rich membrane microdomains by differential treatment with methyl-beta-cyclodextrin and quantitative proteomics, Mol Cell Proteomics 8 [4], pp. 612-23.

[105] Levental, I.; Lingwood, D.; Grzybek, M.; Coskun, U. and Simons, K. (2011): Palmitoylation regulates raft affinity for the majority of integral raft proteins, Proc Natl Acad Sci U S A 107 [51], pp. 22050-4.

[106] Munro, P.; Kojima, H.; Dupont, J. L.; Bossu, J. L.; Poulain, B. and Boquet, P. (2001): High sensitivity of mouse neuronal cells to tetanus toxin requires a GPI-anchored protein, Biochem Biophys Res Commun 289 [2], pp. 623-9.

[107] Bonnon, C.; Wendeler, M. W.; Paccaud, J. P. and Hauri, H. P. (2010): Selective export of human GPI-anchored proteins from the endoplasmic reticulum, J Cell Sci 123 [Pt 10], pp. 1705-15.

[108] Simons, K. and Gerl, M. J. (2010): Revitalizing membrane rafts: new tools and insights, Nat Rev Mol Cell Biol 11 [10], pp. 688-99.

[109] Takeda, M.; Leser, G. P.; Russell, C. J. and Lamb, R. A. (2003): Influenza virus hemagglutinin concentrates in lipid raft microdomains for efficient viral fusion, Proc Natl Acad Sci U S A 100 [25], pp. 14610-7.

[110] Barman, S.; Adhikary, L.; Chakrabarti, A. K.; Bernas, C.; Kawaoka, Y. and Nayak, D. P. (2004): Role of transmembrane domain and cytoplasmic tail amino acid sequences

of influenza a virus neuraminidase in raft association and virus budding, J Virol 78 [10], pp. 5258-69.

[111] Rossman, J. S.; Jing, X.; Leser, G. P. and Lamb, R. A. (2010): Influenza virus M2 protein mediates ESCRT-independent membrane scission, Cell 142 [6], pp. 902-13.

[112] Chen, B. J.; Takeda, M. and Lamb, R. A. (2005): Influenza virus hemagglutinin (H3 subtype) requires palmitoylation of its cytoplasmic tail for assembly: M1 proteins of two subtypes differ in their ability to support assembly, J Virol 79 [21], pp. 13673-84.

[113] Veit, M.; Kretzschmar, E.; Kuroda, K.; Garten, W.; Schmidt, M. F.; Klenk, H. D. and Rott, R. (1991): Site-specific mutagenesis identifies three cysteine residues in the cytoplasmic tail as acylation sites of influenza virus hemagglutinin, J Virol 65 [5], pp. 2491-500.

[114] Wagner, R.; Herwig, A.; Azzouz, N. and Klenk, H. D. (2005): Acylation-mediated membrane anchoring of avian influenza virus hemagglutinin is essential for fusion pore formation and virus infectivity, J Virol 79 [10], pp. 6449-58.

[115] Rossman, J. S. and Lamb, R. A. (2011): Influenza virus assembly and budding, Virology 411 [2], pp. 229-36.

[116] Lai, J. C.; Chan, W. W.; Kien, F.; Nicholls, J. M.; Peiris, J. S. and Garcia, J. M. (2010): Formation of virus-like particles from human cell lines exclusively expressing influenza neuraminidase, J Gen Virol 91 [Pt 9], pp. 2322-30.

[117] Nikolaus, J.; Scolari, S.; Bayraktarov, E.; Jungnick, N.; Engel, S.; Pia Plazzo, A.; Stöckl, M.; Volkmer, R.; Veit, M. and Herrmann, A. (2010): Hemagglutinin of influenza virus partitions into the nonraft domain of model membranes, Biophys J 99 [2], pp. 489-98.

[118] Iwatsuki-Horimoto, K.; Horimoto, T.; Noda, T.; Kiso, M.; Maeda, J.; Watanabe, S.; Muramoto, Y.; Fujii, K. and Kawaoka, Y. (2006): The cytoplasmic tail of the influenza A virus M2 protein plays a role in viral assembly, J Virol 80 [11], pp. 5233-40.

[119] Thaa, B.; Levental, I.; Herrmann, A. and Veit, M. (2011): Intrinsic membrane association of the cytoplasmic tail of influenza virus M2 protein and lateral membrane sorting regulated by cholesterol binding and palmitoylation, Biochem J.

[120] Rossman, J. S.; Jing, X.; Leser, G. P.; Balannik, V.; Pinto, L. H. and Lamb, R. A. (2010): Influenza virus m2 ion channel protein is necessary for filamentous virion formation, J Virol 84 [10], pp. 5078-88.

[121] Thaa, B.; Herrmann, A. and Veit, M. (2010): Intrinsic cytoskeleton-dependent clustering of influenza virus M2 protein with hemagglutinin assessed by FLIM-FRET, J Virol 84 [23], pp. 12445-9.

[122] Elleman, C. J. and Barclay, W. S. (2004): The M1 matrix protein controls the filamentous phenotype of influenza A virus, Virology 321 [1], pp. 144-53.

[123] Burleigh, L. M.; Calder, L. J.; Skehel, J. J. and Steinhauer, D. A. (2005): Influenza a viruses with mutations in the m1 helix six domain display a wide variety of morphological phenotypes, J Virol 79 [2], pp. 1262-70.

[124] Roberts, P. C.; Lamb, R. A. and Compans, R. W. (1998): The M1 and M2 proteins of influenza A virus are important determinants in filamentous particle formation, Virology 240 [1], pp. 127-37.

[125] Schroeder, A.; Kost, J. and Barenholz, Y. (2009): Ultrasound, liposomes, and drug delivery: principles for using ultrasound to control the release of drugs from liposomes, Chem Phys Lipids 162 [1-2], pp. 1-16.

[126] Schroeder, A.; Avnir, Y.; Weisman, S.; Najajreh, Y.; Gabizon, A.; Talmon, Y.; Kost, J. and Barenholz, Y. (2007): Controlling liposomal drug release with low frequency ultrasound: mechanism and feasibility, Langmuir 23 [7], pp. 4019-25.

[127] Hope, M.J.; Bally, M.B.; Webb, G. and Cullis, P.R. (1985): Production of large unilamellar vesicles by a rapid extrusion procedure. Characterization of size distribution, trapped volume and ability to maintain a membrane potential, Biochim Biophys Acta 812, pp. 55-65.

[128] Mayer, L. D.; Hope, M. J. and Cullis, P. R. (1986): Vesicles of variable sizes produced by a rapid extrusion procedure, Biochim Biophys Acta 858 [1], pp. 161-8.

[129] Ong, W.; Yang, Y.; Cruciano, A. C. and McCarley, R. L. (2008): Redox-triggered contents release from liposomes, J Am Chem Soc 130 [44], pp. 14739-44.

[130] Bigay, J.; Casella, J. F.; Drin, G.; Mesmin, B. and Antonny, B. (2005): ArfGAP1 responds to membrane curvature through the folding of a lipid packing sensor motif, Embo J 24 [13], pp. 2244-53.

[131] Zakowski, J. J.; Petri, W. A., Jr. and Wagner, R. R. (1981): Role of matrix protein in assembling the membrane of vesicular stomatitis virus: reconstitution of matrix protein with negatively charged phospholipid vesicles, Biochemistry 20 [13], pp. 3902-7.

[132] Angelova, M. I.; Soléau, S.; Méléard, Ph.; Faucon, J.F. and Bothorel, P. (1992): Preparation of giant vesicles by external AC electric fields. Kinetics and applications, Progr Colloid Polym Sci 89, pp. 127-131.

[133] Dimitrov, D. S. and Angelova, M. I. (1987): Lipid swelling and liposome formation on solid surfaces in external electric fields, Progr Colloid & Polymer Sci 73, pp. 48-56.

[134] Maier, O.; Oberle, V. and Hoekstra, D. (2002): Fluorescent lipid probes: some properties and applications (a review), Chem Phys Lipids 116 [1-2], pp. 3-18.

[135] Stöckl, M.; Plazzo, A. P.; Korte, T. and Herrmann, A. (2008): Detection of lipid domains in model and cell membranes by fluorescence lifetime imaging microscopy of fluorescent lipid analogues, J Biol Chem 283 [45], pp. 30828-37.

[136] Ruan, Q.; Cheng, M. A.; Levi, M.; Gratton, E. and Mantulin, W. W. (2004): Spatial-temporal studies of membrane dynamics: scanning fluorescence correlation spectroscopy (SFCS), Biophys J 87 [2], pp. 1260-7.

[137] Adams, S. R.; Campbell, R. E.; Gross, L. A.; Martin, B. R.; Walkup, G. K.; Yao, Y.; Llopis, J. and Tsien, R. Y. (2002): New biarsenical ligands and tetracysteine motifs for protein labeling in vitro and in vivo: synthesis and biological applications, J Am Chem Soc 124 [21], pp. 6063-76.

[138] Stöckl, M.; Fischer, P.; Wanker, E. and Herrmann, A. (2008): α-Synuclein selectively binds to anionic phospholipids embedded in liquid-disordered domains, J Mol Biol 375 [5], pp. 1394-404.

[139] Wagner, E.; Engelhardt, O. G.; Gruber, S.; Haller, O. and Kochs, G. (2001): Rescue of recombinant Thogoto virus from cloned cDNA, J Virol 75 [19], pp. 9282-6.

[140] Urban, A.; Neukirchen, S. and Jaeger, K. E. (1997): A rapid and efficient method for site-directed mutagenesis using one-step overlap extension PCR, Nucleic Acids Res 25 [11], pp. 2227-8.

[141] Stratagene (2006): QuikChange Site-directed Mutagenesis Kit - Instruction Manual, Stratagene.

[142] Gasteiger, E.; Gattiker, A.; Hoogland, C.; Ivanyi, I.; Appel, R. D. and Bairoch, A. (2003): ExPASy: The proteomics server for in-depth protein knowledge and analysis, Nucleic Acids Res 31 [13], pp. 3784-8.

[143] Laemmli, U. K. (1970): Cleavage of structural proteins during the assembly of the head of bacteriophage T4, Nature 227 [5259], pp. 680-5.

[144] Haugland, Richard P. (2005): The Handbook - A Guide to Fluorescent Probes and Labeling Technologies, Tenth Edition. ed., ISBN: 0-9710636-4-8.

[145] Drin, G.; Casella, J. F.; Gautier, R.; Boehmer, T.; Schwartz, T. U. and Antonny, B. (2007): A general amphipathic alpha-helical motif for sensing membrane curvature, Nat Struct Mol Biol 14 [2], pp. 138-46.

[146] van Iersel, J.; Jzn, J. F. and Duine, J. A. (1985): Determination of absorption coefficients of purified proteins by conventional ultraviolet spectrophotometry and chromatography combined with multiwavelength detection, Anal Biochem 151 [1], pp. 196-204.

[147] Angelova, Miglena I. and Dimitrov, Dimiter S. (1986): Liposome electroformation, Faraday Discuss. Chem. Soc. 81, pp. 303-311.

[148] Angelova, M. and Dimitrov, D. S. (1988): A mechanism of liposome electroformation, Progr Colloid Polym Sci 76, pp. 59-67.

[149] Axelrod, D.; Koppel, D. E.; Schlessinger, J.; Elson, E. and Webb, W. W. (1976): Mobility measurement by analysis of fluorescence photobleaching recovery kinetics, Biophys J 16 [9], pp. 1055-69.

[150] Jacobson, K.; Wu, E. and Poste, G. (1976): Measurement of the translational mobility of concanavalin A in glycerol-saline solutions and on the cell surface by fluorescence recovery after photobleaching, Biochim Biophys Acta 433 [1], pp. 215-22.

[151] Loucaides, E. M.; von Kirchbach, J. C.; Foeglein, A.; Sharps, J.; Fodor, E. and Digard, P. (2009): Nuclear dynamics of influenza A virus ribonucleoproteins revealed by live-cell imaging studies, Virology 394 [1], pp. 154-63.

[152] O'Connell, K. M. and Tamkun, M. M. (2005): Targeting of voltage-gated potassium channel isoforms to distinct cell surface microdomains, J Cell Sci 118 [Pt 10], pp. 2155-66.

[153] Elster, C.; Larsen, K.; Gagnon, J.; Ruigrok, R. W. and Baudin, F. (1997): Influenza virus M1 protein binds to RNA through its nuclear localization signal, J Gen Virol 78 (Pt 7), pp. 1589-96.

[154] Lilie, H.; Schwarz, E. and Rudolph, R. (1998): Advances in refolding of proteins produced in E. coli, Curr Opin Biotechnol 9 [5], pp. 497-501.

[155] Burgess, R. R. (2009): Refolding solubilized inclusion body proteins, Methods Enzymol 463, pp. 259-82.

[156] Greenfield, N. J. (2006): Using circular dichroism spectra to estimate protein secondary structure, Nat Protoc 1 [6], pp. 2876-90.

[157] Böhm, G.; Muhr, R. and Jaenicke, R. (1992): Quantitative analysis of protein far UV circular dichroism spectra by neural networks, Protein Eng 5 [3], pp. 191-5.

[158] Rost, Burkhard (2004): The PredictProtein Server., Nucleic Acids Res 32 [Web Server Issue], pp. W321-W326.

[159] Price, P. A.; Liu, T. Y.; Stein, W. H. and Moore, S. (1969): Properties of chromatographically purified bovine pancreatic deoxyribonuclease, J Biol Chem 244 [3], pp. 917-23.

[160] Gibney, B. R.; Rabanal, F.; Reddy, K. S. and Dutton, P. L. (1998): Effect of four helix bundle topology on heme binding and redox properties, Biochemistry 37 [13], pp. 4635-43.

[161] Cohen, C. and Parry, D. A. (1990): Alpha-helical coiled coils and bundles: how to design an alpha-helical protein, Proteins 7 [1], pp. 1-15.

[162] Dowler, S.; Kular, G. and Alessi, D. R. (2002): Protein lipid overlay assay, Sci STKE 2002 [129], p. pl6.

[163] Dempsey, C. E. (1990): The actions of melittin on membranes, Biochim Biophys Acta 1031 [2], pp. 143-61.

[164] van Veen, M.; Georgiou, G. N.; Drake, A. F. and Cherry, R. J. (1995): Circular-dichroism and fluorescence studies on melittin: effects of C-terminal modifications on tetramer formation and binding to phospholipid vesicles, Biochem J 305 (Pt 3), pp. 785-90.

[165] Janas, T.; Janas, T. and Yarus, M. (2004): A membrane transporter for tryptophan composed of RNA, Rna 10 [10], pp. 1541-9.

[166] Kordyukova, L. V.; Serebryakova, M. V.; Polyakov, V. Y.; Ovchinnikova, T. V.; Smirnova, Y. A.; Fedorova, N. V. and Baratova, L. A. (2008): Influenza A virus M1 protein structure probed by in situ limited proteolysis with bromelain, Protein Pept Lett 15 [9], pp. 922-30.

[167] Heimburg, Thomas (2009): Thermal Biophysics of Membranes, 1st Edition. ed., Wiley-VCH, ISBN: 978-3-527-40471.

[168] Gekara, N. O.; Jacobs, T.; Chakraborty, T. and Weiss, S. (2005): The cholesterol-dependent cytolysin listeriolysin O aggregates rafts via oligomerization, Cell Microbiol 7 [9], pp. 1345-56.

[169] Pinaud, F.; Michalet, X.; Iyer, G.; Margeat, E.; Moore, H. P. and Weiss, S. (2009): Dynamic partitioning of a glycosyl-phosphatidylinositol-anchored protein in glycosphingolipid-rich microdomains imaged by single-quantum dot tracking, Traffic 10 [6], pp. 691-712.

[170] Levental, I.; Grzybek, M. and Simons, K. (2010): Greasing their way: lipid modifications determine protein association with membrane rafts, Biochemistry 49 [30], pp. 6305-16.

[171] Scheiffele, P.; Rietveld, A.; Wilk, T. and Simons, K. (1999): Influenza viruses select ordered lipid domains during budding from the plasma membrane, J Biol Chem 274 [4], pp. 2038-44.

[172] Scheiffele, P.; Roth, M. G. and Simons, K. (1997): Interaction of influenza virus haemagglutinin with sphingolipid-cholesterol membrane domains via its transmembrane domain, Embo J 16 [18], pp. 5501-8.

[173] Feng, M.; Morales, A. B.; Poot, A.; Beugeling, T. and Bantjes, A. (1995): Effects of Tween 20 on the desorption of proteins from polymer surfaces, J Biomater Sci Polym Ed 7 [5], pp. 415-24.

[174] Qiu, D.; Tannock, G. A.; Barry, R. D. and Jackson, D. C. (1992): Western blot analysis of antibody responses to influenza virion proteins, Immunol Cell Biol 70 (Pt 3), pp. 181-91.

[175] Mills, I. G.; Praefcke, G. J.; Vallis, Y.; Peter, B. J.; Olesen, L. E.; Gallop, J. L.; Butler, P. J.; Evans, P. R. and McMahon, H. T. (2003): EpsinR: an AP1/clathrin interacting protein involved in vesicle trafficking, J Cell Biol 160 [2], pp. 213-22.

[176] Sasaki, T.; Sasaki, J.; Sakai, T.; Takasuga, S. and Suzuki, A. (2007): The physiology of phosphoinositides, Biol Pharm Bull 30 [9], pp. 1599-604.

[177] Gregoriades, A. and Frangione, B. (1981): Insertion of influenza M protein into the viral lipid bilayer and localization of site of insertion, J Virol 40 [1], pp. 323-8.

[178] Shishkov, A. V.; Goldanskii, V. I.; Baratova, L. A.; Fedorova, N. V.; Ksenofontov, A. L.; Zhirnov, O. P. and Galkin, A. V. (1999): The in situ spatial arrangement of the influenza A virus matrix protein M1 assessed by tritium bombardment, Proc Natl Acad Sci U S A 96 [14], pp. 7827-30.

[179] Shishkov, A. V.; Bogacheva, E. N.; Dolgov, A. A.; Chulichkov, A. L.; Knyazev, D. G.; Fedorova, N. V.; Ksenofontov, A. L.; Kordyukova, L. V.; Lukashina, E. V.; Mirsky, V. M. and Baratova, L. A. (2009): The in situ structural characterization of the influenza A virus matrix M1 protein within a virion, Protein Pept Lett 16 [11], pp. 1407-13.

[180] Liu, T. and Ye, Z. (2004): Introduction of a temperature-sensitive phenotype into influenza A/WSN/33 virus by altering the basic amino acid domain of influenza virus matrix protein, J Virol 78 [18], pp. 9585-91.

[181] Ye, Z.; Robinson, D. and Wagner, R. R. (1995): Nucleus-targeting domain of the matrix protein (M1) of influenza virus, J Virol 69 [3], pp. 1964-70.

[182] Saad, J. S.; Miller, J.; Tai, J.; Kim, A.; Ghanam, R. H. and Summers, M. F. (2006): Structural basis for targeting HIV-1 Gag proteins to the plasma membrane for virus assembly, Proc Natl Acad Sci U S A 103 [30], pp. 11364-9.

[183] Ford, M. G.; Mills, I. G.; Peter, B. J.; Vallis, Y.; Praefcke, G. J.; Evans, P. R. and McMahon, H. T. (2002): Curvature of clathrin-coated pits driven by epsin, Nature 419 [6905], pp. 361-6.

[184] Stahelin, R. V.; Long, F.; Peter, B. J.; Murray, D.; De Camilli, P.; McMahon, H. T. and Cho, W. (2003): Contrasting membrane interaction mechanisms of AP180 N-terminal homology (ANTH) and epsin N-terminal homology (ENTH) domains, J Biol Chem 278 [31], pp. 28993-9.

[185] Saad, J. S.; Loeliger, E.; Luncsford, P.; Liriano, M.; Tai, J.; Kim, A.; Miller, J.; Joshi, A.; Freed, E. O. and Summers, M. F. (2007): Point mutations in the HIV-1 matrix protein turn off the myristyl switch, J Mol Biol 366 [2], pp. 574-85.

[186] Spearman, P.; Wang, J. J.; Vander Heyden, N. and Ratner, L. (1994): Identification of human immunodeficiency virus type 1 Gag protein domains essential to membrane binding and particle assembly, J Virol 68 [5], pp. 3232-42.

[187] Hamard-Peron, E.; Juillard, F.; Saad, J. S.; Roy, C.; Roingeard, P.; Summers, M. F.; Darlix, J. L.; Picart, C. and Muriaux, D. (2010): Targeting of murine leukemia virus gag to the plasma membrane is mediated by PI(4,5)P2/PS and a polybasic region in the matrix, J Virol 84 [1], pp. 503-15.

[188] Kaadige, M. R. and Ayer, D. E. (2006): The polybasic region that follows the plant homeodomain zinc finger 1 of Pf1 is necessary and sufficient for specific phosphoinositide binding, J Biol Chem 281 [39], pp. 28831-6.

[189] Stenmark, H. and Gillooly, D. J. (2001): Intracellular trafficking and turnover of phosphatidylinositol 3-phosphate, Semin Cell Dev Biol 12 [2], pp. 193-9.

[190] Kutateladze, T. G. (2006): Phosphatidylinositol 3-phosphate recognition and membrane docking by the FYVE domain, Biochim Biophys Acta 1761 [8], pp. 868-77.

[191] Stenmark, H.; Aasland, R.; Toh, B. H. and D'Arrigo, A. (1996): Endosomal localization of the autoantigen EEA1 is mediated by a zinc-binding FYVE finger, J Biol Chem 271 [39], pp. 24048-54.

[192] Bucher, D. J.; Kharitonenkov, I. G.; Zakomirdin, J. A.; Grigoriev, V. B.; Klimenko, S. M. and Davis, J. F. (1980): Incorporation of influenza virus M-protein into liposomes, J Virol 36 [2], pp. 586-90.

[193] Liu, Y. and Atkinson, D. (2011): Enhancing the contrast of ApoB to locate the surface components in the 3D density map of human LDL, J Mol Biol 405 [1], pp. 274-83.

[194] Barman, S.; Ali, A.; Hui, E. K.; Adhikary, L. and Nayak, D. P. (2001): Transport of viral proteins to the apical membranes and interaction of matrix protein with glycoproteins in the assembly of influenza viruses, Virus Res 77 [1], pp. 61-9.

[195] Wang, D.; Harmon, A.; Jin, J.; Francis, D. H.; Christopher-Hennings, J.; Nelson, E.; Montelaro, R. C. and Li, F. (2010): The lack of an inherent membrane targeting signal is responsible for the failure of the matrix (M1) protein of influenza A virus to bud into virus-like particles, J Virol 84 [9], pp. 4673-81.

[196] Gautier, R.; Douguet, D.; Antonny, B. and Drin, G. (2008): HELIQUEST: a web server to screen sequences with specific alpha-helical properties, Bioinformatics 24 [18], pp. 2101-2.

Appendix

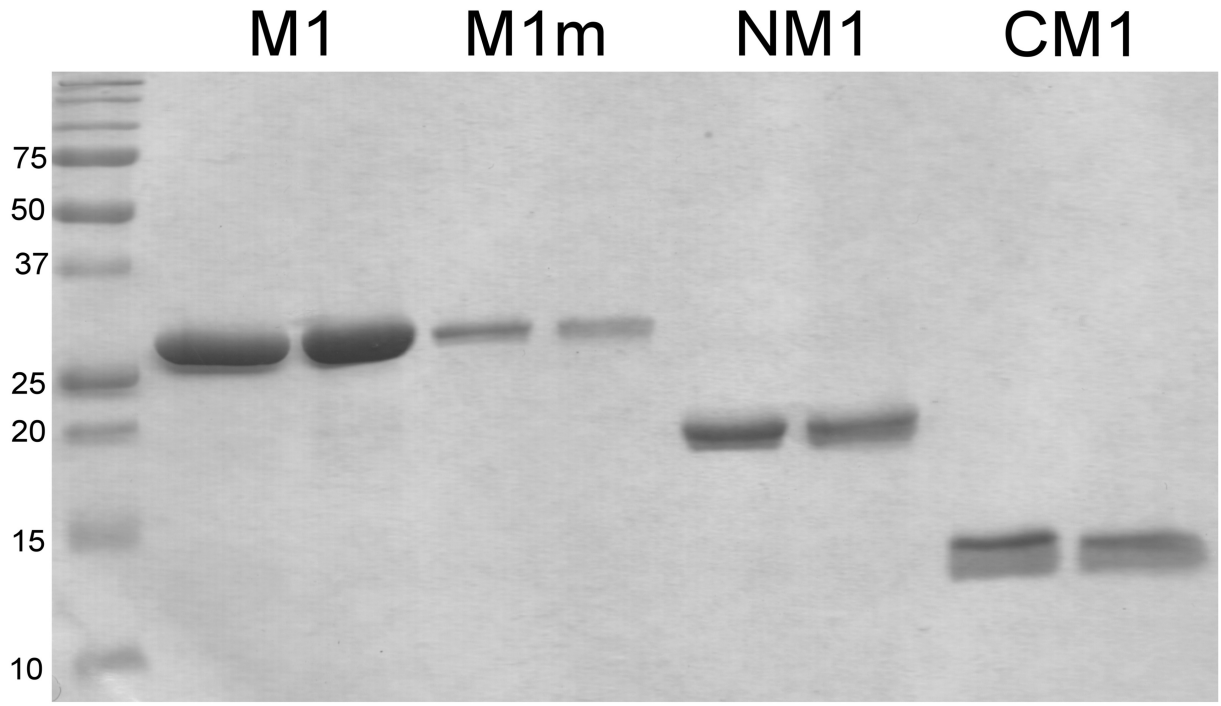

Supplementary Figure 1 Coomassie stained non-reducing SDS-gel for M1m, NM1, NM1m, and CM1. The expressed proteins were consistent in the molecular mass to the predicted values.

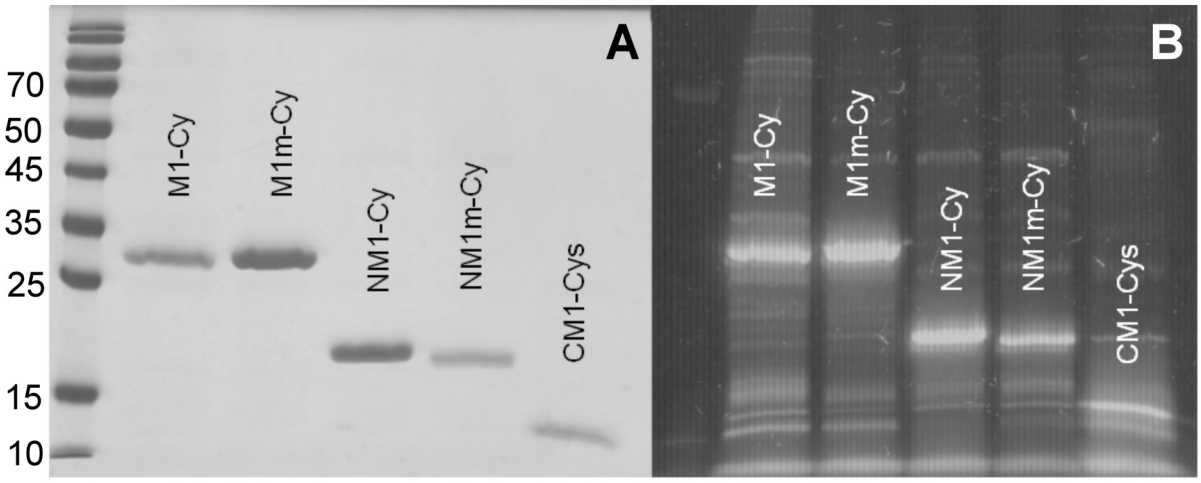

Supplementary Figure 2 FM-labeled M1 mutants. (A) Coomassie stained reducing gel. (B) FM fluorescence of the labeled proteins. A small amount of unbound FM ran at the bottom line

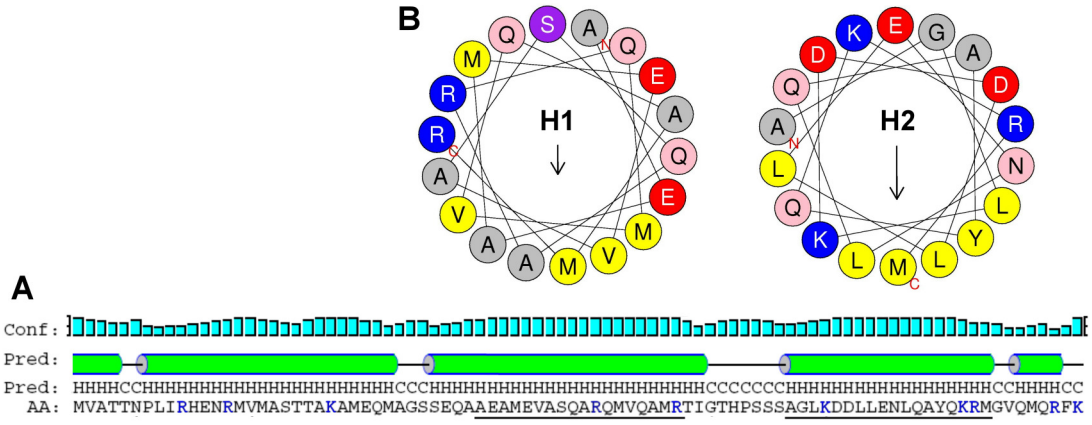

Supplementary Figure 3 (A) Amino acid sequence of the C-terminal part of M1. Basic amino acids are depicted in blue letters. Amino acids used for the calculation of helix properties are underlined. Predicted helix formation in CM1 in green. Confidence values for the prediction in light blue. The prediction was performed according to [158]. (B) Calculation of α-helix properties for the two α-helices with high confidence values. A hydrophobic interface was proposed in both helices (MVMAAV in H1; LMLYL in H2). The calculation was performed on http://heliquest.ipmc.cnrs.fr according to [196].

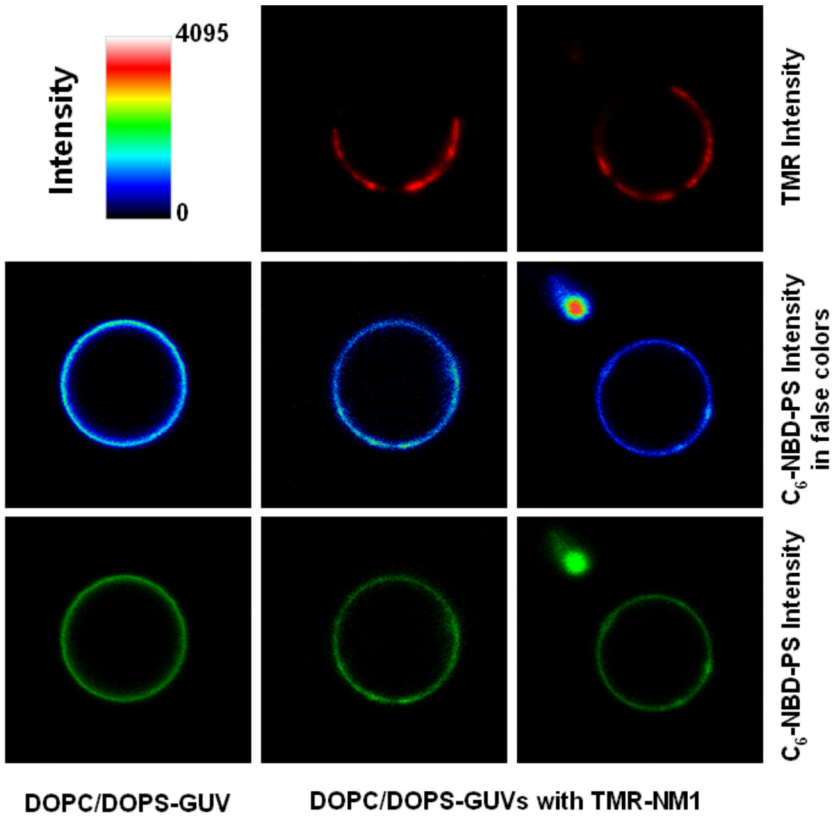

Supplementary Figure 4 Fluorescence intensity of C_6-NBD-PS on GUVs. The intensity of the middle panel depicts the C_6-NBD-PS intensity in false colors. The first column shows a DOPC/DOPS-GUV with NM1-TMR. The second and the third column represent DOPC/DOPS-GUVs with bound NM1 clusters. GUVs were produced by electroswelling. TMR-NM1 was added as mentioned earlier (see Figure 28). Images were recorded after 30 min incubation. The temperature in the microscopy room was set to 24 °C.

Acknowledgment

The presented study was carried out at the Humboldt University Berlin in the workgroup "Molecular Biophysics". I would like to thank all the people who helped to successfully accomplish it.

At first I want to thank Prof. Dr. Andreas Herrmann for providing the exciting topic and for the introduction into the world of influenza and lipid membranes. His encouragement, the fruitful discussions, and his endless patience were essential for finishing this work.

At the Free University Berlin I have to thank PD Dr. Michael Veit for providing plasmids for M1 and NP cloning, Dr. Bastian Thaa for his open ear for all problems concerning M1, and Julia Walter for being so kind to share two of her PIP™ strip samples with Bastian and me for an initial experiment.

I'm grateful to Prof. Dr. Thomas Pomorski, Dr. Anja Arbuzowa, and Dr. Gabi Schreiber who discussed problems in the door angle and gave priceless hints.

I'm thankful to Prof. Dr. Sandro Keller and his group. They kindly welcomed me in their lab at the FMP for the CD measurements. Special thanks go to Natalie Bordag. Her deep insight into the CD methodology and the very fruitful discussions were an important part for the course of this study.

I thank Prof. Bernd Reif at the MDC for the access to the Zetasizer nano.

Jörg Bürger und Dr. Thorsten Mielke from the Ultrastrukturnetzwerk at the Max Planck Institute of Molecular Genetics (Berlin) showed me what can be seen in the nanometer range. Their expertise in electron microscopy and the great working atmosphere was inspiring.

I especially want to thank Dr. Martin Stöckl, Dr. Thomas Korte, and Dr. Martin Loew who introduced me into the complex field of microscopy and always took the time to discuss appearing problems.

In general I want to thank all the members of the group "Molecular Biophysics" for creating the friendly environment, especially Sabine Schiller and Gudrun Habermann for keeping the lab running and Dr. Korte for keeping the IT running. Carina Glöckner provided great technical assistance.

I'm grateful to Natalie Bordag for reviewing parts of this work and Dr. Martin Loew as well as Professor Thomas J. Buckhout for proofreading the final version.

I'm very grateful to all my friends. Your motivation kept me going. My family including my little brother always gave support and great comments.

Finally, I would like to thank my better half Martin for his never ending encouragement and enthusiasm during the writing period. He told me to fight letter for letter, chapter for chapter. Thank you!

Publications

Manuscripts

Gollhofer J, Schläwicke C, Jungnick N, Buckhout TJ (2011) *Members of a small family of nodulin-like genes are regulated under iron deficiency in roots of Arabidopsis thaliana.* Plant Physiol Biochem. 49 (5): 557-64

Nikolaus J, Scolari S, Bayraktarov E, Jungnick N, Engel S, Plazzo AP, Stöckl MT, Volkmer R, Veit M, Herrmann A (2010) *Hemagglutinin of influenza virus partitions into the nonraft domain of model membranes.* Biophys J. 21; 99 (2): 489-98

Socher E, Bethge L, Knoll A, Jungnick N, Herrmann A, Seitz O. (2008) *Low-noise stemless PNA beacons for sensitive DNA and RNA detection.* Angew Chem Int Ed Engl. 47: 9555-9.

Talks

Jungnick N, Gollhofer J, Schläwicke C, Buckhout TJ (2011) *Nodulin-like 1 – a new vacuolar iron transporter in Arabidopsis thaliana*. Cell biology workshop in Hoheneiche.

Posters

Jungnick N, Bordag N, Keller S, Herrmann A. (2010) *Influenza matrix protein M1 membrane binding – an in vitro study*. International Workshop „The Role of Heterogeneity and symmetry of Membranes for their Biological Function“ in Gomadingen.

Jungnick N, Bordag N, Keller S, Herrmann A. (2009) *Influenza matrix protein M1 – a membrane binding study*. International Symposium „Membranes and Modules“ in Berlin.

Jungnick N, Bordag N, Keller S, Herrmann A. (2009) *Influenza matrix protein M1 membrane binding*. 5th International Orthomyxovirus Research Conference in Freiburg.

Jungnick N, Bordag N, Keller S, Herrmann A. (2008) *Insights to the interactions of Influenza matrix protein M1 with model membranes*. Jahrestagung der deutschen biophysikalischen Gesellschaft in Berlin.

Höfer CT*, Jungnick N*, Herrmann A. (2008) *Interaction of Influenza A virus M1 and RNPs with model membranes*. 52nd Annual Meeting of the Biophysical Society in Long Beach (CA), USA. *contributed equally

Eidesstattliche Erklärung

Hiermit erkläre ich, die vorliegende Arbeit selbständig ohne fremde Hilfe verfasst und nur die angegebene Literatur verwendet zu haben.

Ich besitze keinen entsprechenden Doktorgrad und habe mich anderwärts nicht um einen Doktorgrad beworben.

Die dem Promotionsverfahren zugrunde liegende Promotionsordnung ist mir bekannt.

Nadine Jungnick